UNIVERSITY OF SOUTHAMPTON

Development of Methods to Improve Knowledge of Tritium Inputs to the Ocean.

Sheila Stark

This thesis is submitted for

Doctor of Philosophy

Faculty of Science

School of Ocean and Earth Science

October 2003

Graduate School of the
Southampton Oceanography Centre

This PhD dissertation by

Sheila Stark

has been produced under the supervision of the following persons

Supervisor/s

Prof. William Jenkins
Dr. Peter Statham

Member/s of Advisory Panel

Dr. Kelvin Richards

UNIVERSITY OF SOUTHAMPTON

ABSTRACT

FACULTY OF SCIENCE

SCHOOL OF OCEAN AND EARTH SCIENCE

Doctor of Philosophy

DEVELOPMENT OF METHODS TO IMPROVE KNOWLEDGE OF TRITIUM INPUTS TO THE OCEAN

By Sheila Stark

Tritium produced by the thermonuclear weapons tests, which occurred primarily in the 1960s, was released into the atmosphere where it was rapidly oxidised to tritiated water. It then reached the oceans either directly by precipitation and vapour exchange or indirectly via rivers. Over the last thirty years tritium has been exploited as a hydrological tracer, its conservative nature means that its behaviour is solely the result of water mass movement and mixing. The clear tritium spike in precipitation provides oceanographers and modellers with a strong time marker that can be easily seen penetrating into the ocean. This coupled with its short half life provides an ideal tracer to study decadal processes such as thermocline ventilation. However, despite the global tritium in precipitation sampling network set up by the World Meteorological Organisation and the International Atomic Energy Agency, the knowledge of the temporal evolution of tritium input over the oceans is severely limited by lack of data. This poor constraint has led to some workers considering tritium less useful than other tracers, such as the chlorofluorocarbons. This thesis investigates the tritium input function to the oceans using both modelling and laboratory techniques.

The available precipitation dataset is used to construct a global model function which calculates the isotopes concentration in precipitation at any location. This was then used to calculate a North Pacific tritium budget using a simple multi-box model of the shallow circulation of this basin, the results of which were compared with inventories calculated from the WOCE and GEOSECS cruises. The calculated model inventory of 25.1 ± 3.3kg is in close agreement with the WOCE value of 23.4 ± 2.0kg. Once developed, the atmospheric deposition terms and flows in the kinematic model were modified to match the available tritium data. This served to emphasise the importance of vapour deposition to the budget and predicted a value for the Indonesian Throughflow at the upper end of other observational based estimates (15.8Sv). However, the modelling work served to highlight the limitations of tritium in such quantitative circulation studies, as tight constraints could not be placed on any of the advective terms in the model because of the significant uncertainty in the atmospheric deposition terms.

To improve knowledge of the tritium input to the oceans a technique was developed to measure tritium concentrations in annual tree rings, as it was hypothesised that these should reflect ambient precipitation. Measurements were made on cellulose, the primary constituent of wood, as the isotopic signal of its carbon bound hydrogen atoms shouldn't have changed since biosynthesis. Traditional cellulose extraction techniques from softwoods are slow and were found to not give a reproducibly clean product. Therefore a new microwave method was developed which reduced extraction times from 3-5 days to approximately 3 hours. Potential contamination from the hydroxyl groups of the cellulose molecule was subsequently removed by exchange with tritium free NaOH, thus avoiding the dangers of working with large amounts of cellulose nitrate. The validity of this technique and a test of whether the measured tritium concentrations reflect precipitation were provided by a time series from an Irish tree. By comparing the tree ring tritium results with data from the Valentia weather station it is clear that the cellulose is reflecting precipitation. The lack of a 1:1 relationship between cellulose and ambient precipitation indicates that other factors are also involved, and future work should focus on the influence of humidity, groundwater and biological fractionation.

There is clear potential to improve the time history of tritium input to the oceans by measuring historical precipitation concentrations in ocean island tree rings.

Contents

List of Figures

List of Tables

Acknowledgements

I would like to thank all of the people who have made completing this work both successful and enjoyable. Bill Jenkins has been a seemingly endless source of knowledge and his unwavering optimism in the face of the method development was something I will not forget, the same of which is true of his sense of humour and bad jokes. I would particularly like to thank Peter Statham whose keen enthusiasm for a project he was not initially closely involved in has been both inspiring and deeply appreciated. Scott Doney has been of great assistance to me providing me with invaluable advice and the WMO / IAEA data. He has been a great person to work with.

In completing the method development I am indebted to Mike Baillie without whom I would unlikely have found a suitable tree sample to do the work, and who gave sound and much needed advice on how to work with trees. Ray Collins has been critical in helping design and build new parts for the lab work, his patience and good humour were always gratefully received when help was urgently needed.

The other members of Bills harem, particularly Carolyn French, Clare Postlethwaite and Zoë Bond have been of great assistance both as colleagues, particularly in the hardest times in the lab and as friends, giving both moral and emotional support throughout my time in Southampton.

For making sure I had a fantastic time both in the laboratory and in the delights of the Rockies I have to say a huge thanks to Mark Drier, my time in Boulder offered a timely reminder of how much I enjoy science. The rest of the research team at INSTAAR provided invaluable advice and assistance for a stable isotope novice and I would like to thank Jim White for showing huge amounts of interest in tritium in trees.

To all my friends I say a huge thank you for keeping me sane, making me laugh and reminding me that tritium isn't everything. In particular Sue, Nat, Mike and Iain have made being at the SOC a great experience and you will be missed when I go and get a proper job.

To my family all I can say is thanks for supporting me, listening when it was all getting too much and giving me much needed perspective. At last I have finished my education! Finally to John, it is hard to express the thanks I owe you, you have always been there for me and sacrificed many a climbing day to my thesis, here's to catching up!

1. Introduction

1.1 Tritium

Tritium (^{3}H) is the heaviest isotope of hydrogen. It is radioactive and decays with a half life of 12.32 years [*Lucas and Unterweger*, 2000] to the stable helium isotope ^{3}He. In the environment ^{3}H is mainly seen as tritiated water (HTO) though some does exist as molecular hydrogen.

Tritium is constantly formed in the upper atmosphere by the bombardment of nitrogen and oxygen atoms by cosmic rays, as illustrated by Equation 1.1.

$$^{14}_{7}N+^{1}_{0}n\rightarrow^{12}_{6}C+^{3}_{1}T \tag{1.1}$$

The oceanic inventory of this natural tritium is negligible as much of it is lost to space and never reaches the earth's surface. However the onset of the nuclear era resulted in the production of huge quantities of ^{3}H dwarfing the natural inventory. The first nuclear explosion, named *Trinity* was detonated by the United States of America in 1945 [*Jepsen*, 2000] with testing by the then Soviet Union starting in 1949, the UK in 1952 and the French and Chinese starting in the 1960s. Large amounts of artificial ^{3}H started being injected into the atmosphere around March 1954 during the Castle test series in the Pacific [*Libby*, 1963]. The bomb cloud from these Castle tests vaporised enormous quantities of water and carried them into the stratosphere well labelled with bomb ^{3}H [*Begemann and Libby*, 1957]. Fusion bombs produce far more ^{3}H than fission devices, releasing approximately 2kg/Mt of explosive compared with approximately 0.07kg/Mt for fission bombs [*Michel and Suess*, 1975]. The large series of bomb tests in 1962 and 1963 carried out by the United States and the Soviet Union produced three times more ^{3}H than all the previous tests combined [*Eriksson*, 1965]. After the 1963 Nuclear Test Ban Treaty, which banned all nuclear explosions in the atmosphere, outer space and the oceans [*Jepsen*, 2000] relatively little ^{3}H has been produced, though there have been slight increases in the amount of ^{3}H in precipitation as a result of French and Chinese tests.

1.2 Tritium Delivery to the Earths Surface

The mechanisms for the production of bomb tritium, its passage through the atmosphere and its delivery to the earth's surface are reasonably well understood. Once in the stratosphere the bomb derived ^{3}H was rapidly oxidised to form tritiated water molecules and re-entered the troposphere by mid-latitude tropospheric exchange from where it was rapidly rained out, as is illustrated by

Figure 1.1. The residence time of ^3H in the stratosphere ranges from weeks just above the tropopause to several years at higher altitudes [*Fine and Östlund*, 1977], while that in the troposphere is of the order of a few weeks. The fallout of HTO and the height of penetration of the bomb cloud reflects the type of detonation (surface, water or air) the season and the bomb yield [*Taylor*, 1966].

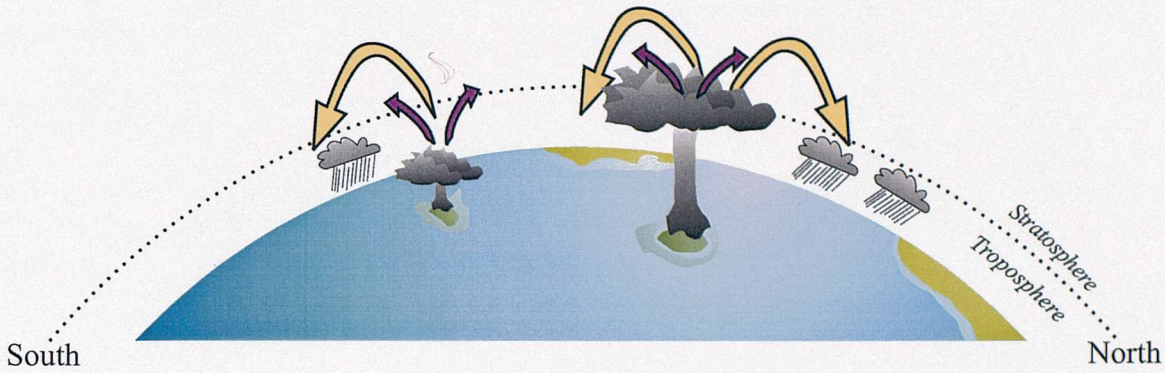

Figure 1.1. Cartoon depicting how bomb ^3H reached the earths surface. Detonation of the devices caused large volumes of ^3H to be injected into the stratosphere after which exchange with the troposphere led to ^3H reaching the earths surface by precipitation and vapour exchange.

Nuclear testing occurred mainly in the northern hemisphere and started on a large scale in 1952. The presence of large amounts of HTO in the troposphere caused rainwater in the 1960s to have greatly elevated tritium levels, up to 10,000TU (where $1TU = 10^{18} \times {}^3H/{}^1H$) in the northern hemisphere in 1963-4 [*Michel and Suess*, 1975]. The clear spike of ^3H in precipitation is clearly evident in Figure 1.2. The isotope then reached the ocean either directly via precipitation and vapour exchange or indirectly by evaporation and continental runoff. Over the bomb spike northern hemisphere surface waters showed ^3H concentrations of up to 40TU [*Michel and Suess*, 1975].

The pattern of tritium input in the northern hemisphere is dominated by three pulses in 1954, 1958-1959 and the strongest in 1963 [*Weiss and Roether*, 1980]. There was much less thermonuclear weapons testing in the southern hemisphere, with none occurring prior to the French test series at islands in the Tuamoto Archipelago in 1968 [*Taylor*, 1971]. This led to the distribution of ^3H being asymmetric between the two hemispheres. The ^3H concentration at continental sites is also elevated compared with marine locations at the same latitude reflecting re-evaporation from soils and vegetation. Re-evaporation of HTO over the oceans is very limited as rapid mixing above the thermocline immediately dilutes precipitation and the mixing ratio of water evaporated from the oceans is always low.

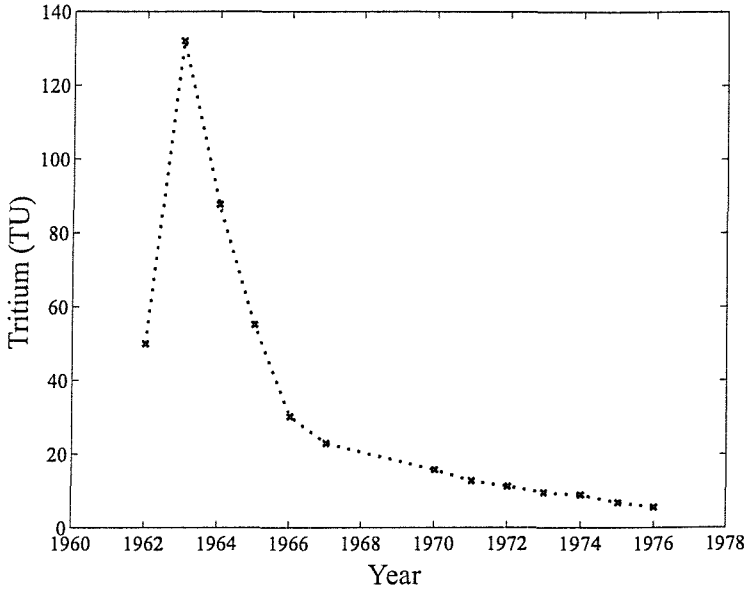

Figure 1.2. The concentration of ^3H in precipitation observed at Wake Island (19.28°N, 166.65°W) in the North Pacific Ocean. The bomb 'spike' is clearly evident in 1963.

Early work [*Eriksson*, 1965] suggested that the exchange of tritiated water vapour across the air-sea interface was the dominant mechanism for the entry of bomb ^3H to the worlds oceans. However this hypothesis assumes concentrations of ^3H in water vapour over the oceans, for which there is very little data [*Koster et al.*, 1989]. Subsequent work has generally supported this hypothesis as the reported observed ^3H inventories are significantly larger than can be accounted for by direct precipitation and runoff alone [*Broecker et al.*, 1986; *Weiss et al.*, 1979] but modelling studies such as *Koster et al.* [1989] still question it and lack of data leaves the issue unresolved.

The majority of ^3H reached the earth's surface north of 15°N reflecting several processes. Firstly the transfer of air from the stratosphere to the troposphere largely occurs at latitudes greater than 35°N and the residence time of water in the troposphere is too brief to allow significant transport of it to the tropics. It has also been shown [*Broecker et al.*, 1986], by water column properties (salinity, nutrients and potential temperature) that there are strong fronts across the Pacific and Atlantic Oceans at around 15°N, which inhibit lateral mixing. Together these processes all act to hold ^3H in northern waters

1.3 Tritium as a Tracer

The existence of tritium as part of the water molecule make it an ideal hydrological tracer. It is conservative and as such has no significant biological or chemical sinks or sources in the worlds

oceans, its behaviour being solely the result of mixing and the movement of water masses [*Jean-Baptiste and Messias*, 1993]

To promote the use of ^{3}H in ocean circulation studies the International Atomic Energy Agency (IAEA) and the World Meteorological Organisation (WMO) joined together and organised a global network of stations to collect monthly precipitation samples for ^{3}H analysis. Unfortunately logistics and cost led to the oceanic coverage of this network being sparse and there are very few long duration records away from the continents. For example, although the record at Valentia, Ireland extends from 1957 to at least 1997, that in Bermuda only covers a seven year period from 1962-1968. Even poorer records are seen at sites such as Madeira where measurements were only made between 1988 and 1993, many years after the initial injection of bomb ^{3}H to the oceans.

Over the last thirty years a significant number of studies have been published which discuss the fate of bomb tritium in the ocean, either qualitatively in terms of flow patterns and advection/mixing processes or quantitatively, with the computation of mass fluxes. For example *Fine* [1985] used ^{3}H data to constrain the flow through the Indonesian Seas from the Pacific to the Indian Oceans to 5 Sv (where $1Sv = 1 \times 10^{6}\ m^{3}.s^{-1}$).

Tritium data has been shown to not only support previous descriptions of the oceans structure but has provided over the last thirty years an improved understanding of the pathways by which tracers enter the ocean interior as well as better knowledge of the timescale of key oceanic processes [*Jean-Baptiste and Messias*, 1993].

1.4 Tritium in Modelling Studies

1.4.1 Climate Models

Climate models are tools used to enhance understanding of the climate system and to aid prediction of future climates. However despite major advances in the field over the last forty years even the most sophisticated models remain far simpler than the full climate system [*McGuffie and Henderson-Sellers*, 2001]. Modelling of the full three dimensional ocean is far more difficult than the atmosphere because of the smaller scales of motion which exist in the ocean, for example ocean eddies are around 10-50km compared to around 1000km in the atmosphere. The inherent limitations of ocean modelling prohibit a perfect simulation of observed property fields, such as temperature and salinity. It is therefore challenging to test models with passive tracers which do not affect the density field [*Heinze et al.*, 1998].

The oceans are a key component of the global climate system as they store and transport heat, absorbing warmth in the topics and releasing it at higher latitudes. They dominate the global

hydrological cycle as they are a huge moisture reservoir and they play a vital role in the regulation of atmospheric gases such as CO_2. Numerical models of the oceans predict ocean currents, temperature and salinity and form a key component of coupled climate models. Checking a models ability to capture water mass formation is limited by its reliance on ocean measurements [*England and Maier-Reimer*, 2001] but chemical tracers can provide detailed pathways and rates of water mass movement.

Natural tracers such as radiocarbon and ^{39}Ar have well known deliveries to the ocean. However their usefulness is limited by uncertainties in the reconstruction of natural pre-bomb ^{14}C concentrations in the surface ocean and areas of deep water formation, and the lack of ^{39}Ar data due to the difficulties in measuring it [*Heinze et al.*, 1998]. Likewise nutrients are not best suited to tracer studies as their use necessitates complete modelling of biological and chemical processes.

To be of optimal use modelling and circulation studies need 'ideal tracers' which may be looked upon as dyes, the distribution of which can be interpreted in terms of ocean currents and mixing processes alone. Such tracers must be chemically stable and have well constrained sources and sinks. Transient tracers such as bomb ^{3}H and chlorofluorocarbons (CFCs) satisfy these criteria and as such the study of these can be used to test how well Ocean General Circulation Models (OGCMs) represent oceanographic processes. These species are the most comprehensively measured transient tracers in the modern ocean, with sections obtained during the 1970s Geochemical Ocean Sections (GEOSECS) expeditions being followed by detailed surveys such as the 1981-1983 Transient Tracers in the Ocean (TTO) programme in the Atlantic. During the 1990s the Atlantic, Pacific and Indian Oceans have all been studied as part of the World Ocean Circulation Experiment (WOCE).

1.4.2 Tritium as a Dye Tracer

Tritium is particularly suited to use as a modelling tool for several reasons. Firstly, the bomb spike produced a very clear time marker that can be seen propagating into the ocean [*Jenkins*, 1998] and this can be considered as a large scale dye experiment. The ability of a model to replicate this is a sure test of performance. Secondly ^{3}H is an ideal and sensitive tool for studying exchange between northern subtropical and tropical waters because of the strong 5-10 fold inter-hemispheric contrast in its delivery. Thirdly the timescale of tritium decay (12.32 years) is ideally matched to study model ventilation over decadal timescales, for example to look at thermocline ventilation or renewal of Antarctic Intermediate Water [*England and Maier-Reimer*, 2001]. The usefulness of ^{3}H to study ventilation is particularly important in modelling work to predict the oceans role in both climate and the uptake of pollutants [*Sarmiento*, 1983].

An example of such a study is that by *Jia and Richards* [1996] in which the ^3H–^3He tracer pair was included in the Atlantic Isopycnic Model. This model has a 1° horizontal resolution and 20 vertical layers, with realistic bathymetry. Inclusion of the tracer pair allowed comparisons to be made between the model ^3H distribution, GEOSECS and TTO observations. The model ^3H pattern clearly showed ventilation of the subtropical gyre south of 35°N and the pathways of the deep overflows from the Greenland Norwegian basin. However the model ^3H distributions on various density layers in the subtropical gyre did not agree with observations, which was attributed to the coarse horizontal resolution of the model and too rapid circulation on the isopycnic layers. In this way the inclusion of ^3H-^3He allowed the model to be calibrated and its performance assessed .

In practise difficulties arise in the use of transient tracers such as tritium in modelling studies because of the limited spatial and temporal sampling of the tracer fields, uncertainties in their boundary conditions and ambiguities in the circulation field [*Memery and Wunsch*, 1990]. One solution is to simultaneously examine the distribution of several different tracers though this requires and understanding of the relationship between tracer fields and their variability over the ocean [*Doney et al.*, 1997].

1.5 The Tritium Input Function

Oceanographic applications of tritium require knowledge of the concentration of the isotope in both precipitation and vapour through time.

Model estimates for the deposition of tritium to the earths surface developed by *Weiss et al.* [1979] and *Weiss and Roether* [1980] have been widely accepted as a tool for defining the ^3H flux boundary condition in ocean modelling work, such as the North Atlantic model study of *Sarmiento* [1983]. However as is pointed out by *Memery and Wunsch* [1990] the estimated uncertainty in the *Weiss and Roether* [1980] formulation of approximately 20%, may be prohibitively large for ocean modelling purposes.

Measurements of surface water tritium concentrations that pre-date the thermonuclear era are few, of questionable reliability and of the order 0.2-0.5 TU [*Begemann and Libby*, 1957, *Dreisigacker and Roether*, 1978]. However after 1960 far more oceanic ^3H measurements have been made and *Dreisigacker and Roether* [1978] and *Fine and Östlund* [1977] have used these to construct surface water ^3H time histories for the North Atlantic (see Figure 1.3) and North Pacific respectively. The 'source function' developed for the Pacific by *Fine and Östlund* [1977] uses an exponential relationship with latitude to describe surface water concentrations such that:

$$TU = -1 + e^{a+b\times latitude} \tag{1.2}$$

where a and b are functions of time, salinity and longitude. It was found that for 81% of the samples the predicted ^{3}H concentration falls within 18% of the observed value. However the function is limited to use south of 51°N as no data north of this latitude was included and the exponential relationship means that it may overestimate ^{3}H concentrations further north. The function is also limited to the Pacific ocean and it is difficult to apply outside of the time period of the data (1963-1974). Subsequently these functions have been used as concentration boundary conditions for both box models and simple circulation models. *Thiele and Sarmiento* [1990] used the North Atlantic boundary condition of *Dreisigacker and Roether* [1978] in a 2 dimensional model of flow along a thermocline isopycnal surface, which showed the importance of ventilation and provided estimates of ventilation age. Ultimately though, the usefulness of such functions is severely limited by the difficulty in extrapolating results from one basin to a global scale.

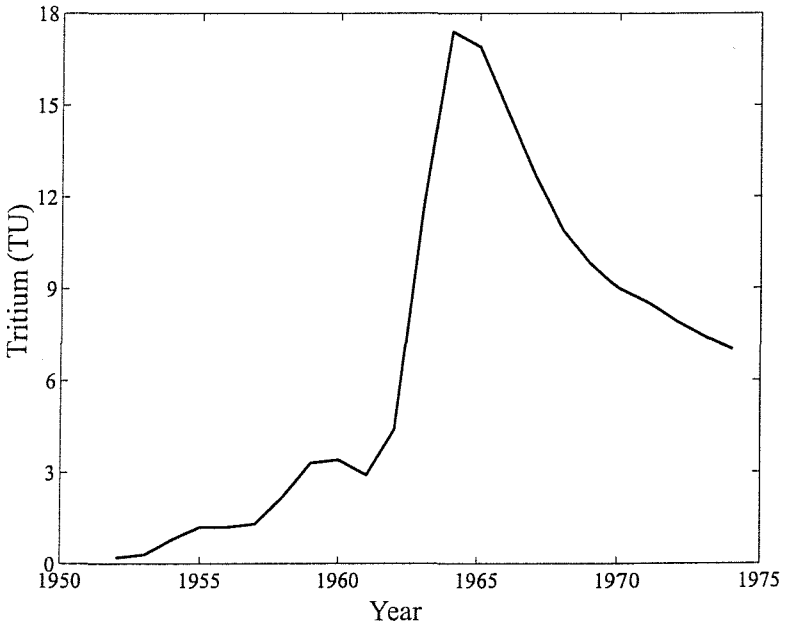

Figure 1.3. The model surface water ^{3}H concentrations for the North Atlantic developed by Dreisigacker and Roether [1978] which has been used as a 'source function' for modelling studies.

Building on the pioneering work of *Weiss and Roether* [1980], *Doney et al.* [1992] developed a global model function of the distribution of bomb ^{3}H in precipitation that fitted the integrated delivery for the WMO/IAEA stations to an accuracy of 5-10%. It is important to note however that the instantaneous temporal fit was not this strong, ranging from 15-35%. Ultimately the integral accuracy of this function was demonstrated by the success of *Doney et al.* [1993] in using the fit to construct a North Atlantic ^{3}H budget which showed good agreement with observations.

This work has done much to address the concerns raised by *Memery and Wunsch* [1990] about the utility of ^{3}H as a diagnostic of ocean model performance but problems remain in the ^{3}H source function which need to be addressed. The remaining uncertainties can be summarised thus:

1. Tritium in precipitation data is extremely sparse over the oceans leading the *Doney et al.* [1992] error maps to show significant uncertainties over the oceans.

2. The factor analysis maps produced by *Doney et al.* [1992] overestimate the ^{3}H delivery to the ocean due to over-extrapolation of continental influence [*Doney et al.*, 1993]. To accommodate this the North Atlantic budget was calculated by adopting a uniform transition scale of 500 km, a choice which needs to be tested.

3. Knowledge of the surface ocean response to the bomb transient is sparse in the early years due to both lack of data and the difficulty at the time of doing low level ^{3}H measurements.

In conclusion despite recent advances the utility of ^{3}H as a tracer in circulation and modelling efforts is fundamentally limited by uncertainties in its input function. The main focus of this thesis is to address these issues by developing a technique to improve deposition knowledge over the oceans by reconstructing records of ^{3}H in precipitation in tree rings.

1.6 Trees as Recorders of Past Climates

The latter half of this thesis is concerned with reconstructing records of tritium in precipitation from tree rings.

1.6.1 Tree Physiology

The stems or trunks of trees store water, carbohydrates and minerals, conduct water and minerals up from the roots and transport food and hormones from where they are synthesised to where they are either respired or stored [*Kozlowski and Pallardy*, 1997]. A tree stem is typically composed of tapering columns of xylem (wood) composed of a thin series of annual layers or rings. When xylem is young it is known as sapwood and conducts sap, which is primarily water, strengthens the stem and can also act as a storage reservoir for food. On average only about 10% of the sapwood cells are alive [*Kozlowski and Pallardy*, 1997] and as it ages the cells die and the tissue often becomes darker in colour and is known as heartwood. Heartwood provides mechanical support but no longer participates in physiological processes.

In temperate trees the annual rings stand out prominently in both stem and branch cross sections and are the basis of climatic reconstructions. At temperate latitudes active growth and addition of wood to the stem occurs during the warmer months of the years and ceases during the cold

season, making ring boundaries extremely distinct. In contrast, trees in tropical locations with continually warm and wet climates may add xylem to the stem during most, if not all of the year resulting in growth rings either being absent or very indistinct. A tree grows by increasing both its height (apical growth) and breadth (radial growth). In general a tree deposits wider rings when it is young and the stem is small and as it ages radial growth slows as the stem diameter increases.

Tree roots absorb water and minerals from the soil, store reserved food and synthesise some growth hormones. Water that flows in through the roots moves up in the xylem of the sapwood portion of a tree to the leaves from where it is subsequently lost to the atmosphere via transpiration [*White et al.*, 1985]. Variations among species in the extent and distribution of roots are critical in climate reconstructions as they determine how much of a groundwater signal is recorded by the tree. It should be noted that the extent of spread of roots varies significantly both between species and with site and soil type for any individual species.

Leaves are crucial in the growth and development of trees as they are the principal photosynthetic organ. They are also storage sights for carbohydrates and mineral nutrients and the primary site for water exchange with the atmosphere. Leaf tissue has abundant intercellular spaces connected to the atmosphere by microscopic openings known as stomata [*Kozlowski and Pallardy*, 1997]. Stomata play an essential role in plant physiology as they are the passages through which most water is lost and CO_2 is gained by the tree.

1.6.2 Photosynthesis

Photosynthesis is the process by which all green plants use light energy to synthesise reduced carbon compounds from CO_2 and water. Both energy capture and CO_2 fixation occur predominantly in the chloroplasts of tree leaves and simply put, photosynthesis is the reduction of atmospheric CO_2 to glucose using light energy with a release of oxygen from water (Equation 1.2).

$$6CO_2 + 12H_2O \rightarrow C_6H_{12}O_6 + 6O_2 + 6H_2O \tag{1.3}$$

Although carbohydrates are the principal products of photosynthesis large quantities of these are rapidly converted into other compounds such as lipids and amino acids, which are equally important to plant metabolism [*Kozlowski and Pallardy*, 1997].

Many environmental factors affect photosynthesis including light, temperature, atmospheric CO_2 concentration, water supply, humidity and soil fertility [*Fritts*, 1976].

1.6.3 Dendroclimatology

The modern science of dendrochronology was pioneered by A.E. Douglass, an astronomer who investigated sunspot cycles by tracing climatic factors that were reflected in the growth of trees. Specifically *dendroclimatology* uses tree rings to reconstruct the past climate of an area and initial work focused on the link between past climate and tree ring width which results from plant growth being affected by conditions in the forest environment [*Fritts*, 1976]. In many climates the width of a tree ring is most strongly influenced by rainfall and temperature. In general, harsh winters, hot summers and droughts encourage narrow ring growth while mild winters and mild or wet summers encourage the formation of wide rings.

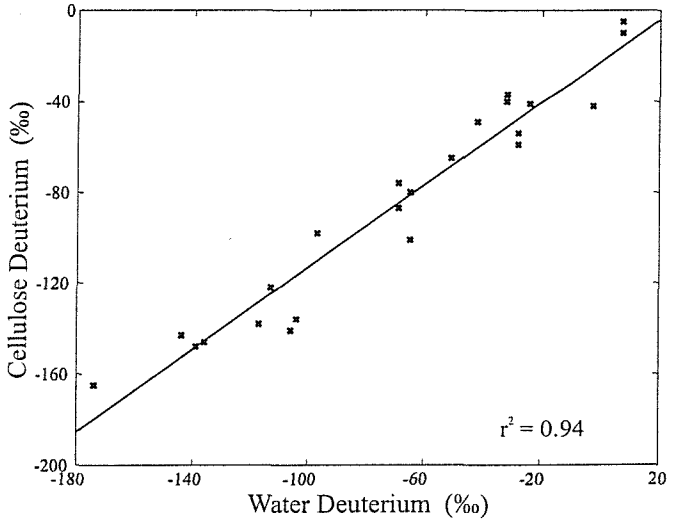

Figure 1.4. A graph illustrating the relationship between the deuterium content of tree ring cellulose and the trees water source. The correlation coefficient of 0.94 highlights the strength of the relationship, which forms the basis of the methods developed in this thesis to improve knowledge of the ^{3}H input function. The data presented is that of Epstein et al, [1976].

Tree growth is undoubtedly controlled by the movement of water and as this is the only source of hydrogen available to a tree for photosynthesis the isotopic signal recorded in a tree ring should reflect the water used by the tree in that year. This principle has been the foundation of hydrogen climatic reconstructions from tree rings and strong correlations have been found between the deuterium content of tree ring cellulose and their associated waters [*Epstein et al.*, 1976; *Yapp and Epstein*, 1982a]. The strength of this relationship is clearly illustrated by Figure 1.4, though the lack of a perfect 1:1 relationship indicates that other factors are also important. For example the transpiration of water through leaf stomata has an important effect on deuterium reconstructions, as until water is transpired its isotopic signal remains unchanged under most common conditions of plant growth [*Yapp and Epstein*, 1982a]. In this thesis this premise is exploited using the assumption that the primary signal reflected in the soil moisture used by trees is precipitation. In

this way the ^3H signal recorded in an easily datable tree ring provides a mechanism to determine historical concentrations of ^3H in precipitation.

1.7 Aims of the Thesis

The primary aim of this thesis is to investigate the tritium input function and to develop a method to improve knowledge of it. This aim is addressed by first developing a global model function of the distribution of the isotope in precipitation. The usefulness of this function to both modelling efforts and circulation studies is then explored by looking at the results of a simple multi-box model of the shallow circulation of the North Pacific. This first half of the work highlights the importance of improving knowledge of the temporal evolution of the deposition of ^3H to the earth's surface. The second half of the thesis is concerned with the development of a method to reconstruct time histories of ^3H in precipitation from tree rings.

Overall the aims of this work can be summarised as follows:

1. To model the input of ^3H to the earths surface with a particular interest in the delivery to the oceans (*Chapter 2*).

2. Use this model to calculate a North Pacific ^3H budget for comparison with integrated ^3H inventories from the WOCE and GEOSECS cruises (*Chapter 2*).

3. Use the model to make simple deductions about the evolution of the distribution of ^3H in the North Pacific from 1950 to 1997 and investigate the sensitivity of the budget to each of the model terms (*Chapter 2*).

4. Develop a technique to reconstruct ^3H in precipitation time histories at oceanic islands to allow knowledge of the input of ^3H to the oceans to be improved (*Chapter 3*).

5. Assess how well the technique works by constructing a ^3H time history from an Irish tree for comparison with precipitation data from the Valentia weather station (*Chapter 4*).

Throughout this study the following definitions are used:

- Tritium concentrations are expressed in Tritium Units (TU) which are defined as (^3H /^1H) x 10^{18}. To allow ^3H to be treated as a pure 'dye like' tracer the effect of radioactive decay needs to be taken into account. To do this all concentrations are decay corrected to a common date and, for example, TU97N refers to the ^3H concentration on January 1st 1997.

- The deviation in per mil (parts per thousand) of the isotopic ratio of deuterium of a sample compared with SMOW (Standard Mean Ocean Water) is defined as:

$$\delta D = \left[\frac{\left({}^{2}H/{}^{1}H \right)_{sample} - \left({}^{2}H/{}^{1}H \right)_{SMOW}}{\left({}^{2}H/{}^{1}H \right)_{SMOW}} \right] \times 1000 \qquad (1.4)$$

2. The Deposition and Recirculation of Tritium in the North Pacific Ocean

2.1 Introduction

Tritium (^3H) entered the North Pacific via several pathways: precipitation, vapour deposition, lateral transport, and river inflow. These four pathways and advective transport and mixing within the ocean determine the temporal evolution of the ^3H concentration at any particular location. Ocean surface waters in the northern hemisphere had ^3H concentrations as high as 40TU over the bomb spike in 1963-1964 compared to natural background levels of ~0.5 TU [*Michel and Suess*, 1975], where 1TU = $1x10^{18}$ $^3H/^1H$.

The distribution of tritium in North Pacific waters can be understood broadly by dividing the basin into three layers [*Fine et al.*, 1981]. The surface layer includes the depth range of the winter mixed layer and is therefore ventilated locally on an annual basis. This water has received ^3H directly from atmospheric fallout and lost some by lateral transport or exchange with deeper waters. Below this layer, the upper thermocline (second layer) receives ^3H from above and penetrates to the depth of the maximum winter outcrop isopycnal for the basin (26.8 σ_θ). Waters deeper than this isopycnal in the lower thermocline comprise the third layer and have only received ^3H by vertical diffusion and intermediate water formation in the Sea of Okhotsk. In the 1990s there was significant bomb ^3H at depth, indicating that the North Pacific can act as a sink for atmospheric constituents despite the lack of significant deep water formation in the area [*Fine et al.*, 1981].

Along with radiocarbon and CFCs, tritium is the most extensively measured transient tracer in the modern ocean. The ^3H samples collected as part of the World Ocean Circulation Experiment (WOCE) provide us with the most extensive data set of this isotope presently available. In particular, the WOCE data set allows the North Pacific ^3H inventory to be calculated with much better accuracy (~10% as shown below) and to constrain circulation issues for the basin associated with tropical-subtropical exchange, the Indonesian Throughflow, and intermediate water formation.

North Pacific tritium data has been used extensively to identify the pathways for water mass penetration into the subtropical gyre and the equatorial system [*Jean-Baptiste and Messias*, 1993]. Lateral advection along isopycnals transports ^3H from high latitudes to the subtropics and tropics

[*Fine et al.*, 1981], and one of the most prominent features of the ^{3}H distribution in the tropics is the presence of a maximum centred between 125° and 145° W. This has been interpreted as direct evidence of an "interior water pathway" from the subtropics to the equator [*M^{C}Phaden and Fine*, 1988; *Fine et al.*, 1987].

M^{C}Phaden and Fine [1988] suggested that the ^{3}H maximum arises because of the positive wind stress curl and negative Ekman pumping between 3° and 14°N, allowing a southward geostrophic flow to cross the North Equatorial Counter Current (NECC) in the central Pacific. Using a thermocline model and OGCM, *Liu and Huang* [1998] extended this work to incorporate the vertical structure of the geostrophic flow and to show that the ^{3}H maximum is a result of transport both in the interior and in the Mindanao current. This process represents part of the North Pacific subtropical cell. Subduction of surface waters in the subtropics feeds a subsurface flow towards the equator where the water is upwelled and then moves poleward at the surface, affecting sea surface temperature and exchanging heat and freshwater with the atmosphere [*Johnson*, 2001]. The timescale for the subducted pathway has been inferred from ^{3}H measurements to be of the order 10 years [*Fine*, 1985; *Fine et al.*, 1987], and estimates of the magnitude of the flux are of the order 30Sv (33.1Sv [*Qiu and Huang*, 1995], 28.35Sv [*Huang and Russell*, 1994]).

The flow through the Indonesian Seas represents a path of surface and thermocline water transport from the Pacific to the Indian Ocean [*Fieux et al.*, 1996]. The flow is difficult to constrain since the water passes through a complex series of channels with intricate topography and coastlines. The Indonesian Throughflow is driven by a pressure gradient between the western Pacific and the Indian Ocean set up by easterlies in the equatorial Pacific. North Pacific water is supplied to the Throughflow by the Mindanao current and eddy [*Godfrey*, 1996; *Rodgers et al.*, 1999] which are part of the low latitude western boundary circulation of the basin. Estimates of the magnitude of the flow vary widely from an estimate based on ^{3}H data of 5.1Sv [*Fine*, 1985] through model based estimates of a nine year mean of 7.4Sv [*Potemra et al.*, 1997] to 16.4Sv [*Morey et al.*, 1999]. The depth range of the flow is also much debated, with it often being considered to be a warm surface water flow [*Morey et al.*, 1999]; but some models suggest that more than half of the transport may occur below the mixed layer [*Fine*, 1985]. There is seasonal and interannual variability in the magnitude of the throughflow associated with the regional monsoon and the El Nino Southern Oscillation [*Gordon*, 1986].

One of the most striking features of the North Pacific subtropical gyre is a well defined salinity minimum at depths of 300-800m associated with North Pacific Intermediate Water (NPIW) [*Yasuda et al.*, 1996]. Intermediate water formation in the North Pacific occurs via ventilation in the subpolar gyre, especially in the Sea of Okhotsk, and is likely to be due to a combination of

cooling and brine rejection during seasonal sea ice formation [*Reid*, 1965; *Warner et al.*, 1996]. Waters with a density greater than $26.8\sigma_\theta$ do not outcrop in the open North Pacific, but water densities up to $27.7\sigma_\theta$ are seen in the Sea of Okhotsk [*Talley*, 1991]. The general circulation in the Sea of Okhotsk is a broad cyclonic gyre [*Wong et al.*, 1998] connected to the North Pacific through the Kuril Islands. The outflow waters can sink to depths of 1000m, though the effects can be spread to at least 2000m by high rates of vertical mixing [*Talley*, 1991]. The presence of two ^{3}H maxima in the subpolar North Pacific suggests that although North Pacific Intermediate Water (NPIW) is formed in the north west it may be further ventilated downstream in the Gulf of Alaska [*Van Scoy et al.*, 1991].

Modelling efforts over the last two decades provide an increased understanding of the pathways by which tracers reach the ocean interior and the timescales of key oceanic processes. Chemical tracers can constrain models in a way that temperature and salinity (T-S) alone cannot [*England and Maier-Reimer*, 2001]. A model with a good representation of T-S can have major errors in its simulated circulation so it is important to check the models ability to capture tracer distributions.

In this chapter the usefulness of tritium in circulation problems is explored by developing a model North Pacific ^{3}H budget that is compared with inventories calculated from the WOCE and GEOSECS cruise datasets. The usefulness of ^{3}H to such calculations is limited by how well one can constrain its input function. Therefore a new estimate of the delivery of bomb ^{3}H to the North Pacific by precipitation, vapor deposition, rivers, and lateral advection for the period 1960-1997 is developed. Building on the work of *Doney et al.* [1992], a global model function of the ^{3}H distribution in precipitation using World Meteorological Organisation (WMO) / International Atomic Energy Agency (IAEA) data is calculated. This model function allows the atmospheric delivery of ^{3}H to the North Pacific to be calculated using the standard *Weiss and Roether* [1980] hydrological model. The sensitivity of the model to circulation and surface input assumptions are explored with a view to ascertaining the usefulness of ^{3}H to such quantitative circulation problems.

2.2 North Pacific Tritium Inventories

2.2.1 The WOCE Tritium Distribution

The tritium data from the WOCE series of cruises reveals that by the mid 1990s the ^{3}H distribution in the North Pacific was characterised by significant depth penetration at high latitudes and high concentrations in the subtropical gyre. The main features of the WOCE

distribution are illustrated in Figure 2.1 by a zonal section along 9.5° north and a meridional section along 135° west.

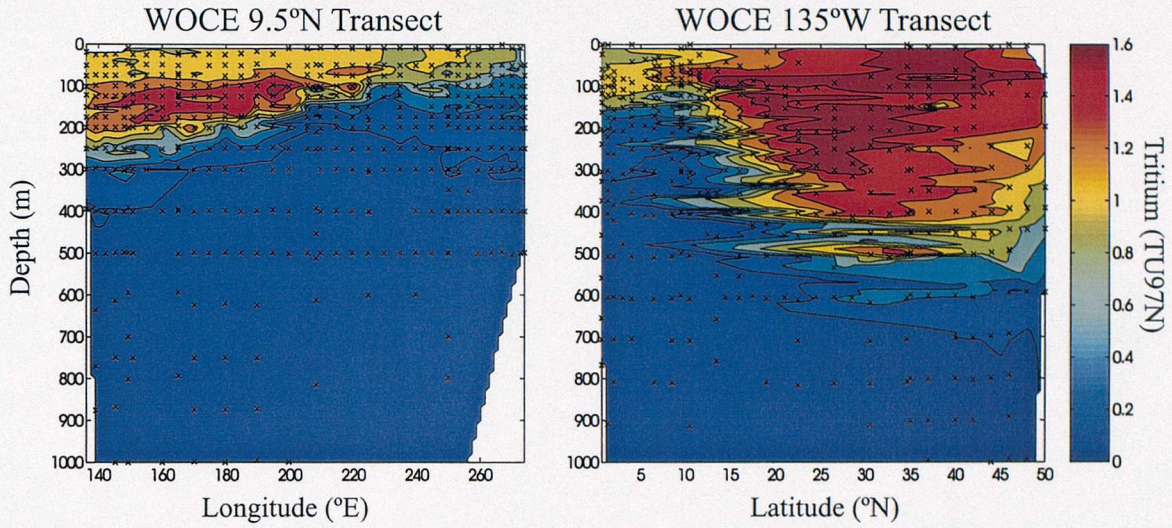

Figure 2.1. Contour plots showing the tritium distribution on a zonal section (along 9.5°N) and a meridional section (along 135°W) in the North Pacific from the WOCE series of cruises. The locations where samples were collected are shown by crosses and all tritium concentrations are decay corrected to January 1st 1997 (TU97N).

The meridional section shows that the highest surface water tritium concentrations are at mid latitudes, reflecting the location of maximum ^{3}H rainout even three decades after the weapons testing. This transect also illustrates that the majority of ^{3}H in the North Pacific is in the subtropical gyre, where concentrations are uniformly greater than 1.2 TU97N in the top 200 metres. Overall the subtropical and subpolar regions are significantly richer in ^{3}H than tropical latitudes, with there being far lower concentrations of the isotope in the top 200 metres equatorward of 15° north. It would appear that the predominately east-west plane of the North Equatorial Current (NEC) is an effective barrier to significant penetration of ^{3}H rich waters from the subtropical gyre into the equatorial region. However the zonal section at 9.5° north shows relatively high ^{3}H concentrations in the top 300 metres of the water column, especially in the central and western Pacific, which is typical of tropical latitudes in the WOCE data, though there is little appreciable ^{3}H below this. An increase in equatorial ^{3}H levels can occur as the NEC will receive water with higher ^{3}H from both the California Current in the east and from the subtropical gyre via a Hadley cell circulation. The 'tongues' of relatively high ^{3}H seen penetrating equatorward between 200 and 400 metres depth in the meridional section are evidence of such a Hadley cell circulation. The distribution of ^{3}H at 9.5° north also shows that higher concentrations of the isotope are seen in the west of the basin, which is likely due to the upwelling of low ^{3}H water which is characteristic of the eastern North Pacific at this latitude.

It is strikingly clear from the section at 135° west that ^{3}H penetrates to significantly greater depth at higher latitudes, with concentrations of 0.4 TU97N being seen at 600m polewards of 30° north. This depth distribution is a clear reflection of the effect of intermediate water formation in the North Pacific, which is visible at a site distant from the main areas of intermediate water mass formation in the west of the basin.

2.2.2 WOCE and GEOSECS Tritium Inventories

Two data sets were used to describe the changing North Pacific tritium inventory, namely the 1989 to 1995 WOCE and the 1973-1974 GEOSECS (Geochemical Ocean Sections) cruise data sets.

Samples for the WOCE tritium data used here were collected between January 1989 and April 1995 and subsequently analysed in the Woods Hole Oceanographic Institution Helium Isotope Laboratory. Samples were collected from 57°N to the equator and from between 71.5°W and 126.5°E, making it the most detailed study of ^{3}H in this ocean so far. Samples were collected throughout the water column down to a depth of 6089 metres, although samples from depths greater than 3 km were taken solely for the purpose of providing blanks.

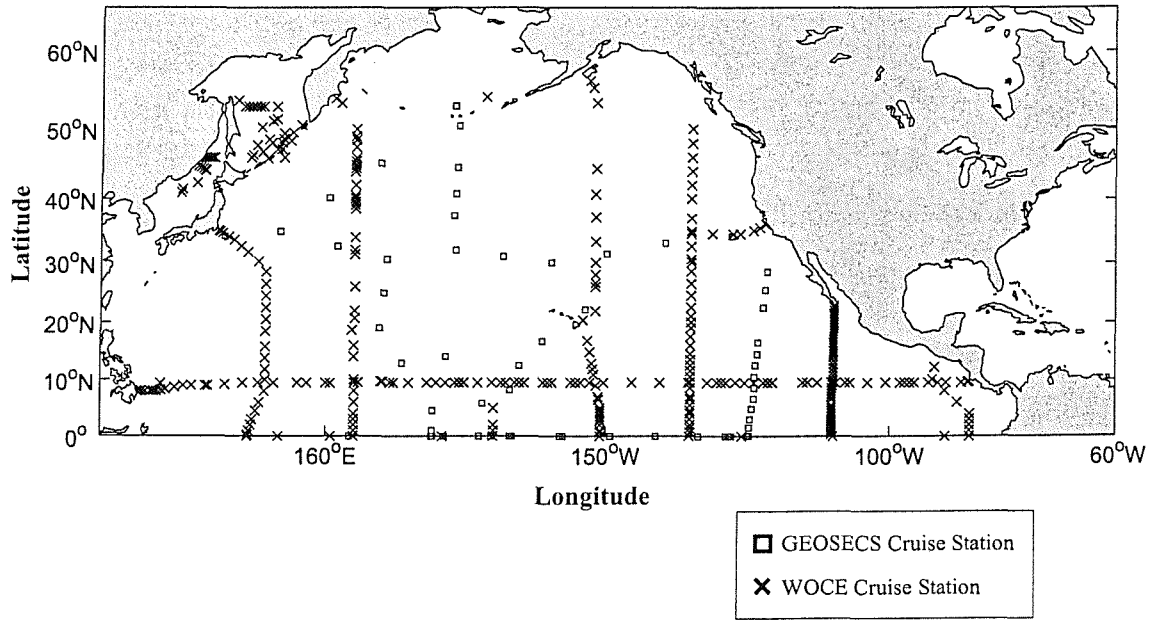

Figure 2.2. Map of the North Pacific basin showing the location of the sample stations on the WOCE and GEOSECS cruises. Much less data is available to calculate the GEOSECS inventory as there were only 42 stations in the North Pacific compared with 326 during the WOCE series of cruises.

The GEOSECS dataset was collected between January 1973 and October 1974, and sampling extended from the equator to 53.1°N. The longitudinal extent of these cruises was less than in the later WOCE survey, with few samples being taken in the west or in the low latitude east of the basin. The location of the sampling stations from both series of cruises is shown in Figure 2.2.

For each data set the tritium inventory was calculated by vertically integrating the data at each station from the surface to the deep ocean and averaging over horizontal spatial bins that cover the basin, as shown in Figure 2.3. The data were decay corrected to a uniform date (January 1st, 1997 TU97) using the revised tritium half life of 12.32 years [*Lucas and Unterweger*, 2000]. The decision to have fewer bins longitudinally was due to the poorer spatial resolution of the cruise stations in this direction. Uncertainties in these inventories were calculated from the standard deviations of the column integrated values in each bin (Figure 2.3). Bins that contained no data were assigned a ^3H concentration by interpolating from surrounding bins, and the error was set as equal to this value. The quoted errors are likely to be an underestimation of the total uncertainty as no account was taken of the potential longitudinal variability of the ^3H distribution within the large 50° wide bins.

Data Set	Inventory (kg)	Author
WOCE	23.4 ± 2.0	This study
GEOSECS	21.1 ± 4.7	This study
GEOSECS	16.2[1]	Van Scoy et al. (1991)
GEOSECS	16.3 ± 2.4[1] to 15°N[2] 19.8 ± 3.0[1] to 10°S[2]	Broecker et al. (1986)
Long Lines	15.8[1] ± 1.6[3]	Van Scoy et al. (1991)

1. These inventory calculations were not calculated using the revised tritium half life of *Lucas and Unterweger* [2000]. Errors introduced by this will be less than 1%.
2. Error value based on the quoted error for the global ocean of ~15%.
3. Error value based on the quoted tritium sample measurement error of 10% (1σ). This is a minimum value as errors will also be introduced by the spline interpolation and spatial averaging procedures used to calculate the overall inventory.

Table 2.1. Comparison of observed North Pacific Tritium Inventories. All values are corrected to January 1st 1997.

Table 2.1 shows the calculated, decay corrected tritium inventories from the two data sets and compares them with those from earlier studies. All estimates of the North Pacific inventory calculated from datasets that pre-date the WOCE survey are smaller than the WOCE value. This is

primarily a reflection of the improved sampling of the WOCE cruises. For example the northwest subpolar and subtropical gyre regions, which have been shown to contain high water column ^{3}H inventories, were poorly sampled by the GEOSECS cruises, which may have resulted in low biases in the calculated GEOSECS inventory.

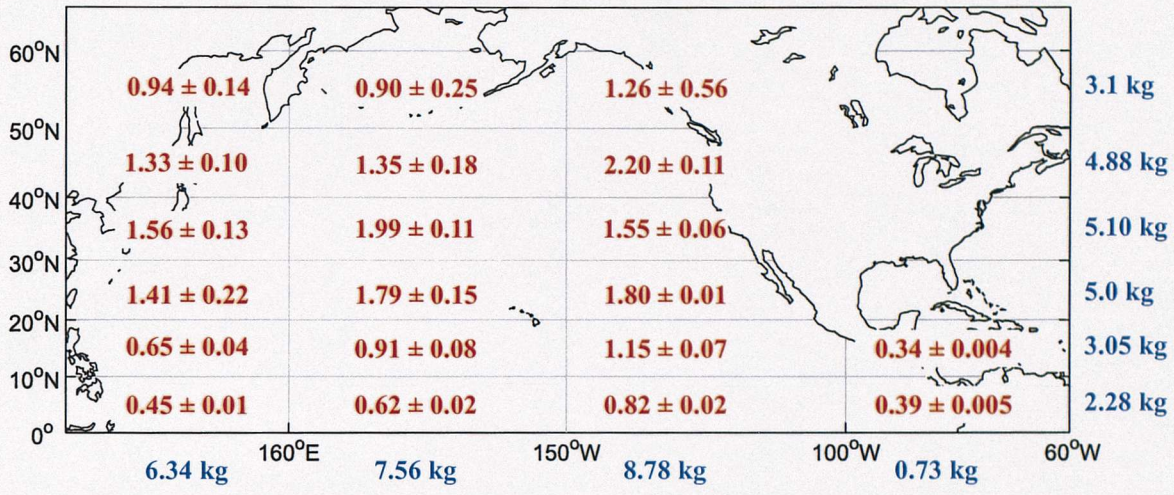

Figure 2.3. Map showing the distribution of the total depth integrated tritium inventory and the associated error in this value (one standard deviation) in each of the bins used in the calculation. The boxes represent the bins that were used to calculate the overall inventory. All values are in kg and the blue values represent the total in each 10° latitude or 50° longitude range.

Strong spatial gradients exist in the distribution of ^{3}H in the North Pacific. Latitudinal variability which reflects the location of the thermonuclear weapons tests and the location of maximum ^{3}H rainout at mid latitudes is still very evident in the WOCE distribution, even after three decades of circulation and mixing. Earlier work has highlighted the importance of good longitudinal sampling as deeper ^{3}H penetration is seen in the west of the subtropical gyre following the downward slope of isopycnals from east to west [*Fine et al.*, 1981]. Much of the finer structure of the North Pacific ^{3}H distribution will have been missed by the GEOSECS cruises as there were very few stations north of 40°N, with extremely sparse sampling in the west and north east of the basin (see Figure 2.1). The WOCE data has also highlighted the importance of better depth sampling than in earlier studies as there is clearly ^{3}H at intermediate depths in the basin that needs to be included.

The calculated value from the GEOSECS data is larger but broadly consistent with the values from *Broecker et al.* [1986] and *Van Scoy et al.*, [1991] considering the large error in the

calculated value. Direct comparisons are hard to make as the error fields are poorly defined for the earlier estimates.

The greater uncertainty in the GEOSECS value compared to the WOCE one is the result of the poorer areal resolution of the GEOSECS cruises. This means that a lot of interpolation was needed to calculate an overall inventory and the resulting uncertainty remained large.

2.3 The Changing Distribution of Tritium in the North Pacific

The larger error in the GEOSECS inventory makes it difficult to elucidate the temporal evolution of the total, decay corrected inventory for the basin, which has not changed within the errors of the measurements between the two datasets. This is in contrast to the North Atlantic, where a real increase in the ^{3}H inventory over time is seen due to Arctic inflow [*Doney et al.*, 1993]. However in the years between the two surveys, there have been significant changes both laterally and vertically in the water column distribution of ^{3}H in the North Pacific, which reflect the mean circulation of the basin.

Comparing the latitudinal distribution of the decay corrected tritium inventory in the North Pacific between GEOSECS and WOCE (Figure 2.4) shows that the majority of the ^{3}H is in the subtropical gyre (20-40° N), in good agreement with earlier studies [*Broecker et al.*, 1986; *Van Scoy et al.*, 1991]. Stronger latitudinal gradients are evident in the top 1000m of the water column in the GEOSECS data, which shows a more pronounced subtropical maximum. The loss of strong latitudinal gradients in the WOCE data is due to negligible ^{3}H entering the ocean in the intervening years coupled with continued homogenisation by circulation and mixing. This reduction was already evident by the time of the Long Lines cruises in 1983-1985 [*Van Scoy et al.*, 1991]. The latitudinal variations seen in the WOCE data are more striking deeper in the water column, especially the pronounced maximum at 40-50° N below 1000m (Figure 2.4) in comparison to the GEOSECS values which are quite low at that depth. This is clear evidence of an increase in depth penetration between the two surveys as is seen with bomb radiocarbon [*Peng et al.*, 1998].

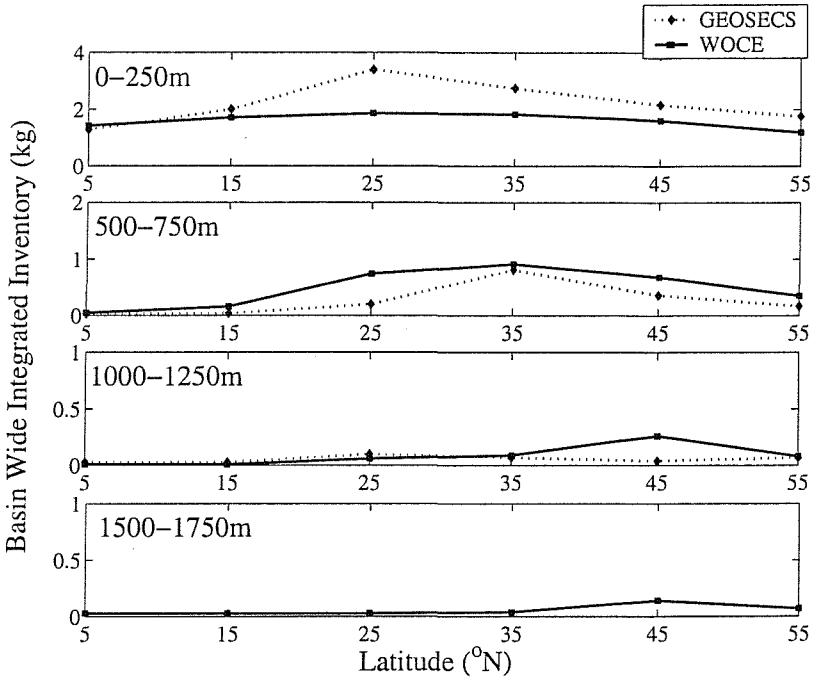

Figure 2.4. A comparison of the latitudinal distribution of ^3H from WOCE and GEOSECS data at three different depths. No ^3H data was collected from depths greater than 1500m during the GEOSECS cruises so the 1500-1750m plot only shows the distribution from the WOCE dataset. All of the inventory values presented have been decay corrected to January 1st 1997.

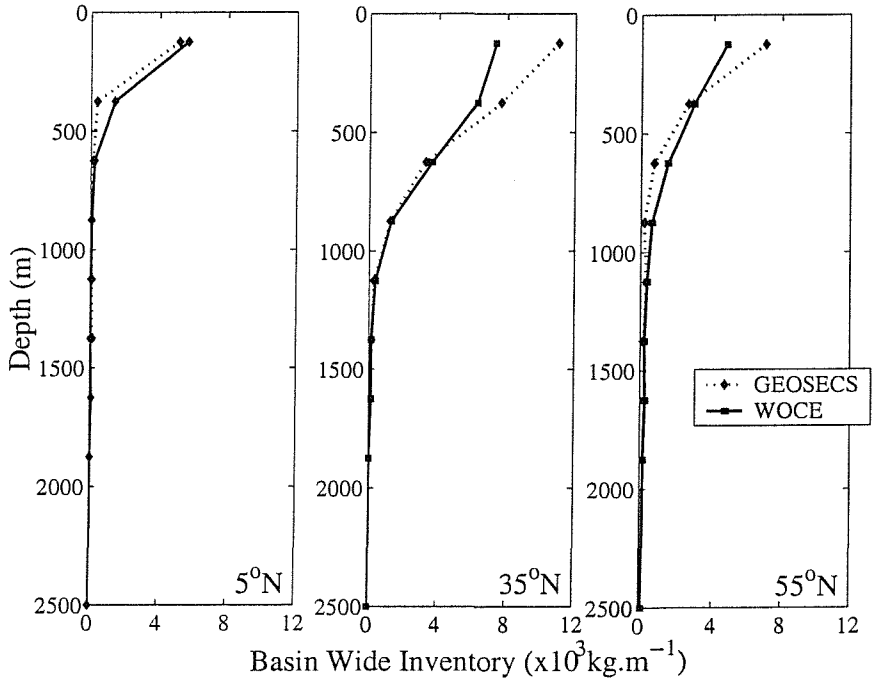

Figure 2.5. A WOCE and GEOSECS comparison of the depth distribution of ^3H in the North Pacific at three different latitudes. The inventories have all been decay corrected to January 1st 1997.

The overall depth distribution of decay corrected tritium has not changed dramatically between the two surveys, although there is deeper penetration in the WOCE data (see Figure 2.5). The highest concentrations are seen in surface waters and there is little ^{3}H below 1000m. In the WOCE data there is more ^{3}H at intermediate depths with 23% of the inventory being at depths greater than 500m compared with 11% in the GEOSECS data. The depth profile at 0-10°N shows that very little ^{3}H has penetrated below 1000m and that it is truly a shallow water phenomenon in the tropics. In contrast the profiles at 30-40° and 50-60°N show that at higher latitudes a greater proportion of the inventory is at intermediate depths, with detectable amounts of ^{3}H down to 2500 metres. Although there is a more noticeable increase in depth penetration at high latitudes, there is a larger ^{3}H inventory between 500m and 1000m for 30-40°N than at 50-60°N. This pattern reflects the location of intermediate water formation in the subpolar gyre, especially in the Sea of Okhotsk and the Bering Sea [*Warner and Roden*, 1995], and its subsequent transport to and modification within the subtropical gyre [*Talley*, 1991]

Figure 2.5 illustrates that by the time of the later survey there is an increase in the amount of tritium in surface equatorial waters and a decrease in the shallow waters of the subtropical gyre. This shift of ^{3}H from intermediate to low latitudes is the result of a Hadley cell movement of properties from the subtropics to the tropics, a shift that is also seen in bomb radiocarbon [*Key*, 1997; *Mahadevan*, 2001].

The improved estimates for the inventory and distribution of tritium in the North Pacific provided by the WOCE cruise data allows us to use the isotope to constrain circulation and total atmospheric deposition in the basin. To this end a simple multi-box model of the North Pacific is used to construct a ^{3}H budget to compare with the inventory results.

2.4 Atmospheric Tritium Deposition to the North Pacific

2.4.1 Total Atmospheric Deposition

The total atmospheric delivery of tritium to the ocean consists of three components, the precipitation flux, the downward vapour flux and finally the vapour back-flux from the ocean due to re-evaporation, such that:

$$D_{atm} = PC_P + E\frac{h}{1-h}C_V - E\frac{1}{\alpha(1-h)}C_S \qquad (2.1)$$

where E, P and h are the hydrological parameters evaporation, precipitation and relative humidity, C_P, C_V and C_S are the tritium concentrations in precipitation, vapour and surface water respectively and α is the isotopic equilibrium factor for HTO / H_2O in liquid-vapour exchange.

This relationship was proposed by *Weiss and Roether* [1980], and it has become the generally accepted model for the tritium flux to the oceans. But over recent years several areas of the analysis have been questioned [*Koster et al.*, 1989; *Memery and Wunsch*, 1990]. Investigators have assumed that ^3H concentrations in marine precipitation and vapour are in isotopic equilibrium. This assumption was based on a limited number of simultaneous observations of vapour at ships height and precipitation, which show considerable scatter [*Roether*, 1989], and allows the ^3H concentration in vapour at any time t, $C_V(t)$, to be related to that in precipitation and set equal to $\frac{1}{\alpha} C_P(t)$ or ~0.89 $C_P(t)$. It is important to consider the validity of this assumption as, particularly over the bomb spike when precipitation ^3H concentrations were high, it will have a significant effect on the total ^3H deposition. Considering Equation 2.1 it is clear that as surface water ^3H concentrations are much smaller than those in precipitation the third term represents a minor correction only. It also follows that as $E \approx P$ and $h \approx 0.75$ the input from vapour exchange should greatly exceed that from precipitation so the chosen value of the C_V / C_P ratio is critical to the total calculated ^3H deposition.

The work by *Jouzel et al.* [1987] showed that rain is never in complete isotopic equilibrium with water vapour, even at the sea surface, and that ^3H concentrations in rain are always much higher than in the surrounding water vapour. Unfortunately there is very little data to quantify the degree of isotopic equilibration, and the lack of data means that a precise constraint on the vapour deposition to the world ocean is problematic. Table 2.2 summarises the values of the C_V / C_P ratio from models and data that are presently available.

There is a significant difference between values of the C_V / C_P ratio calculated from observations and the atmospheric modelling result of *Koster et al.* [1989]. The smaller simulated value may be due to the model failing to capture an important pathway for ^3H transport within the atmosphere, as it appears that the models' downward vapour transport is too slow. Also the model had a limited representation of continental re-evaporation and did not recreate the large observed gradient between continental and marine precipitation [*Roether*, 1989]. The cloud model of *Lipps and Hemler* [1992] highlighted the importance of the treatment of ^3H transport between rainwater and vapour to model deposition ratios. In convective rain as air moves up the condensate formed at any stage falls down through the foregoing ones, mixing with other droplets and taking up new vapour as it does so [*Dansgaard*, 1964]. Therefore the downward flux of ^3H in the atmosphere is

strongly affected by the ice phase as the isotope is much freer to exchange and escape to the surrounding atmosphere from raindrops than from falling ice particles. Therefore modelling studies such as *Koster et al.* [1989] need a careful treatment of the isotopic adjustment of ^3H between rain and vapour since this process allows ^3H to escape from the raindrop and ultimately diffuse to the surface. *Lipps and Hemler* [1992] concluded that a more detailed treatment of deep convection in the *Koster et al.* [1989] GCM study would not result in a higher C_V / C_P ratio.

Source	C_V / C_P Ratio
Isotopic equilibrium	0.89
Koster et al. [1989] (Model)	0.35 ± 0.05
Weiss et al. [1979] (Data)	0.76 ± 0.05
Doney et al. [1993] using *Östlund and Mason* [1985] Miami data	0.60 ± 0.05
Doney et al. [1993] comparison of *Östlund and Mason* [1985] data with IAEA precipitation at Baring Head Lighthouse New Zealand	0.81 ± 0.03

Table 2.2. Summary of the work done to date on the relationship between the tritium concentration in water vapour (C_V) and precipitation (C_P).

In their tritium budget for the North Atlantic *Doney et al.* [1993] used a C_V / C_P ratio of 0.7 ± 0.1, which represents the mean of the values from Miami, New Zealand and the *Weiss et al.* [1979] results. The same value is used here to calculate the atmospheric delivery of ^3H to the North Pacific.

It is also important to note that the C_V / C_P ratio is unlikely to be constant and may have changed over the course of the tritium transient [*Doney et al.*, 1993]. As surface water ^3H concentrations increase relative to those in precipitation, the ratio is likely to do the same as the vapour back flux from the ocean surface becomes increasingly tritiated.

2.4.2 Precipitation

The concentration of tritium in precipitation that is needed to compute the atmospheric deposition of ^3H to the North Pacific was calculated using a global ^3H precipitation model

function. Following the work of *Doney et al.* [1992] the global distribution of ^3H in precipitation can be modelled using R-mode factor analysis.

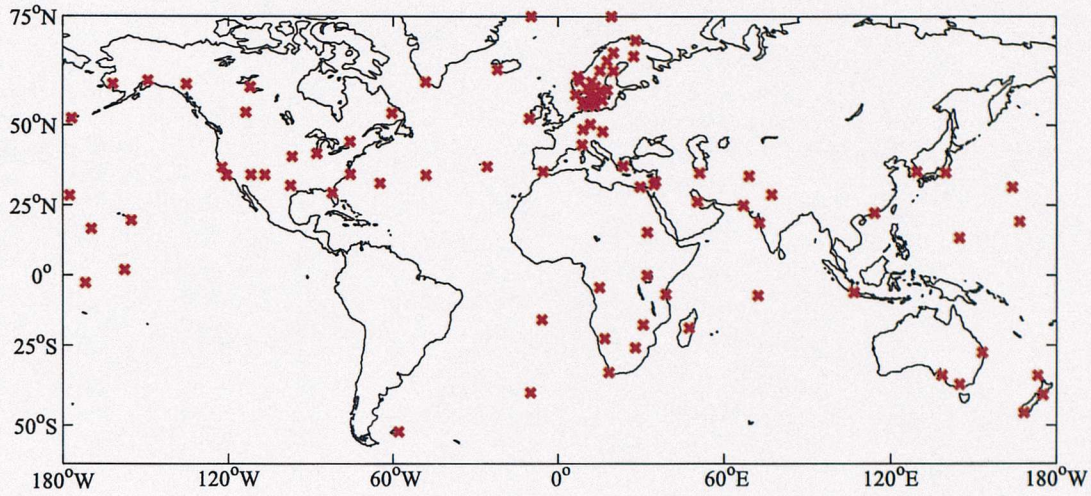

Figure 2.6. A map showing the location of the WMO/IAEA sampling stations used to construct the ^3H in precipitation model function. It is clearly visible that the majority of the stations are located on the continents in the northern hemisphere. Of the 93 sampling stations included in the model only 16 are at ocean island locations that can be termed truly oceanic.

To produce the model the WMO/IAEA tritium in precipitation data set from 1960 to 1997 was used. Data before 1960 was excluded as very little data was collected before this year. The IAEA data set is sparse in both space and time as measuring stations are unequally spaced around the globe (Figure 2.6), with few being away from the continental margins, and do not cover the same time periods at all stations. In this study only the 93 stations with at least five years of ^3H data including the major bomb transient between 1962 and 1964 were included. The aim of the model function was to construct a set of reference curves that could be used to reconstruct the ^3H time history at any location.

To account for the sparse coverage of the station data, the annually averaged tritium concentrations were zonally averaged into 10° latitude bands from 50°S to 70°N. A simple linear interpolation was used to account for areas with very sparse data. These steps resulted in zonal mean ^3H concentration data which could be represented by $C_P(t,\varphi)$, a 38x12 matrix. Building on the work of *Doney et al.* [1992] this was modelled in *R*-mode factor analysis as a linear combination of n factors such that:

$$C_P(t,\varphi) = \sum_i^n \left(\hat{c}_p(t,i) l(i,\varphi)\right) + \varepsilon(t,\varphi) \tag{2.2}$$

In Equation 2.2 $\hat{c}_p(t,i)$ is the ith vector of the factor scores (the time records from 1960 to 1997), $l(i,\varphi)$ is the ith vector of the factor loadings (the latitudinal patterns from 50°S to 70°N), and $\varepsilon(t,\varphi)$ is the error matrix.

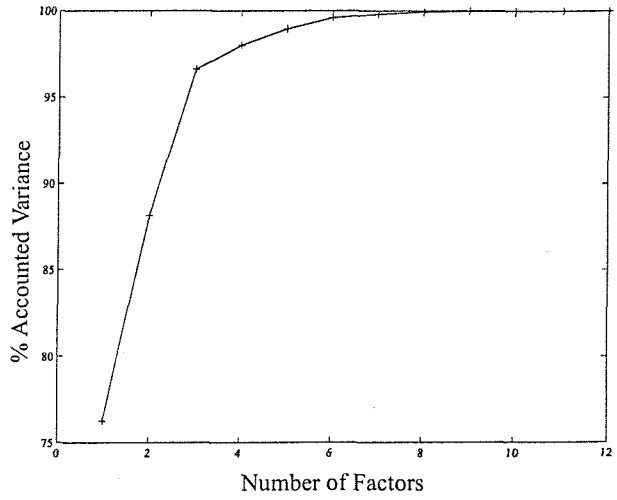

Figure 2.7. Plot of the variance accounted for versus the number of factors for the factor analysis of zonally averaged ^3H data. Including more than 3 factors did not substantially improve the performance of the model function at predicting the concentration of ^3H in precipitation.

Before doing the factor analysis, the data was standardised and normalised to have a variance of one and a mean of zero. This was done by subtracting the mean over all years from each latitude band and then dividing by the standard deviation. If this step is ignored the weaker, more diffuse southern hemisphere signal would be overwhelmed by the larger northern hemisphere spike.

The covariance matrix of $C_P(t,\varphi)$ was then solved for its eigenvectors, and the n eigenvectors with the largest eigenvalues were retained as the n factors of $C_P(t,\varphi)$. The n eigenvectors were then varimax rotated to localise the variance from each latitude band onto a smaller number of factors. As can be seen from Figure 2.7 three factors account for more than 96% of the original variance in $C_P(t,\varphi)$. Their resulting factor loadings ($l(\varphi)$) and factor scores ($\hat{c}_p(t)$) are shown in Figure 2.8.

2.4.2.1 Factor Distributions

The distribution of the factors can be explained in terms of the global hydrological cycle of tritium.

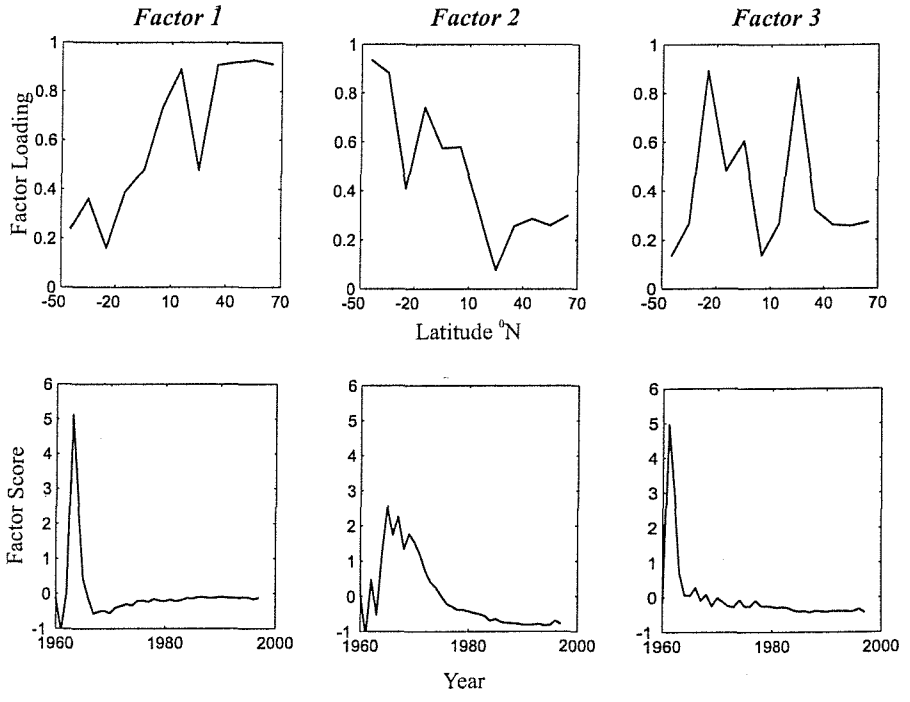

Figure 2.8. Factor loadings and factor scores calculated for the zonally averaged ^3H data with no decay correction applied.

As can be seen from Figure 2.8 the temporal and spatial distributions of the first two factors are broadly consistent with the *Doney et al.* [1992] analysis and can be interpreted as a northern hemisphere (factor 1) and a southern hemisphere (factor 2) factor. The time history of the first factor shows the expected northern hemisphere "spike" in 1963, while the second factor shows the delayed and more diffuse signal that is typical of the southern hemisphere, arising because of the slow communication between the stratospheres of the two hemispheres. The dominance of the northern hemisphere factor, which accounts for 76% of the variance in $C_P(t,\varphi)$, is a reflection of the location of the largest bomb tests in the northern hemisphere, the penetration of this signal well into the tropics, and weighting of the zonal average data set towards the northern hemisphere.

The third factor, which was not seen in the *Doney et al.* [1992] analysis shows a peak that precedes the main pulse of the first factor in 1963. This may be a reflection of tropospheric fallout occurring soon after the first bomb tests. For example debris from the Bravo Test of 1954 was rapidly removed by ice crystals formed by the large quantities of seawater carried aloft by the

bomb cloud [*Taylor*, 1966]. The deposition of ^3H to the Earth's surface is composed both of this early fallout and the delayed stratospheric component.

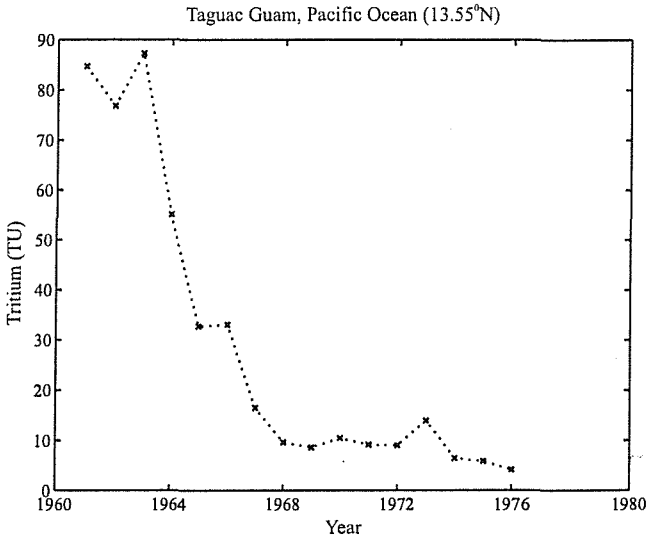

Figure 2.9. The ^3H in precipitation time history from Taguac, Guam Island in the North Pacific Ocean which clearly shows high ^3H ratios in the two years preceding the main bomb spike in 1963.

Evidence of the importance of direct, early deposition is seen in the WMO/IAEA data from Taguac, Guam. As is shown in Figure 2.9 the ^3H in precipitation records from this island in the North Pacific show high ^3H concentrations in 1961 and 1962 prior to the main, northern hemisphere peak signal in 1963.

2.4.2.2 Discussion of Model Function Performance

Using Equation 2.3, the annual mean tritium concentration at an individual station $c_P(t)$ can be calculated from a linear combination of the three reference curves $\hat{c}_P(t,1)$, $\hat{c}_P(t,2)$ and $\hat{c}_P(t,3)$ such that:

$$c_P(t) = f_0 + f_1\hat{c}_P(t,1) + f_2\hat{c}_P(t,2) + f_3\hat{c}_P(t,3) + \varepsilon_a(t) \tag{2.3}$$

The three coefficients (f_1, f_2 and f_3) and mean (f_0) are unique for each individual station and were calculated from the least squares solution of Equation 2.3. The residual error, $\varepsilon_a(t)$ represents the

mismatch between the reconstruction and the measured data at each station. For each station the standard deviation of the residuals was estimated as a measure of the goodness of the fit from Equation 2.3 such that:

$$\sigma_a = \left(\frac{1}{N-3} \sum_{i=1}^{N} \varepsilon_a{}^2 \right)^{\frac{1}{2}} \tag{2.4}$$

where N is the number of years, t_i for which there is ^{3}H data at a particular station.

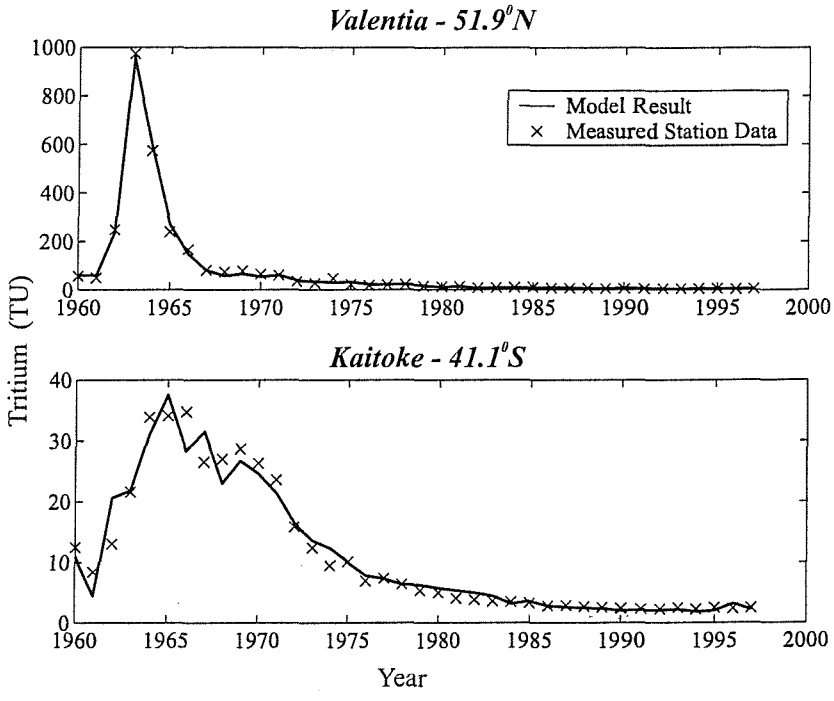

Figure 2.10. Model function performance compared with data at two different continental locations, Valentia (Ireland) and Kaitoke (New Zealand). Note the very different TU scales (no decay correction) on the two plots which is a reflection of the much higher ^{3}H in precipitation concentrations in the northern hemisphere.

The performance of the model at two key continental locations is shown in Figure 2.10. It is clear that the model recreates well the annual ^{3}H in precipitation time histories at both a northern hemisphere location (Valentia) and a southern hemisphere location (Kaitoke), each of which has a small standard deviation (9.62 TU and 2.42 TU respectively).This good model performance is typical of continental sample stations, where there is plenty of raw data. To prevent the model overestimating the ^{3}H concentration at stations with temporally sparse data after the spike, such as

Bermuda and Hawaii (see Figure 2.11), a simple linear interpolation was fitted to a typical pre-bomb concentration of 5 TU in 1997. As is shown by Figure 2.11 this allows the model to perform well at these two typical oceanic locales.

The tritium time-history at any arbitrary point on the globe can be estimated by spatially interpolating the three coefficients f_1, f_2 and f_3 for the ^{3}H reference curves derived for the individual stations and then calculating a new time-history using Equation 2.3. The coefficients for each of the 93 stations included in the model and the results of a seasonal cycle solution of Equation 2.3 are shown in Appendix 1. A number of issues arise, however, because of the sparse global sampling network, strong latitudinal gradients, and the marked transitions between oceans and land in the ^{3}H precipitation record. Of the 93 stations included in the model only 16 are truly oceanic (island), and several are in coastal locations, which are likely to move in and out of the marine boundary layer. This is a major weakness of this model function as ^{3}H concentrations in precipitation are typically 2-5 times higher over the continents than the oceans at the same latitude [*Doney et al.*, 1992]. This contrast is the result of the faster removal of HTO and larger water vapour levels over the oceans compared with the continents.

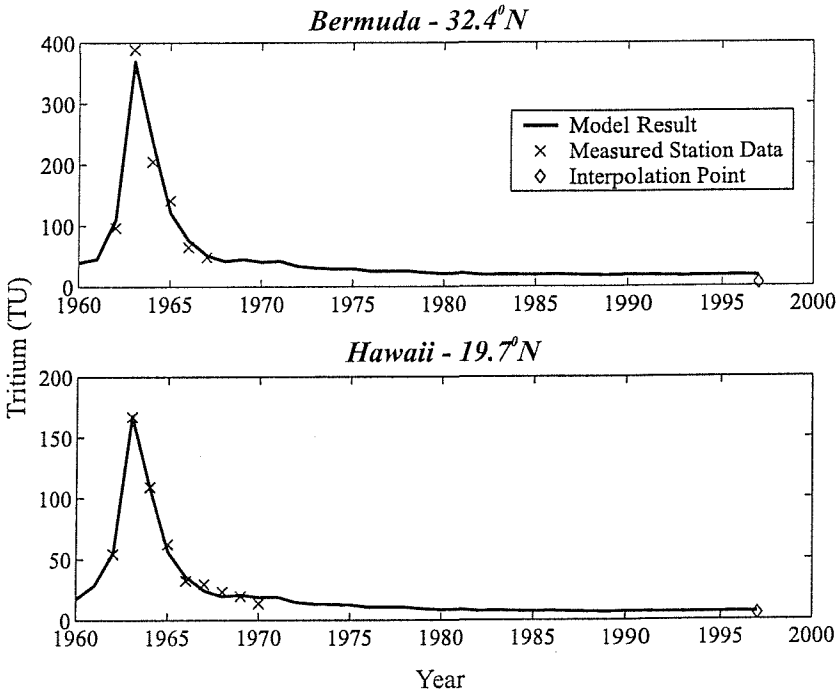

Figure 2.11. Model function performance compared with data at two oceanic locations, Bermuda (North Atlantic) and Hawaii (North Pacific). Again the two plots have different tritium scales (no decay correction) reflecting the strong latitudinal gradient of the ^{3}H concentration in precipitation. Included in the plot is the interpolation point that was used to improve model performance at locations where data is sparse.

The length scale for the continental / marine transition was estimated to be of order 1000 km [*Weiss and Roether*, 1980], but the spatially interpolated model exhibits a much broader layer due to the lack of available data from stations at oceanic locations. This effect can be corrected for by adjusting the computed $c_P(t)$ fields to take into account how far the continental ^3H signal penetrates over the oceans. In lieu of suitable ^3H data this penetration distance can be estimated from precipitable water (w) data [*Doney et al.*, 1993]. Precipitable water represents the amount of liquid water that would result if all of the water vapour in the atmosphere were condensed [*Peixoto and Oort*, 1983]. Evaporation over the oceans, especially in the subtropics, increases the precipitable water (net E-P) and lowers the water vapour ^3H concentration through dilution and ocean uptake. Hence the length-scale over which the continental ^3H signal is removed should be comparable to or less than that of the transformation of low w continental air into high w marine air [*Doney et al.*, 1993]. The transition in w extends 500-1000 km from the continents [*Prabhakara et al.*, 1982], and a length scale of 500 ± 250 km was used in the model calculations as in the *Doney et al.* [1993] North Atlantic ^3H budget. Using this length scale the precipitation input to the North Pacific was calculated by assuming that the ^3H profile falls off exponentially from the precipitation function continental end member to a minimum marine value, taken from the available WMO / IAEA oceanic station data.

The total atmospheric deposition of tritium to the North Pacific was calculated using Equation 2.1. The hydrological parameters were taken from the *Da Silva et al.* [1994] climatology, and the deposition was calculated over a 2.4° grid for the North Pacific from the equator to 60°N.

2.5 Model of the North Pacific Tritium Budget

A simple multi-box model of the circulation of the North Pacific was developed to use the calculated WOCE inventory and regional patterns to constrain the atmospheric and advective terms in the tritium budget. Once developed some of the flows in this general kinematic model were modified to match the available ^3H data.

2.5.1 Continental Runoff of Tritium to the North Pacific

The input of tritium to the North Pacific from continental runoff is very small compared with that from the atmosphere so a simple runoff scheme was deemed sufficient. The flux was calculated using the *Weiss and Roether* [1975] river model and the land precipitation ^3H concentrations C_P. *Weiss and Roether* [1975] developed the model based on the Rhine River drainage system and found that it could be represented as a series of boxes with varying residence times as shown below. In the model 25% of the river water has a residence time of a year or less,

35% has a mean residence time of 5 years with the remaining 40% being ground water containing no bomb tritium.

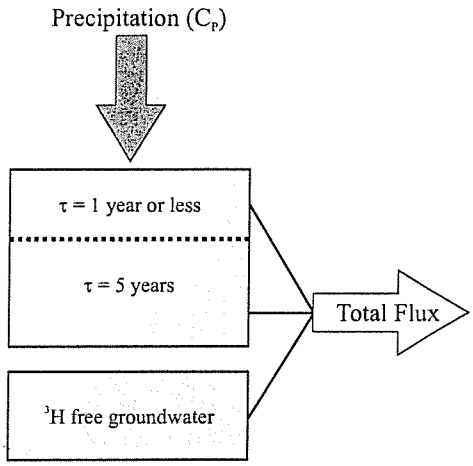

Figure 2.12. Schematic of the simple box model used to calculate the input of ^{3}H to the North Pacific from rivers.

The calculated ^{3}H time histories for the major rivers that drain into the North Pacific were multiplied by *Baumgartner and Reichel* [1975] annual runoff volumes to get annual ^{3}H runoff fluxes into each of the model boxes. The model is very simple and may only be applicable to mid-latitude rivers such as the Rhine; tropical and high latitude rivers will behave in a qualitatively different manner [*Doney et al.*, 1993]. For example high latitude rivers such as the Amur may have shorter residence times and lower groundwater contributions because of subsurface permafrost layers [*Östlund*, 1982].

2.5.2 Kinematic Model

To calculate the total atmospheric deposition of tritium to the North Pacific, a box model of the shallow circulation was used to simulate the surface water time histories needed to calculate the re-evaporation term. The basin was split into tropical, subtropical and subpolar boxes, the depth of which were chosen on the basis of observed ^{3}H distributions. The tropical box was chosen to extend to 20°N to include the North Equatorial Current (NEC), which is the northernmost current of the equatorial system flowing westward between 10° and 20°N. The subtropical box extends to 40°N beyond which constitutes the subarctic region [*Michel and Suess*, 1975], separated from the subtropical gyre by an abrupt change in temperature and salinity.

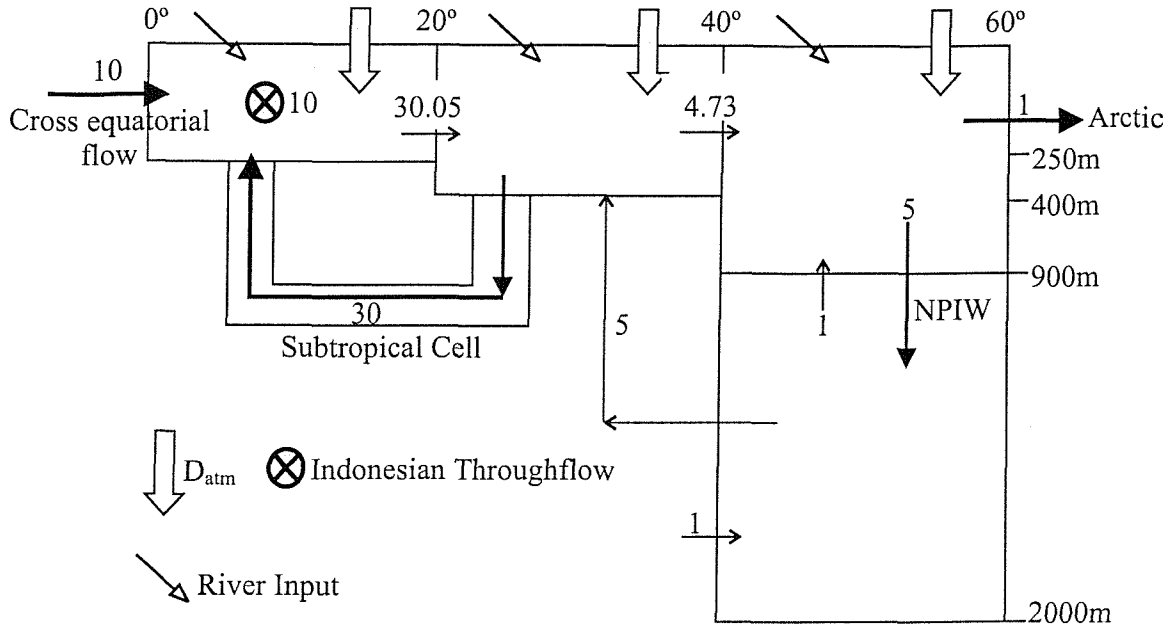

Figure 2.13. Schematic of the multi-box model of the shallow circulation of the North Pacific. All of the fluxes are in Sv (1Sv = $1x10^6 m^3.s^{-1}$) and the model was run with a time step of 0.5 years. The timescale of subtropical-tropical exchange is of order 10 years [Liu and Philander, 2001] and the model subtropical cell applies a 10 year delay to waters flowing from the subtropics to the tropics. After formation NPIW is transported to and modified within the subtropical gyre, where it is seen as a low salinity signal [Talley, 1991].

The model circulation, including all advective fluxes, is shown in Figure 2.13. An inflow of intermediate waters from the South Pacific is needed to balance the flow of North Pacific water into the Indian Ocean [*McCreary and Lu*, 2001]. To calculate the ^3H flux into the model from its southern boundary, the water flux (10 Sv) was multiplied by a time history of ^3H concentrations in the equatorial South Pacific. This time history was constructed from data from the top 250m of the water column from the WOCE, GEOSECS and RSMAS series of cruises. The northward surface flows in Figure 2.13 have been adjusted to account for the net input of mass to the basin from rivers and the balance of precipitation and evaporation.

2.5.3 Model Tritium Budget

The results of the North Pacific Budget Model are shown in Figures 2.14 and 2.15. Figure 2.14 shows the annual ^3H contribution from each of the terms in the model.

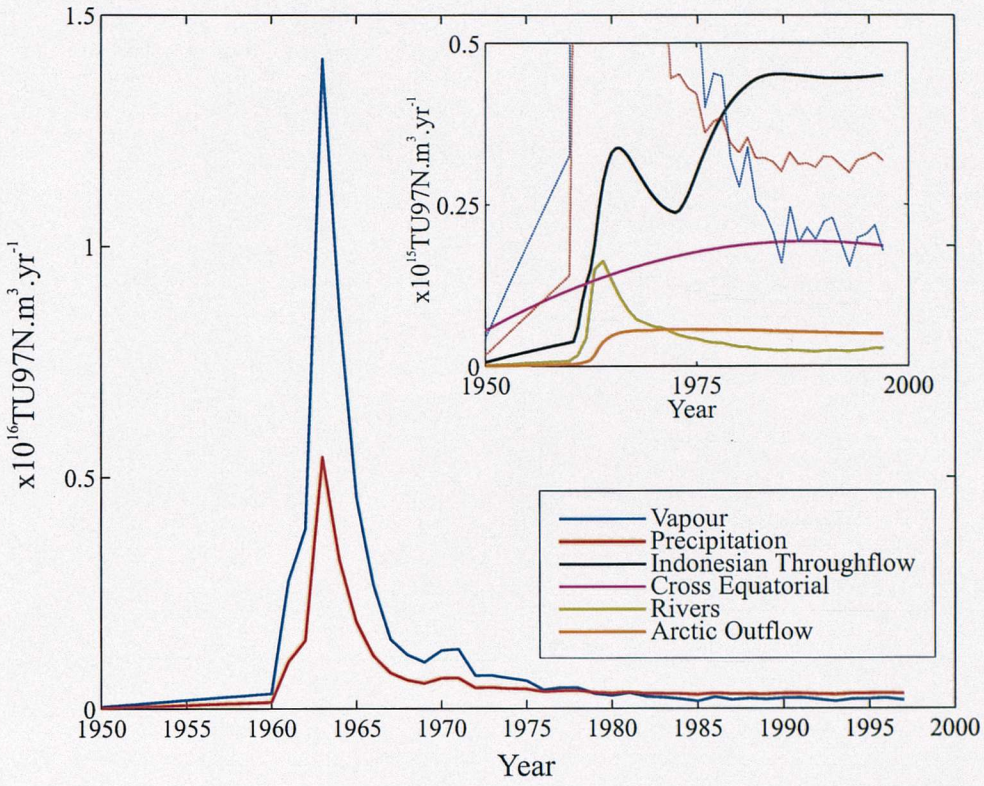

Figure 2.14. Time histories of the atmospheric deposition of ^3H to the North Pacific and each of the advective terms in the model budget. Note the different inventory scales on the two plots, which highlight the dominance of atmospheric deposition to the ^3H budget of the North Pacific. The ^3H contribution from each of the terms has been decay corrected to January 1st 1997 (TU97N). The vapour exchange curve (blue) has been corrected for the re-evaporation of HTO from the ocean surface

It is clear that the main source of bomb ^3H to the North Pacific has been atmospheric vapour deposition, which exceeds direct precipitation by a factor of two. This is consistent with earlier work [*Doney et al.*, 1993], which found that ^3H by vapour deposition exceeds that by direct precipitation by a factor of 2-5. A small ratio may be expected in the North Pacific because of its large ocean to coastline ratio, which allows evaporation from the sea surface to have a significant effect on the oceanic, near surface water vapour concentration. After 1980 deposition from direct precipitation starts to exceed the net vapour input, which reflects the growing relative importance of the vapour back flux term after the main bomb spike.

Inputs from rivers and the modelled circulation contribute over an order of magnitude less than the atmospheric deposition to the overall budget, with the loss through the Indonesian Throughflow contributing more than the other advective terms. The maximum river contribution is seen to lag the atmospheric spike as 35% of the water in the river model has a residence time of 5 years (Figure 2.12) and consequently shows a delayed and broader ^3H peak than precipitation and vapour deposition. The importance of the river contribution to the budget is minimal after the

delayed main bomb spike. The relative importance of the advective terms to the budget increases after 1975 as deposition continues to decline after the main bomb transient. In particular the Indonesian Throughflow output and cross equatorial ^{3}H input become comparable in importance to atmospheric deposition after this year.

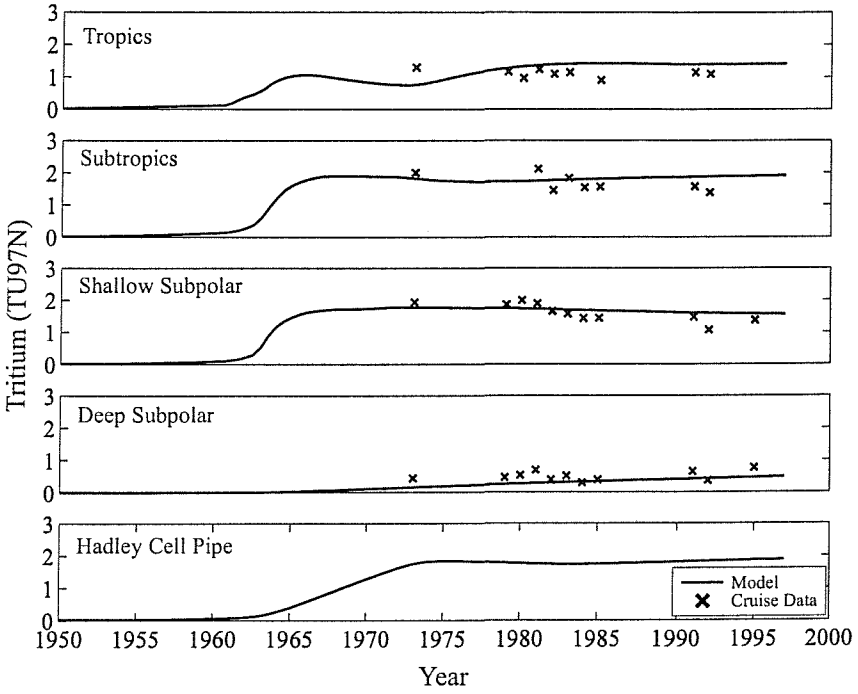

Figure 2.15. Model ^{3}H ratios for the 4 boxes in the model and the lower limb of the Hadley cell compared with cruise data. All ratios have been decay corrected to January 1st 1997 (TU97) and the value in each box is the average over the bounding boxes shown in Figure 2.12. The cruise data shown is from the WOCE, GEOSECS and RSMAS (Rosenstiel School of Marine and Atmospheric Sciences, University of Miami) cruises.

The model output can also be used to evaluate the changing distribution of ^{3}H in the North Pacific. Figure 2.15 and Table 2.3 show that the majority of the bomb ^{3}H remains in the upper ocean with the highest concentrations being seen in subtropical waters, reflecting the location of the bomb tests and of maximum stratospheric tropospheric exchange. The maximum in the surface box ^{3}H concentrations is seen to lag the atmospheric 'spike' of 1963 by two to three years, consistent with the work of *Fine and Östlund* [1977]. The increase in the amount of ^{3}H at intermediate depths in the subpolar region is a reflection of intermediate water formation. There is a net movement of ^{3}H from the subtropics to the tropics, in agreement with the WOCE observations. The model produces a double peak in the tropical box time history due to the delayed arrival of the tritium input via the subtropical cell. A delayed but weaker signal is also seen in the subtropical box due to the surface limb return flow of the Hadley cell.

The overall tritium inventory for the North Pacific calculated from the model is 25.1 ± 3.3 kg which falls within the error margins of the WOCE inventory value of 23.4 ± 2.0 kg. The error in the model inventory is derived by combining the uncertainties in each of the advective and atmospheric deposition terms in the model assuming they are uncorrelated.

Area	WOCE Inventory (kg)	Original Model (kg)	Inverse Model (kg)
Tropics	5.36	6.60	5.87
Subtropics	10.09	9.54	9.17
Subpolar Shallow	6.09	6.55	5.65
Subpolar Deep	1.90	2.46	2.43
Subpolar Total	7.99	9.01	8.08
North Pacific	23.40	25.10	23.12

Table 2.3 – A comparison of the original and inverse model inventories with those calculated from the WOCE cruise data. The inverse model is described and discussed in 2.6.

This good agreement, within errors, between the model and WOCE inventories indicates that generally the model is working well with there being a realistic amount of ^{3}H present in the North Pacific basin. It is also clear from the good broad agreement between the model and cruise concentrations in Figure 2.15 and inventories in Table 2.3 that the model produces a reasonably realistic distribution of ^{3}H in the basin. From the mid-1980s onward, the original model somewhat overestimates the concentrations and WOCE inventories in the tropical and shallow subpolar boxes by 10-20% and underestimates the levels in the deep subpolar box by a similar amount. These local discrepancies between the model and WOCE data indicate that there are some problems with the way ^{3}H is redistributed within the model basin. The error may reflect regional variability in the atmospheric deposition. Both the value of the C_V / C_P ratio and the continent-marine transition length scale may not be the same for each of the model boxes. For example in the subpolar box, where the model overestimates the inventory, there is only one oceanic station in the WMO / IAEA precipitation data set north of 40°N which is located at the edge of the marine boundary layer and therefore may not be truly representative of open ocean conditions.

Alternatively the ^{3}H distribution may be reflecting errors in the models circulation. The overestimation of the tropical inventory coupled with the underestimation of that in the

subtropical box could be evidence of an overly vigorous Hadley cell or weak Indonesian Throughflow in the model. Likewise the overestimation in the deep subpolar box could reflect an unrealistic representation of the formation and modification of NPIW. The sensitivity of the model to each of these terms is further explored using inverse techniques.

2.6 Inverse Calculation

The sensitivity of the model to each of the major advective and atmospheric terms was explored using an inverse calculation. The prime objective of the inverse was to improve the model's total and regional distribution of ^{3}H. The system is over-determined and poorly conditioned, and therefore the parameters were determined in a least squares fashion. The constraints for the inverse were the WOCE regional inventory values as this captures all of the information available for the WOCE period, namely the total inventory and regional distribution.

The control variables for the calculation were the atmospheric deposition (namely the C_V / C_P ratio) and the advective fluxes (Table 2.4). The cost function reads:

$$J = \left(I_{R\mathrm{mod}} - I_{Robs}\right)^T R_I^{-1}\left(I_{R\mathrm{mod}} - I_{Robs}\right)$$

$$+\left(P_{\mathrm{mod}} - P_{obs}\right)^T R_P^{-1}\left(P_{\mathrm{mod}} - P_{obs}\right) \qquad (2.5)$$

where I_{Rmod} and I_{Robs} are vectors of the modelled and observed regional inventories, P_{mod} and P_{obs} are vectors of the initial and optimised control parameters and R_I and R_P are the covariance matrices for the inventories and control parameters respectively. In minimising Equation 2.5, it was assumed that the individual inventory observations and the control parameters are all uncorrelated, and thus R_I and R_P are simple diagonal matrices. The diagonal terms in the covariance matrices are the variances in each of the inventories and control parameters. As the overall error in the WOCE North Pacific inventory is approximately 10% (Table 2.1) a 10% uncertainty in each of the regional inventory values was assumed in Equation 2.5. Mass was conserved at all times as model mass balance was calculated at each iteration during the inversion. Equation 2.5 was minimised using a multi-dimensional unconstrained non-linear minimisation approach (MATLAB™ *fminsearch*), which is a Nelder-Mead type scheme. The first guess at each of the parameter values (x_0) were those used in the original model run and are given, along with

their associated uncertainty in Table 2.4. An additional constraint was also placed on the C_V / C_P ratio to prevent it from exceeding the isotopic equilibrium value of 0.89.

Parameter	x_0	Optimal Value	Range (16 runs)
C_V / C_P	0.7 ± 0.1	0.67	0.60 – 0.74
Indonesian Throughflow	10 ± 10 Sv	15.8 Sv	10.6 – 19.1 Sv
Subduction rate	30 ± 5 Sv	26.4 Sv	20.9 – 28.8 Sv
Subduction timescale	10 ± 2 years	9 years	8 – 10 years
NPIW	5 ± 5 Sv	5.5 Sv	4.9 – 6.3 Sv
Arctic outflow	1 ± 0.2 Sv	1.0 Sv	1.00 – 1.01 Sv
NPIW outflow	5 ± 2 Sv	5.7 Sv	4.5 – 7.0 Sv
J	8.18	3.17	1.10 – 10.64

Table 2.4. The results of the inverse calculation showing the optimised value for each of the terms in the model and the reduction in the cost function, J, by the optimisation. The range of optimal values shown in the third column is the result of the second Monte Carlo Analysis where I_{Robs} was randomly perturbed to see how well the model and data can constrain the deposition and circulation terms.

2.6.1 Stability of the Solution

The cost function surface was explored in three ways to assess the stability of the solution. First the values of x_0, the initial guess of the parameter values were varied from $0.1x_o$ to $10x_{0,}$ which did not change the value of J or the optimal values of the control parameters. Secondly a simple Monte Carlo analysis was done where the starting point was perturbed using a set of Gaussian distributed random values. The values, generated using the MATLAB™ *randn* function, had a mean of zero and a standard deviation which was set as equal to the uncertainty in each term (Table 2.4). All optimisations with these randomly generated perturbations yielded the same values for both the control parameters and the cost function, J. The robustness of the minimisation under these two tests led to the conclusion that the solution is stable and indicates that the minimisation scheme has not found a local minimum.

Finally a second Monte Carlo analysis was performed to assess the robustness of the optimal parameters and determine how well the combination of the multi-box model and WOCE data is constraining them. To do this the WOCE regional inventories, I_{Robs}, were randomly perturbed,

again using a set of Gaussian distributed random values, this time with a mean of zero and standard deviation set to 10% of the inventory values, the uncertainty in the WOCE regional ^{3}H inventories. The results of 16 such randomly generated analyses are shown in Table 2.4 and show that the values of the control parameters vary by up to 30% depending on the inventories used, with only the magnitude of the Arctic outflow being unaffected. This implies that to further constrain atmospheric deposition and North Pacific circulation using ^{3}H data the ^{3}H inventory and distribution within this ocean needs to be better constrained. The tight constraint on the Arctic outflow may indicate that small changes in its value have a significant impact on the inventory in the subpolar surface box, which as is discussed below is not recreated well by the model.

2.6.2 Results of the Inverse Solution

The inventory values presented in Table 2.3 indicate that the minimisation has improved the agreement between the model and the WOCE data, as is borne out by the reduction in the value of the cost function (Table 2.4). The overall inventory for the basin produced by the optimisation is in very close agreement with the calculated WOCE value (23.12 kg compared with the WOCE value of 23.40 kg) and regionally the ^{3}H distribution is also improved. The tropical and total subpolar inventories are now within 10% of the WOCE values which was not true of the original model run. However, looking at the depth distribution in the subpolar boxes indicates that although the optimisation improves the agreement with the data the inventory in the deep box is still overestimated. This indicates that the model may not be capable of recreating the WOCE ^{3}H distribution north of 40°N and that some aspect of the circulation in the basin is not being represented. It may be the lack of intermediate depth circulation at subtropical and tropical latitudes that is causing the model to have difficulty replicating the ^{3}H distribution, as it is assumed that water only flows from intermediate subpolar depths to the subtropical surface box.

The optimal vales of the model parameters are presented in Table 2.4, which shows that they all fall within the range of literature estimates, highlighting tritium's ability to constrain circulation. It is clear that the overall inventory requires a C_V / C_P ratio of around 0.67 (range 0.60 – 0.74) which is less than isotopic equilibrium but certainly not as small as was indicated by the *Koster et al.* [1989] modelling work. Similar results were found for the North Atlantic [*Doney et al.*, 1993]. The observed ^{3}H inventories for these two basins are simply too large to be supported mainly by direct precipitation input and thus require a substantial vapour transport pathway as river input and ocean lateral transport are insufficient to make up the difference. This discrepancy emphasises the need for a more thorough examination of the isotopic transport pathways for liquid and vapour forms of water in the atmosphere.

The inverse model simulations tend to indicate an Indonesian Throughflow on the higher end of observation based estimates, which is likely driven by the model in an attempt to lower the excess ^{3}H inventory in the tropics. It is somewhat striking that the ^{3}H based estimate of the throughflow by *Fine* [1985] is, in contrast, at the lower end of the observational range (~5 Sv). If that number is believable then either the ^{3}H deposition is poorly represented in the tropics or another mechanism, such as the subtropical cell, is required to decrease the tropical budget.

2.6.2.1 Sensitivity to Southern Hemisphere Inflow

The sensitivity of the model budget was further explored by allowing the concentration of the water flowing across the equator from the southern hemisphere to vary. It was seen that varying the ^{3}H concentrations from 0.25 to 4 times the original values only affected the inventory in the tropical and subtropical boxes. Increasing the concentrations caused the total inventory and that in the subtropical and tropical boxes to increase, the reverse being seen when the concentration of inflowing water was decreased. However even reducing the values by 75% does not prevent the model from overestimating the tropical box and the overall North Pacific inventory. In conclusion the results are relatively insensitive to the magnitude of these concentrations.

2.6.2.2 Mixing Experiments

As a final assessment of the performance of the model some simple mixing experiments were carried out to simulate a reverse exchange or eddy flux at the boundary between the surface boxes. Doing this allows the waters of the surface boxes to mix and may be a more realistic simulation of the behaviour of the oceans. These eddy fluxes were included as surface fluxes flowing south and the northward flows in Figure 2.13 were adjusted so that the net mass balance was always maintained. Including a mixing term at the boundary between the tropical and subtropical and between the subtropical and shallow subpolar boxes had absolutely no effect on the results, even if the mixing was made unrealistically large. Therefore the simple approach of excluding horizontal mixing was justified in this case.

2.7 Summary

In this chapter tritium data from the WOCE series of cruises was used to construct improved basin-scale and regional ^{3}H inventories for the North Pacific. These were then used as constraints to develop a budgetary model of the basin to explain the evolving ^{3}H distribution for this ocean. To achieve this, an improved precipitation function was constructed and both this and the budgetary model performed well when compared with the available observations. In calculating

the precipitation function a third factor emerged that was not seen in the *Doney et al.* [1992] analysis, the temporal evolution of which highlighted the importance of direct ^3H deposition at the time of the thermonuclear weapons tests. As with earlier calculations [*Doney et al.*, 1993] the uncertainty associated with the atmospheric deposition of ^3H to the oceans is the greatest weakness of the model. The relationship between the ^3H concentration in water vapour and precipitation remains problematic, as does the air-sea vapour flux and the length scale of the continent-marine transition.

The unadjusted ^3H budget model overestimates the basin inventory based on the WOCE data by ~7%, but this error is well within the uncertainty of the atmospheric deposition. The solution of an inverse calculation highlights that despite the uncertainty in the atmospheric deposition terms it is possible to put constraints on circulation using ^3H data. However for tighter constraints to be placed on circulation terms it would be necessary to have a better spatial knowledge of ^3H in the North Pacific to reduce the errors in the estimated inventories.

The lack of oceanic tritium in precipitation data, the limited data available on the C_V / C_P ratio and the continent – marine transition length scale are likely to be the main sources of model error. It is clear that these factors limit the usefulness of ^3H in constraining and testing circulation and ocean models at present, as is highlighted by the model's difficulty in reproducing the depth partitioning of ^3H at high latitudes. Without more knowledge about these terms high resolution model ^3H simulations should be treated with care, though a GCM run could provide a far more detailed spatial structure of ^3H in the North Pacific, or any other basin, than was possible in this work. To optimise the use of ^3H in such roles, for which the isotope could be very useful due to the large number of measurements made as part of the WOCE program, it is essential to improve the surface boundary condition and in particular the C_V / C_P ratio. To improve the knowledge of the C_V / C_P ratio there either needs to be a detailed field study of ^3H concentrations in maritime air masses or a high resolution atmospheric model of vapour transport in the atmosphere needs to be run.

However it is possible that the lack of oceanic ^3H in precipitation data may be improved in the future. Tritium bound in the cellulose of tree rings at oceanic islands has the potential to provide a record of past precipitation which could be used to improve the isotopes surface boundary condition. Such reconstructions have been done for deuterium (^2H) and a strong correlation has been found between the cellulose deuterium concentrations and those of their associated waters [*Epstein et al.*, 1976; *Schiegl*, 1974]. In such reconstructions the precipitation signal can be complicated by that from groundwater, vapour and fractionation during biosynthesis. However a careful choice of tree and study of the fractionation steps involved should allow precipitation ^3H

reconstructions to be made. The remainder of this thesis focuses on developing a technique to make such reconstructions, which have not been done before for low level ^{3}H measurements. In the next chapter there is a detailed description of the method developed to reconstruct ^{3}H measurements from tree rings, including a new rapid technique to extract cellulose, and a method to minimise contamination in the final measurement. In Chapter 4 this technique is tested and results are presented from Valentia, Ireland where there is a complete record of ^{3}H in precipitation to compare the tree ring record to. With the information that this technique has the potential to provide, ^{3}H could become a very powerful tool to study circulation and constrain general circulation models.

3. Development of a Method for Preparation of Tree Ring Cellulose for Tritium Measurement

3.1 Introduction

The usefulness of climatic reconstructions from isotopic studies of tree ring cellulose is well documented [*Schiegl*, 1974; *Lawrence and White*, 1984; *Tang et al.*, 2000]. Additionally we can improve knowledge of tritium deposition to the oceans using reconstructions of ^{3}H concentrations in precipitation based on tree ring data at oceanic islands. As there have been few attempts to measure ^{3}H in tree rings, a time series from Valentia, Ireland has been compared with the ^{3}H in precipitation records from the Valentia weather station. However, studies have shown that individual fractions of plant matter have very different isotopic signatures. For example the lignin in *Pinus radiata* is more than 50‰ depleted in deuterium with respect to cellulose while the other extractives are depleted by more than 100‰ [*Grinsted and Wilson*, 1979]. It is for this reason that chemical data from wood is typically derived from cellulose which is chemically stable and physiologically sensitive to environmental changes [*Sheu and Chiu*, 1995]. Cellulosic compounds are also relatively immobile and remain confined to the growth ring in which they were formed [*Leavitt and Danzer*, 1993] whereas whole wood contains some mobile compounds which can cross ring boundaries smearing isotopic signals.

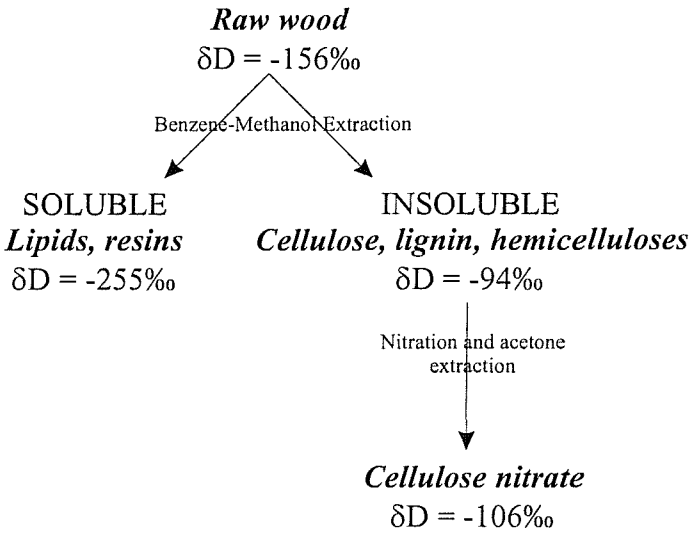

Figure 3.1. Schematic of the deuterium content of different fractions of whole wood, highlighting the importance of making isotopic measurements on cellulose (or cellulose nitrate) for climatic reconstructions. The deuterium measurements were made on rings from the years 1561-1576 from a Bristlecone Pine from the White Mountains of California. Adapted from Epstein et al. [1976].

Cellulose is a polysaccharide common to all plant materials and is composed of individual molecules that are 3-5μm long. A single molecule of cellulose is a linear polymer of 1,4-β-D-glucose, the empirical formula for which is $C_6H_{10}O_5$ [*Percival*, 1962]. It should be noted that although pure cellulose is composed only of linked glucose units it is not possible to extract and isolate pure cellulose from whole wood. The term α-cellulose is used to describe the predominantly cellulosic fraction that can be extracted from whole wood. Along with cellulose there are commonly traces of xylose and other sugars. Pure α-cellulose is white and any remaining sugars and lignins produce a product with a characteristic yellow colouring. The importance of extracting pure cellulose for climatic reconstructions is highlighted by Figure 3.1 which shows the deuterium signal from different fractions of wood from a Californian Bristlecone Pine. It is clear that even trace amounts of impurities will significantly affect the final isotopic signal seen.

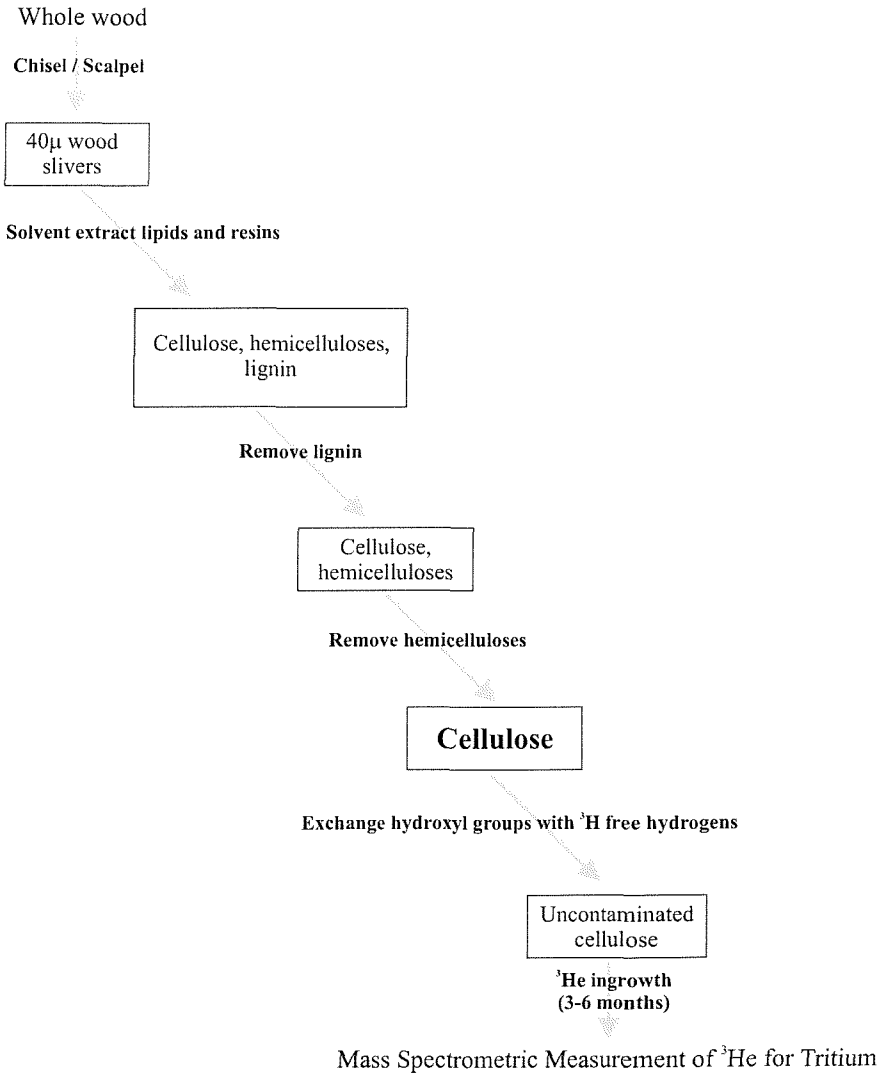

Figure 3.2. Flow chart of the stages involved in the preparation of tree ring samples for tritium analysis.

All of the stages involved in extracting cellulose needed for the reconstruction of ^{3}H time series from tree rings are shown in Figure 3.2. This chapter outlines all of the methods that have been used to reconstruct ^{3}H time series from tree rings starting with the initial extraction stage and finishing with the final mass spectrometric measurement.

3.2 Cellulose Extraction

Assessing α-cellulose purity by colour has been routine in the literature with the review of cellulose extraction procedures by *Sheu and Chiu* [1995] concluding that extraction in a benzene-ethanol Soxhlet followed by lignin removal "consistently gave extracted cellulose of whiter appearance". In the method development that follows purity will again be assessed in this way with products being compared to a white surface in natural light.

3.2.1 Cellulose Extraction from Hardwoods

Broadly wood is termed as either 'hard' or 'soft' with hardwood being from *Angiospermae* which are trees with encased seeds, such as oak. In contrast softwoods are *Gymnospermae* which have naked seeds and are of the order conifer. Chemically softwoods contain higher concentrations of lipids, resins and hydrocarbons than hardwoods, which necessitates an extra solvent extraction stage to isolate α-cellulose (see Figure 3.2).

The extraction of α-cellulose from hardwoods is relatively simple due to the low concentrations of lipids and other resinous materials. Cellulose was routinely extracted in the current work from oak wood following the procedure of *Loader et al.* [1997], which is a modified version of the sodium chlorite delignification technique of *Green* [1963]. Using this method lignin is dissolved and removed from wood slivers by repeated chlorine bleaching treatments using a combination of sodium chlorite and glacial acetic acid. Hemicelluloses, which are non-glucan polysaccharides [*Gray and Song*, 1984] are then removed from the white residue by treating it with a base (sequentially 10% and 17% NaOH) leaving behind a relatively pure cellulose product [*Hedges*, 1990]. Full details of the method are given in Appendix 2.

3.2.2 Cellulose Extraction from Softwoods

The extraction of cellulose from softwoods is a lengthy process that has traditionally involved an initial multi-day Soxhlet extraction stage to remove lipids, oils and resins. The most commonly used solvent systems for such extractions are an azeotropic mixture of benzene and methanol [*Epstein et al.*, 1976; *Sheu and Chiu*, 1995], a 2:1 toluene-methylated spirit azeotrope [*Loader et al.*, 1997] and a 2:1 mixture of toluene and ethanol [*Leavitt and Danzer*, 1993]. It was noted by

Green [1963] that extraction time will vary depending on the nature of the sample being analysed but 12-24 hours is typical.

Soxhlet extraction has been used for many years to remove solvent soluble material from solid matrices. The sample is placed in a permeable glass thimble and the extractor is constructed so that as the solvent is heated from below by a hot plate or heating mantle the vapour rises, cools, condenses and falls into the thimble. Once the thimble is full a siphon tube removes the solvent taking it back to the flask of boiling solvent and this cycle is repeated over many hours. This method has many disadvantages:

1. Once the solvent reaches the sample it has cooled and condensed so is no longer at boiling point.
2. Large volumes of solvent are required.
3. Extraction takes up to 24 hours, or longer in some cases.
4. There is often a less than complete extraction.

Here the motivation to find a new technique was the difficulty in obtaining a good □-cellulose product with no colouration from cedar wood using the Soxhlet approach. The main focus of this work was to see if the ^{3}H signal recorded in tree rings reflected ambient precipitation. To this end a ^{3}H time series reconstructed from the cellulose of an Irish cedar tree was compared with the ^{3}H data from the Valentia weather station. Wood from a cedar tree was used as this was the only tree sample available with wide enough rings to provide the large amounts of material needed for low level ^{3}H analysis. The more abundant Irish oak trees typically had rings which were too thin to sub-sample (<1mm) and would not provide enough wood for the analysis. As cedar is a softwood it contains a significant amount of resinous material that must be removed. Two solvent systems were tried with the conventional Soxhlet system:

1. The classic 24 hour benzene-methanol extraction followed by a further 24 hour acetone extraction.
2. A scheme comprising a 24 hour 2:1 chloroform-ethanol extraction, followed by ethanol alone for 24 hours and finally a 24 hour water extraction.

For both procedures cedar samples were cut into thin (~40μm) slivers using a chisel and scalpel and for each extraction 2g of wood was placed in a borosilicate Soxhlet extraction thimble. Each

extraction stage was carried out by placing 250ml of the relevant solvent into the reservoir flask and running the Soxhlet for 24 hours. After shutdown and cooling samples were removed from the Soxhlet and rinsed twice with the next solvent to be used before the following extraction was carried out. Once all extraction stages were complete the sample was transferred from the Soxhlet thimble to an Erlenmeyer flask and allowed to dry before the final delignification step (see section 3.2.1). At the end of both procedures the wood slivers appeared slightly paler but retained their overall structure. In this study after the initial solvent extraction stage α-cellulose was retrieved using the same sodium chlorite oxidation procedure that was used for hardwoods and which is outlined in Appendix 2.

Unfortunately samples extracted using these procedures were all strongly discoloured and no improvement was seen by increasing extraction times to 48 hours even with the injection of fresh solvents after the first 24 hour period. Finally the two solvent systems were combined as chloroform and benzene are likely to extract very different compounds. However this also did not yield a good product. The impurity of the product, long extraction times and large amount of solvent being used made finding a new, more rapid technique highly desirable.

3.2.3 Microwave Assisted Extraction

Microwave energy has been used to enhance chemical digestions since 1975 [*Richter et al.*, 2001] and *Ganzler et al.* [1986] reported the first use of microwave technology for the extraction of organic compounds from soils and plants. By the early 1980s the use of closed vessels had allowed higher pressures and temperatures to be achieved resulting in greatly reduced reaction times.

Comparisons between this and traditional techniques have been made [*Ganzler and Salgo*, 1987; *Lopez-Avila et al.*, 1994] and have shown that microwave methods give an improved yield and better protection of the compounds to be analysed. The main disadvantages of Soxhlet extraction (variable extraction efficiency, time consuming, solvent volume and solvent temperature) are mainly eliminated by microwave extraction techniques. The ability to precisely control temperature makes the technique more reproducible and costs tend to be lower due to the smaller solvent volumes required.

Traditional methods such as Soxhlet extraction depend on conductive heating which is slow. In contrast microwave extractions work by heating polar solvents and sample with microwave energy. It is a cold *in situ* process only producing heat when the solution absorbs the microwave energy [*Richter et al.*, 2001].

Microwave energy is a non-ionising radiation which causes motion by ion migration and dipole rotation, without affecting molecular structure. The electric field causes the sample and solution molecules to align with the field, which is known as dipole rotation. The applied electric field oscillates, forcing the aligned molecules to move and the solution is heated by the resulting friction [*Richter et al.*, 2001]. Domestic microwaves have a frequency of 2450 MHz and the molecular alignment and return to thermal disorder occurs 4.9×10^9 times per second causing rapid heating [*Jones Williams*, 1997]. Heating is also caused by ionic conductance whereby ions migrate according to the polarity of the electromagnetic field. In this mechanism heating is the result of the accelerated ions meeting resistance to their flow. These two mechanisms lead to greatly improved extraction efficiency as the instant uptake of radiation throughout the solution heats much faster than conduction. Using sealed vessels also allows a greater boiling point to be reached than is possible at atmospheric pressure. Polar solvents such as acetone and dichloromethane are heated to around 100°C above their atmospheric boiling points [*Barnabas et al.*, 1995]. In conclusion it is this combination of rapid heating and elevated reaction temperatures that greatly increase extraction efficiency and reduces extraction times. *Fischer* [1986] found that using microwave energy reduced the sample preparation time for isotope dilution analysis of trace metals by approximately 80%, in a variety of geological matrices. The intense internal heating and the effects of differential polarisation may also generate enough mechanical stress to rupture the surface layers of the sample exposing new layers to solvent attack [*Fischer*, 1986]. This process may lead to a faster and more complete extraction than is possible in a Soxhlet.

The nature of the solvent system used dictates the polarisability of the solvent molecules. For any given frequency the heating is more rapid the greater the relative permittivity of the solution as more thermal energy will be released [*Barnabas et al.*, 1995]. Non-polar solvents such as benzene and hexane which have low relative permittivities are unaffected by microwave energy and require the addition of a polar solvent to be used in microwave digestions.

In the following sections a new technique is presented which replaces the multi-day Soxhlet stage in the extraction of α-cellulose from whole wood with a microwave extraction procedure that takes only three hours. The technique was developed using cedar wood from Tollymore Forest Park in Northern Ireland and samples were routinely extracted for subsequent helium ingrowth and ^3H analysis. Cedar wood was a good choice for the development of a new technique as it contains large quantities of resinous and other natural compounds, and is therefore a rigorous test of the extraction efficiency of the method.

3.2.4 Microwave System

All extractions were carried out in a 650W MDS-2000 microwave sample preparation system (CEM Corp., Matthews, NC). This systems allows the temperature and pressure of the reaction to be both monitored, and controlled by varying the magnetron output. To monitor and control pressure, tubing is attached to one sample vessel (the control vessel) which is routed outside the microwave and connected to the pressure sensing transducer in the base of the system. Temperature is controlled via a microwave transparent fibre optic temperature probe which has a phosphor temperature sensor tip that is inserted into the control vessel. Maximum temperature and pressure settings can be programmed into each heating stage and microwave power is cut when either of these is reached. The microwave process will then resume when the temperature or pressure falls to acceptable levels. This is an essential safety feature that is, however, not called upon during routine operation of the microwave system.

3.2.4.1 Apparent Power Output

As the energy output from a magnetron varies with age and usage it is important to consider the instrument's Apparent Power Output (APO). This parameter needs to be calculated and regularly monitored to ensure consistent extraction conditions are used. The APO of the MDS-2000 system was calculated by measuring the temperature increase of a known volume of distilled water that was heated for 2 minutes at full power. The temperature before and after heating was measured after stirring to homogenise the water. The temperature change of the water was used to calculate the Actual Power Absorbed by the sample (APA), which was assumed to equal the APO using the following relationship:

$$APA = \frac{C_P K \Delta T m}{t} \tag{3.1}$$

where Δt is the temperature change, m the mass of water, t the time, C_P the thermal capacity of water (0.99869 at 21°C) and K, which is equal to 4.184, converts from thermochemical calories to watts.

Using Equation 3.1 the APO of the MDS-2000 was determined to be 542.0 ± 24.2 W (10 runs) so the magnetron was operating at 83% of its rated output of 650W. Regular monitoring of the machines APO is necessary to ensure that consistent extraction conditions are maintained.

3.2.5 Extraction Vessels

The major risk in microwave extractions is the over-pressurisation of the vessels leading to vessel failure and the leakage of solvent fumes into the microwave cavity. This puts the operator of the instrument in danger and will also significantly shorten the lifespan of the machine. In this work flammable solvents such as benzene and ethanol were used which could lead to a potentially explosive situation if solvent vapours were to leak from the vessels. The carcinogenic nature of benzene further necessitates the careful choice of appropriate vessels.

During the initial development of the technique microwave extractions were carried out in vessels manufactured by Savillex® Corporation in the United States. The vessels were rated to a pressure of 150psi, had a capacity of 120ml and were fitted with an internal spring in the cap. If the pressure within the vessel exceeded the maximum the internal spring in the cap moved upwards opening the exhaust aperture thus releasing the pressure by venting. Once the pressure was released the spring would return to its original position and the extraction could continue. However these vessels were found to be unreliable and vented frequently, sometimes within 30 seconds of the onset of heating. Comprehensive testing of the vessels by heating 10ml of water and 1g of wood slivers for 15 minutes at 15% power showed that the vessels behaviour and ability to hold pressure changed with use. A vessel that had coped with a heating cycle would often vent when exposed to the same conditions at a later date. The onset of venting within a minute of the start of a heating cycle led to the conclusion that not all of the vessels could actually hold the pressure to which they were rated. It must be stressed though that this is a purely qualitative conclusion as there is no way to monitor either pressure or temperature with this system. The springs in the caps of the vessels that were proving problematic were subjected to mechanical tests which showed that individual springs had very different strengths and many did not obey Hooke's Law. It was concluded that the unreliable and changing nature of these vessels was prohibitively dangerous for the extractions due to the explosive and toxic nature of the solvents used (benzene, methanol, chloroform, acetone and ethanol). It was decided to change to vessels and a microwaving system where the temperature and pressure within the vessels could be directly monitored and controlled.

All subsequent extractions were carried out in CEM Advanced Composite Vessels which have a Teflon© PFA body and a composite sleeve. These materials are microwave transparent which allows the vessel contents to absorb the maximum amount of the incident microwave energy. The seal on the vessels between the base and the cap is provided by the external threaded polyetherimide locking rings which are screwed together to hand tightness. As the vessels are heated the expansion of the vessel liner ensures that a good seal is made. However it was found that when low boiling point solvents such as chloroform and benzene were used a good seal was

not formed indicating that the vessel was not hot enough to expand sufficiently to make a good seal. This was rapidly evident as the polyetherimide caps were attacked by the leaking solvents and quickly damaged.

Replacement caps were manufactured at the Southampton Oceanography Centre from Teflon© PTFE which is chemically inert and microwave transparent. The use of Teflon© PTFE for vessels caps has to be approached with some caution as the material has a tendency to flow and creep, especially at temperatures above 150°C [*Matusiewicz*, 1999]. For all of the extractions carried out here the microwave temperature sensor was programmed to not exceed 120°C and the dimensions of the vessel caps were checked with callipers. To test for creep of the caps 10ml of water was placed in a vessel and heated for 10 minutes at 16% power. It was found that after heating the cap dimensions had changed slightly (less than 2%) but that the original dimensions were regained once the vessel had cooled. The expansion seen was no more than would be expected from normal thermal expansion of Teflon© PTFE (coefficient of thermal expansion = 0.000122mm per °C). This test was repeated six times and cap dimensions were also noted periodically during routine extractions with the same result. Therefore it was concluded that at the temperatures and pressures used there is no significant dimensional changes (creep) in the PTFE material and no further problems were encountered with the caps.

The 110ml vessels are rated to 200°C and 200psi. Pressure release is controlled by a safety rupture membrane which is made of Teflon© PFA. Should the maximum pressure be exceeded gases can escape through the exhaust port as the membrane ruptures (see Figure 3.3.). Six vessels, one of which was the control vessel for temperature and pressure monitoring were routinely used at a time. They were all connected to a central containment vessel via 1/8 inch Teflon tubing to prevent solvent fumes from entering the microwave cavity should any of the vessels over-pressurise and vent. Should any fumes enter the cavity the MDS-2000 system is also fitted with a fan which vented to a fume cupboard for safe disposal. As a final precaution the microwave was always placed so that its door faced the fume cupboard in case there should be an explosion of sufficient strength to destroy the door. The liner cover of the control vessel had Teflon© PFA fittings to allow the pressure tubing to be connected and for the insertion of a quartz thermowell for the temperature probe. The quartz thermowell runs through the vessel cap down to near the bottom of the vessel and houses the temperature probe, protecting it from solvent attack. A schematic of the vessels is shown in Figure 3.3.

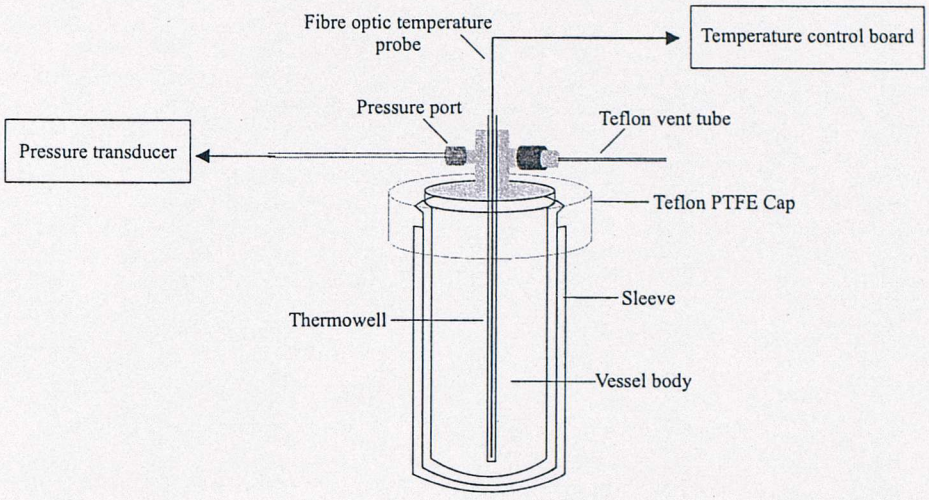

a) control vessel with temperature and pressure control

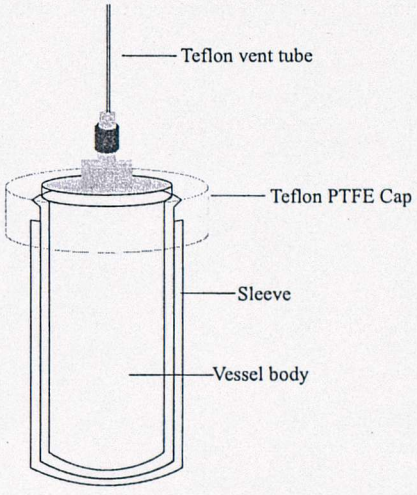

b) digestion vessel without temperature and pressure control

Figure 3.3. Schematic of the lined digestion vessels routinely used for microwave extractions.

The microwave transparent nature of the vessel and liner mean they remain relatively cool during the heating process. This improves the vessels' reflux capability as the cooler the walls are the more efficient they are at removing solvent molecules from the vapour phase. The higher condensation rate leads to lower internal pressures at higher temperatures. This relationship between temperature and pressure is complicated by the exact nature of the reagents and sample being used and the condensation rate varies with vessel geometry and materials, liquid volume, duration of heating and the systems ability to dissipate energy [*Richter et al.*, 2001].

When microwaves enter the oven they are dispersed and reflect from metallic surfaces which results in a variation in the amount of energy absorbed by samples at different positions in the oven [*Hall*, 1993]. The MDS-2000 is fitted with a rotating carousel which continuously moves the sample vessels a full 360° during any heating cycle. To test the uniformity of heating the APO

using 10ml samples of water in the control vessel in each of the six positions used was measured. There was no significant difference in the measured APO at each position leading to the conclusion that the rotating carousel is maintaining even heating conditions.

3.2.6 Development of the Microwave Extraction Procedure

To develop an efficient microwave extraction protocol several initial experiments had to be done to determine the optimum parameters to use as there was no published literature on how to proceed. It was decided to use the same solvent systems in the microwave as in the Soxhlet extractions to try and give a direct comparison between the two methods.

Initial microwave experiments focused on using the benzene-methanol and chloroform-methanol solvent systems for short reaction times (15-20 minutes) at high powers. For all microwave extraction development α-cellulose was subsequently retrieved using the *Loader et al.* [1997] technique, as in the Soxhlet tests.

3.2.6.1 Benzene-methanol extractions

An azeotropic mixture of benzene and methanol is composed of 39.5% methanol by weight, which corresponds to a mixture of 150ml benzene and 108.3ml methanol. Pure hydrocarbon solvents such as benzene do not absorb microwave energy so a percentage of a polar solvent such as methanol must be added, which will heat the benzene *in situ*.

Extractions were carried out by placing 1g of wood slivers and 20ml of solvent in a PFA digestion vessel. Tests were run using 2 sample vessels which were placed directly opposite each other in the microwave, to ensure even heating. The samples were run for 15 minutes at 60% power after which they were placed in a cold water bath for 30 minutes to cool. The vessels were then opened and the solvent decanted off. The wood slivers were then washed twice in acetone and 20ml of fresh acetone was then added to each vessel. They were then run for 10 minutes at 60% power before cooling. Finally the solvent was decanted and the sample was transferred to an Erlenmeyer flask and left to dry overnight in the fume cupboard.

3.2.6.2 Chloroform-ethanol extractions

The chloroform-ethanol extractions were carried out in a very similar manner to the benzene-methanol ones. The azeotrope is composed of a 2:1 mixture of chloroform and ethanol. Two vessels containing 1g of wood slivers and 20ml of solvent were heated for 20 minutes at 55% power. After cooling and removal of the solvent the sample was washed twice with absolute ethanol before 20ml of fresh ethanol was added. The vessels were then heated at 50% power for 15 minutes, cooled and the sample washed twice with Q-water. Finally 10ml of water was added

and the samples heated for 10 minutes at 25% power. Acetone was not used for this final cleaning stage as it is incompatible with chloroform. Again the cooled samples were transferred to an Erlenmeyer flask and allowed to dry overnight in the fume cupboard.

It was immediately apparent that material was being extracted from the wood slivers with both of the above solvents systems, as the solvents were strongly coloured after heating. However the cellulose products achieved from these experiments were significantly discoloured indicating that impurities remained. Product purity was not improved with either solvent system by doing a second run in the microwave using fresh solvent or by increasing the length of each extraction by 50%. These power ratings also led to high pressures developing inside the vessels that on occasion led to over-pressuring and venting. It was therefore concluded that a better approach would be to operate the microwave at lower powers and have longer extraction times. Once the solvent and sample solution is boiling the addition of microwave energy will not improve extraction but will increase the pressure inside the vessel. It was therefore decided to heat the samples in a cyclic manner, with a short period of time at high power to heat the sample followed by a longer 'maintenance' period at lower power. This cycle is then repeated several times so that the sample remains hot but the vessel pressure is better managed. This approach eliminated the problem of vessels over-pressuring though the product was still impure using a single solvent system.

The difficulty in achieving a good white α-cellulose product using either the benzene-methanol or the chloroform-ethanol approach led to the decision to combine the use of both solvent systems. Experiments were conducted where samples were first extracted in chloroform-ethanol before a second extraction in the benzene-methanol azeotrope. Initial experiments were carried out using 2 vessels and focused on the length of extraction, the ratio of time at high and low power and the pressure of the solvent system. This procedure proved to be highly successful in reproducibly yielding a pure white product. Subsequent experiments focused on scaling the method for running 6 vessels at once and it was found that if the number of vessels was tripled then the microwave power had to be doubled.

During the development of the technique it was found that longer extraction times, of up to 90 minutes did not improve product purity, yield or reproducibility. Smaller volumes of wood and solvent can be used in each vessel but the microwave power should be changed accordingly. The method was developed for 1g of wood because of the large amounts of cellulose needed to get a good ^{3}H detection limit. However CEM advised not having more than 1g and 20ml of solvent in a vessel as it is important to have a significant percentage (82% here) of the total volume available for solvent expansion.

The single solvent system tests that were carried out indicated that using both chloroform and benzene is critical to achieving a good extraction. This is probably a reflection of the very different chemistries of the two and it may be that the wood contains phenolic compounds that benzene will be more successful at removing. It is likely that neither solvent system alone is capable of extracting the wide range of chemicals in the wood. To optimise the technique further one final test was to combine the two solvent systems to try and reduce the total extraction time. An extraction solution was made up by adding 10ml of benzene to 10ml of 2:1 chloroform-ethanol. The tests were run using 2 vessels containing 1g of wood and 20ml of solvent each. An hour long extraction was performed as 4 cycles of 5 minutes heating at 30% power followed by a 10 minute maintenance period at 6% power. After cooling it was immediately evident that the solvent was far less coloured than had typically been seen with either of the solvents on their own. After decanting off the solution the wood slivers were washed twice with acetone before adding a fresh 20ml to each vessel and heating for 5 minutes at 30% power followed by 10 minutes at 6%. The cellulose product that was achieved after lignin removal was yellow coloured indicating that, as was hinted at by the lack of colour of the solvent, the extraction was incomplete. It was concluded that this was not a viable approach and that the extraction may be being inhibited by side reactions between the three solvents and was unlikely to improve efficiency.

Parameter	Value
Rated power of the microwave	650W
Calculated microwave APO	542.0 ± 24.2W
Mass of wood per vessel	1g
Solvent volume per vessel	20ml
Maximum extraction temperature	‡120°C
Maximum extraction pressure	‡110psi
Stage 1 (chloroform-ethanol)	3x (5 minutes at 350W followed by 10 minutes at 65W)
Stage 2 (benzene-methanol)	3x (5 minutes at 325W followed by 10 minutes at 65W)
Stage 3 (acetone)	5 minutes at 325W followed by 10 minutes at 65W

‡ These levels were chosen on the advice of CEM based on their experience of working with petroleum hydrocarbons.

Table 3.1. The final microwave parameters used to routinely extract α-cellulose from Irish cedar wood.

The final set of microwave parameters which has been routinely used to extract α-cellulose from cedar wood are outlined below in Table 3.1. A more detailed description of the final procedure is given in Appendix 3.

3.2.7 Discussion

The temperature and pressure within the control vessel was closely monitored during the first sample run and the results are shown in Figure 3.4.

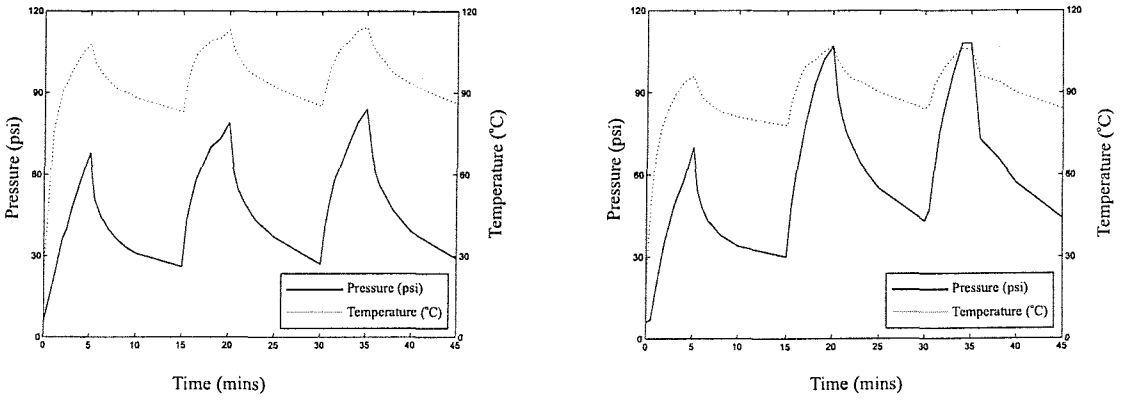

a) chloroform-ethanol extraction

b) benzene-methanol extraction

Figure 3.4. Graphs of the temperature and pressure time histories in the control vessels during a) a chloroform-ethanol extraction and b) a benzene-methanol extraction. The cyclicity in the 2 parameters due to the microwave heating pattern used is immediately apparent.

It is clear from Figure 3.4 that the temperature and pressure within a PFA digestion vessel directly mirrors the cyclicity in microwave power. Both parameters increase rapidly at the onset of a period of high power and then rapidly decrease when the power is reduced for the maintenance period. These elevated temperatures give microwave extractions a kinetic advantage over those carried out in a Soxhlet [*Richter et al.*, 2001]. During the extractions illustrated in Figure 3.4. the temperature within the vessels reached much higher levels than is possible for those solvent systems at atmospheric pressure. The maximum temperature reached in the chloroform-ethanol extraction was 114°C, almost double the azeotrope boiling point of 59.4°C with a mean temperature of 97°C during the whole run. During the benzene methanol run the mean temperature was 89°C with a maximum of 107°C compared to an atmospheric pressure boiling point of 58.3°C. As the mean temperature in each run exceeded the atmospheric boiling point by more than 50% it is no surprise that the extraction time is significantly reduced compared to that in a Soxhlet.

It is shown by Figure 3.4. that higher temperatures are reached during the chloroform-ethanol extraction. However it is also apparent that the internal vessel pressure in the benzene-methanol

run exceeds that in the chloroform-ethanol extraction. The mean pressure during the benzene-methanol run was 60psi with the highest pressure reached being 108psi. These are considerably greater than the corresponding values attained in the chloroform-ethanol extraction (49psi and 84psi respectively). These differences are likely to be a reflection of the different thermal properties of the two solvent systems but they highlight the importance of monitoring the pressure in such microwave procedures. The slopes of the lines in Figure 3.4. indicate that there was a large increase in vessel pressure for a small temperature change and it seems important that the cyclic heating approach was used. From the plots it seems unsurprising that the initial experiments using uniformly high microwave powers frequently resulted in venting as the pressures are likely to have continued to rise. The highly flammable and toxic nature of the solvents being used make it essential to run such extractions in a system that monitors vessel pressure and cuts the microwave power if a pre-described maximum is reached. It is for this reason that the use of pressure monitoring and control is more important than temperature control.

In the above sections a new rapid technique has been described that extracts α-cellulose from softwoods. The advantages afforded by this technique are outlined in Table 3.2.

Variable	Soxhlet	Microwave
Solvent volume	250-350ml	20ml
Solvent temperature	Condensed from atmospheric boiling point (58.3°C benzene-methanol, 59.4°C chloroform-ethanol)	Average of 89.2°C for benzene-methanol and 96.8°C for chloroform-methanol
Time in chloroform-ethanol	24 hours	45 minutes + 30 minutes cooling
Time in benzene-methanol	24 hours	45 minutes + 30 minutes cooling
Time in acetone	24 hours	15 minutes + 30 minutes cooling
Total time	6g wood in 72 hours	6g wood in 3¼ hours
Ease of control	Hard to control – often a high degree of variability in the extraction	Microwave power, maximum temperature and pressure can all be controlled.
End product colour	Variable from cream to yellow – significant levels of impurities remain	White – excellent reproducibility

Table 3.2. A direct comparison of the speed and efficiency of microwave and soxhlet extraction for the extraction of α-cellulose from Irish cedar wood.

From Table 3.2 it is possible to conclude that not only is microwave extraction faster and easier to control but it also gives a purer final product. Once all of the equipment has been purchased the method is also cheaper as far less solvent is used and it should be noted that it is also more ecological as less waste is produced.

This novel use of microwave technology offers an extremely time efficient method to routinely extract α-cellulose from soft woods which can be carried out safely with the use of a pressure controlled system and reliable vessels. However the chemical heterogeneity between different softwood species may require some modifications of the method described and shorter or longer extraction times may be needed, depending on the species under study and the range of natural products present in the raw wood sample.

3.3 Removal of Hydroxyl Group Contamination

The following sections describe the procedure that has been developed and routinely used to ensure that the tritium signal seen is a reflection of conditions the year that the cellulose was formed. The initial method development was carried out in collaboration with Rachel Stanley, a Fulbright Scholar from MIT who worked with me on the technique for nine months. The collaboration yielded the initial ideas and development of the exchange technique as an alternative to nitration, and Rachel was involved in the preparation of the first three exchanged samples (E1-E3). All subsequent samples and modifications to the technique I completed alone.

3.3.1 Cellulose

As can be seen in Figure 3.5. the cellulose molecule contains oxygen and carbon bound hydrogen, with 70% being bound to carbon. Of the remaining 30% half are in the amorphous regions of the polymer and half in the crystalline regions [*Grinsted and Wilson*, 1979]. To make ^{3}H measurements that reflect meteoric water it is necessary to remove all of the hydrogens whose isotopic ratio may have changed since biosynthesis. The hydroxyl (*-OH*) groups of the cellulose polymer are the most reactive substituent group of the molecule and will readily exchange isotopically with ambient water hydrogen [*Schimmelmann*, 1991]. The stronger carbon – hydrogen bond means that the isotopic composition of this hydrogen is not affected by water encountered after the tree grew. For this reason it is necessary to remove the 'exchangeable' hydroxyl group hydrogen from cellulose to allow a ^{3}H measurement to be made on the carbon bound fraction.

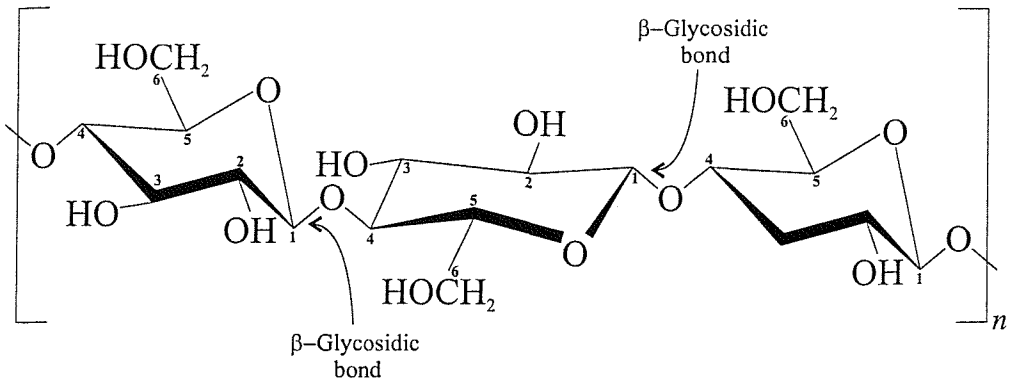

Figure 3.5. The structure of cellulose showing 3 of the D-glucose ($C_6H_{10}O_5$) repeating units joined by β(1,4) glycosidic linkages. Structurally cellulose is a polysaccharide composed of several thousand such units.

Cellulose molecules are large and are thought to be the largest of all known polysaccharide molecules [*Whistler and Smart*, 1953]. The polymer is seen to have a predominantly fibrous nature though it also has partially crystalline regions within which there are amorphous, or less ordered regions.

Cellulose has a tendency to aggregate into partially crystalline bundles which are known as micelles or fibrils, of mainly parallel chains of anhydroglucose units [*Percival*, 1962]. X-ray diffraction studies have shown that these small crystalline regions are separated by less ordered amorphous regions with no sharp line of demarcation between the two. The structure of cellulose allows for chain packing as a result of both intramolecular and intermolecular hydrogen bonding [*Dawsey and M^{C}Cormick*, 1990]. These strong interactions lead to the stiffness and mechanical strength of the cellulose polymer but make complete reaction or modification very difficult. Reactions occur far slower in the crystalline regions of cellulose where the hydroxyl groups are hydrogen bonded in a regular, ordered manner, and only a limited fraction of these hydroxyl groups will undergo exchange or substitution [*Mann and Marrinan*, 1956].

To aid reactions and achieve a good degree of substitution it is advantageous to swell the fibre structure before or during reaction. Swelling of the amorphous regions occurs first, with the loosening of long portions of cellulose chains so they become free to move in the swelling agent [*Whistler and Smart*, 1953]. As these regions swell to a gel, penetration of the crystalline regions starts to occur as the stronger associative forces there are disrupted. However, even with a fully swollen complex, complete reaction is difficult to achieve as the three hydroxyl groups in the glucose monomer are not equally reactive. The relative reactivity of the three is dependent on their position in the residue and other steric effects associated with the introduced and reacting group. It has been proposed by *Kurahashi et al.* [1999] that the formation of hydrogen bonding networks and positive charge delocalisation is mainly responsible for the relative reactivities of

carbohydrate hydroxyl groups. Generally the primary hydroxyl group (see Figure 3.5), OH(6) is more reactive than both OH(2) and OH(3) [*Dawsey and M^{C}Cormick*, 1990].

3.3.2 Removal of Exchangeable Hydrogen

Most dendroclimatological studies [*Epstein et al.*, 1976; *Pendall et al.*, 1999; *Schiegl and Vogel*, 1970] have measured the isotopic ratios of cellulose nitrate. The formation of cellulose nitrate is an inorganic esterification reaction that replaces the hydrogen atoms on the hydroxyl group with nitrate ($-NO_2$) groups. Fuming nitric acid (HNO_3) alone will nitrate cellulose but the addition of a catalyst will yield products with a higher nitrogen content [*Whistler and Smart*, 1953]. The most commonly used nitrating mixtures combine the fuming nitric acid with acetic anhydride [*DeNiro*, 1981], 98% sulphuric acid and redistilled dichloromethane [*Short et al.*, 1989] or phosphoric acid and phosphorous pentoxide [*Epstein et al.*, 1976]. The maximum degree of substitution (DOS) achieved in these nitration reactions is always well short of the theoretical maximum of three and varies with acid mixture [*Short and Munro*, 1993]. The DOS increases with time, levels off and then decreases over a period of a few days. Strong acids such as sulphuric acid will denitrate cellulose so the DOS of the final product is a balance between the competing nitration and denitration reactions.

Cellulose nitrates with a nitrogen content that exceeds 13.1% are highly unstable [*Marsh and Wood*, 1938] and cellulose nitrate is commonly known as 'gun cotton' and is highly explosive in oxygen. On the basis of the glucose residue ($C_6H_{10}O_5$) cellulose tri-nitrate should contain 14.2% nitrogen, the di-nitrate 11.1% and the mononitrate 6.8%.

Epstein et al. [1976] found that one nitration of sufficient duration followed by an acetone extraction provides enough replacement of the exchangeable hydroxyl groups to ensure that the measured isotopic ratio is that of the carbon bound hydrogen, to a good precision (1σ=2‰). Stable isotope studies such as this involve very small (milligram) samples. However for ^{3}H analysis, larger samples of up to 5g were routinely flame sealed in glass bulbs for helium ingrowth. The larger sample sizes and the danger of combusting the highly explosive cellulose nitrate in oxygen while sealing make this a dangerous proposition. There is also the possibility that the very strong acids that are used to nitrate cellulose may exchange some of the carbon bound hydrogens [*Grinsted and Wilson*, 1979]. A different approach was therefore used so that a non-explosive substance could be sealed for helium ingrowth.

3.3.3 The Cellulose – Water Exchange Reaction

The alternative approach to obtain the isotopic ratio of the non-exchangeable hydrogen in cellulose is to control the composition of the hydroxyl groups by equilibration of the cellulose

with water (or vapour) of a known isotopic composition [*Feng et al.*, 1993]. This reaction makes use of the fact that the hydroxyl hydrogens in the cellulose polymer readily exchange with water according to Equations 3.2 and 3.3.

$$HOD + R.OH \leftrightarrow R.OD + H_2O \tag{3.2}$$

$$HOT + R.OH \leftrightarrow R.OT + H_2O \tag{3.3}$$

In both equations *R* represents the cellulose polymer and Equation 3.2. shows an exchange with deuterated water (D) and Equation 3.3. illustrates an exchange with tritiated water (T). This approach has been widely used in deuterium studies [*Feng et al.*, 1993; *Grinsted and Wilson*, 1979; *Schimmelmann*, 1991] and the δD of the exchanged material can be taken to be the weighted average of that of the unexchanged and the exchanged hydrogens such that the mass balance of the system is described by:

$$\delta D_T = (1 - x_e)\delta D_U + x_e \delta D_e \tag{3.4}$$

where δD_T is the measured cellulose δD, x_e is the fraction of hydrogens that have exchanged, δD_U is the δD of the unexchanged hydrogen and δD_e is the δD of the exchanged hydrogen. The isotopic ratio of the exchanged hydrogens, δD_e, is determined by the ratio of the water and the isotopic fractionation associated with exchange.

The exchange reaction is a very straightforward procedure that involves sitting a sample of cellulose in water, or vapour of a known isotopic composition. The initial fast exchange of the hydroxyl groups in the amorphous regions of the polymer and on the surface of the crystalline arrays takes place in the first 30 minutes. However this phase is of limited extent and the subsequent reaction proceeds much slower [*Frilette et al.*, 1948] with full equilibration occurring only after approximately 30 days at 92 ± 2°C [*Grinsted and Wilson*, 1979], as can be seen in Figure 3.6.

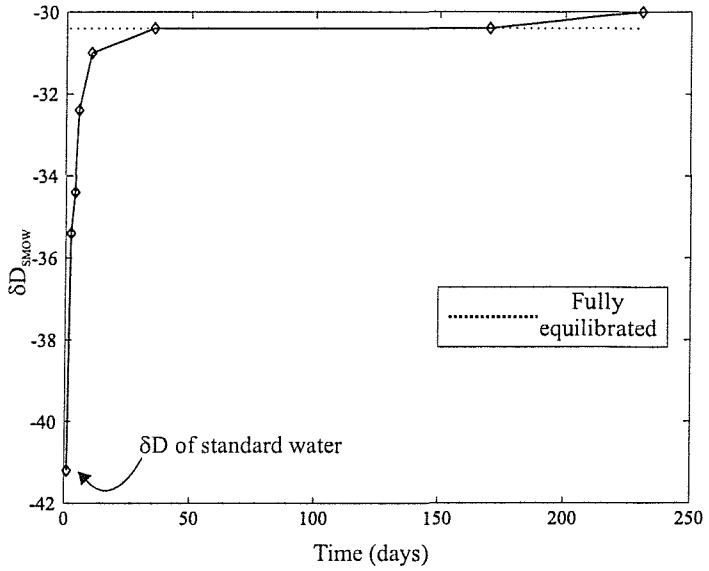

Figure 3.6. The effect of equilibration time on the hydrogen exchange between cellulose and a standard water with a known D/H ratio at 92 ± 2°C. The untreated wood cellulose had a δD_{SMOW} of −67.9 ± 0.5‰ and it can be seen that full equilibration was seen after about 30 days. Adapted from Grinsted and Wilson [1979].

3.3.3.1 Effect of temperature and pH

Carrying out an exchange at elevated temperatures offers a kinetic advantage as it is controlled by diffusion of hydrogen species through the substrate [*Schimmelmann*, 1991]. However *Frilette et al.* [1948] ran exchanges between cellulose and deuterated water at room temperature and 70° and at two different acidities (pHs 3.9 and 10.25) and found that neither variable affected the reaction to any significant degree. The exchange reaction can also be carried out using water vapour of known isotopic composition to an accuracy of ± 3‰ [*Schimmelmann*, 1991], though the reaction is slower than in the liquid phase [*Mann and Marrinan*, 1956]. The reaction was seen to vary with temperature with an exchangeability of 23.1% being achieved at 104°C compared with 26.7% at 114°C and 26.8% at 156°C. These contrasting results may be due to the more elevated temperatures used than in the earlier work or be due to the exchange being carried out in the vapour phase or on cellulose from different trees.

3.3.4 The Reaction of Cellulose with NaOH

Infra-red spectroscopy shows that only 40-42% of hydroxyls, those on the surface of the fibrils, will react [*Short and Munro*, 1993] so in order to exchange the hydroxyl groups in the interior of the polymer it is necessary to penetrate the more strongly bound crystalline regions.

Sodium hydroxide causes swelling of cellulose fibres and penetrates into the interior of the chain bundles, making more of the hydroxyl groups available for reaction. This reaction is one of the best understood and most important reactions of cellulose. When an alkali is added to cellulose both physical and chemical reactions take place which depend on temperature, alkali concentration and the nature of the alkali being used [*Whistler and Smart*, 1953]. With concentrations of NaOH up to 8%, at room temperature, there is only reaction within the amorphous regions of the polymer. At higher concentrations there is also reaction within the crystalline lattice forming a swollen addition complex. In 12-18% solutions it is thought that the complex formed is $(C_6H_{10}O_5)_2.NaOH$ while at concentrations above 21% $C_6H_{10}O_5.NaOH$ is formed [*Whistler and Smart*, 1953]. This effect is even more pronounced at low temperatures [*Feng et al.*, 1993] and is lost on drying as the cellulose will then recrystallise.

Subsequent developments of the exchange technique have made use of the ability of NaOH to aid fibre accessibility. *Feng et al.* [1993] followed the method of *Grinsted and Wilson* [1979] but introduced a series of treatments to increase the extent of exchange and overcome the heterogeneous exchangeability of cellulose samples. Their results show that with no chemical pre-treatment equilibration still hadn't occurred to any significant degree after 2 days. However equilibration was rapidly achieved if the cellulose was soaked in 17% w/v NaOH for 15-18 hours at 0-5°C prior to a 24 hour exchange with water of a known isotopic composition. By including this step in the reaction the high temperatures and long reaction times of the original technique were avoided. A direct comparison was made between this technique and nitration and the resolution of the deuterium measurements was 2.5‰ (1σ) which is slightly poorer than is seen with nitration (1σ = 2‰). However the average fraction of hydroxyl groups exchanged compared well with nitration. Cellulose can be nitrated so that less than 4% of the hydroxyl hydrogens remain [*Grinsted and Wilson*, 1979] which agrees with the average of 4.5% achieved by *Feng et al.* [1993] using exchange. The use of NaOH to swell the cellulose fibres appears to have increased the degree of exchange as *Grinsted and Wilson* [1979] only achieved an average fraction of exchange of 22.4%, or 7.6% of hydroxyls remaining, with no pre-treatment.

It has been found that despite the varying crystallinity of cellulose the degree of exchange should be uniform among samples from an individual tree. *Grinsted and Wilson* [1979] found no evidence for variability in the degree of exchange for one type of cellulose so confidence in using the technique to construct isotopic time series is high. Overall it can be concluded that isotopic reconstructions from exchanged cellulose should be as robust as those from cellulose nitrate.

3.3.5 Optimised NaOH Exchange Technique for Tritium Measurement

It was decided to modify the exchange technique further by carrying out the reaction in NaOH so that the cellulose remains swollen during the whole procedure. Cellulose samples were routinely exchanged by sitting them in a large excess of ^3H free NaOH for 24 hours at room temperature which should deprotonate the exchangeable hydrogens. After 24 hours the samples were flushed with ^3H free phosphoric acid (H_3PO_4) and copious amounts of ^3H free water to reprotonate the exchangeable hydrogens, this time with hydrogens that contain no ^3H. As the exchange was carried out with ^3H free reagents the problem of fractionation during the reaction that is seen with deuterium was avoided. Room temperature was chosen for the reaction to balance the competing effects of swelling increasing at low temperatures and the kinetic advantage offered by high temperatures. It was intended that the use of NaOH to swell the cellulose fibres would give a better degree of exchange than was seen in one of the few studies of ^3H in tree rings by *Kozák et al.* [1989], who removed the exchangeable hydrogens by equilibrating with ^3H free water alone. By heating the cellulose with ^3H free water for 4 hours in an autoclave at 175°C *Kozák et al.* [1989] report that 92% of the hydroxyl groups underwent exchange, less than has been seen with the use of NaOH [*Feng et al.*, 1993].

3.3.6 Production of Tritium Free Reagents

In order to effectively carry out the exchange a supply of tritium free NaOH and H_3PO_4 was needed. Therefore methods were found and refined to produce both reagents from ^3H free water and reactants that contain no hydrogen.

3.3.6.1 Tritium Free Water

To produce tritium free reagents it was first necessary to find a supply of ^3H free water. Tritium free water was collected from Calypso Soft Drinks in Wrexham, North Wales. The water derives from a spring which has its source in the Lincolnshire Limestone beds that underlie the factory site. Water is collected through a borehole directly underneath the factory floor. The water has been carbon dated and found to have an average age of 4938 ± 500 years old (the company data report gave no error on this value but ± 10% is typical for such a measurement). Tritium was also measured using electrolytic enrichment and a liquid scintillation counter optimised for low level counting, and showed no detectable ^3H activity. It should be noted that a detection limit of order 1TU is typical for this type of measurement.

Water was collected and stored in 1 litre glass bottles with polypropylene caps with polycone liners. Prior to filling at the factory the bottles were baked at 200°C for at least 8 hours under an argon atmosphere to remove adsorbed water. The bottles were cooled to room temperature and

sealed with argon inside. The caps which had been evacuated to 1 x 10^{-3} torr and flushed with argon were secured under tension with electrical tape to prevent opening. Throughout this discussion pressures are given in torr which is a non SI unit equivalent to 133.322Pa, so the bottle caps were evacuated to a pressure of 0.13Pa prior to flushing with argon.

Water was introduced to the bottles from a tap with a gentle flow. The bottles were kept vertical at all times to maintain a blanketing layer of argon overlaying the water, thus minimising contamination.

Samples of the water were degassed as described in 3.3.9 for subsequent analysis of the helium ingrown by tritium decay to give a more sensitive measurement of the waters ^{3}H content than is possible by liquid scintillation. Details of the analytical procedure are described in 3.4. Samples were degassed after each water collection trip to 'quality control' the exchange procedure and the results are shown in Table 3.3.

Sample	Tritium (TU)
1	0.002 ± 0.003
2	< 0.001 ± 0.002
3	0.001 ± 0.002
4	< 0.008 ± 0.012
5	0.009 ± 0.01
6	< 0.005 ± 0.009
7	0.005 ± 0.011
8	0.008 ± 0.006
9	< 0.009 ± 0.014
10	< 0.006 ± 0.019

Table 3.3. Tritium ratios measured by helium ingrowth for borehole water collected from Calypso Soft Drinks in Wrexham, North Wales. Where a sample is given a ratio preceded by a less than symbol then the ratio in the sample is lower than the detection limit, the number quoted.

The results in Table 3.3 indicate that the water is indeed tritium free to as good a detection limit as is currently possible. The good agreement of the results suggests that the water is not in contact with any source of contamination at the source, in the factory, in transport and storage or during the degassing procedure.

3.3.6.2 Tritium Free NaOH

Tritium free NaOH was routinely synthesised for the exchange reaction from ^3H free water and metallic sodium following *Cornog* [1921]. Considerable care was taken in the preparation because of the explosive nature of the reaction between sodium and water in the presence of oxygen.

To make 900ml of 17% NaOH 87.9g of sodium needs to be added to the water. However this tended to yield NaOH with concentrations nearer 19%, as the heat of the reaction caused significant evaporation, and experience led to approximately 70g of sodium being used routinely. The ^3H free water was placed in a separating funnel to which anhydrous ethyl ether was added. The flask was then shaken to mix the 2 liquids which allowed the anhydrous ether to take up some of the water into its structure. Small pieces of metallic sodium were then carefully added to make NaOH. The ether layer prevents explosion as the sodium reacts with small pockets of water within it before sinking into the water below as NaOH. It was noted by *Cornog* [1921] that as long as the ether layer thickness was 3-4 times the diameter of the sodium pieces the reaction proceeded safely. Once all of the sodium has been added the NaOH was drained from the bottom of the funnel into a round bottomed flask. Any remaining ether was then removed by heating the solution under an argon atmosphere in a spark free heating mantle, to prevent atmospheric contamination. Full details of the procedure are given in Appendix 4.

After each batch of NaOH had been made its strength was determined by titrating against 1.19M HCl using Phenolphthalein as an indicator, which turned from colourless to pink when the end point was reached. If the solution was found to have a concentration greater than 17% then an appropriate amount of ^3H free water was added, conversely if the concentration of the base was less than 14% it was strengthened by allowing it to boil under argon. To minimise subsequent contamination the NaOH was carefully transferred to an argon filled bottle (prepared as described in 3.3.6.1) for storage.

3.3.6.3 Tritium Free H_3PO_4

Phosphoric acid was chosen to reprotonate the hydroxyl groups in the exchange reaction as it is relatively easy to synthesise and it exerts a less degrading effect on cellulose and has less tendency to esterify it than other acids, such as H_2SO_4 [*Whistler and Smart*, 1953]. Tritium free H_3PO_4 can be made by reacting phosphorous pentoxide (P_4O_{10}) with ^3H free water according to the reaction:

$$P_4O_{10} + 6H_2O \rightarrow 4H_3PO_4 \qquad (3.5)$$

Phosphoric acid behaves as a strong acid in dilute aqueous solutions but only one of the hydrogens is readily ionisable. Solutions of the acid were produced by slowly adding 135g of P_4O_{10} to 800ml of ^3H free water in a fume cupboard. Care must be taken as the reaction is exothermic and produces significant quantities of vapour. However the production of the acid is not this straightforward as the strongly hydroscopic nature of P_4O_{10} causes significant ^3H contamination, with the first acid solutions made having ^3H concentrations 50 times that of the Wrexham water (see Tables 4 and 5). As soon as P_4O_{10} is exposed to air it adsorbs enough water to form a thick paste. As the vapour in the lab may contain significant amounts of tritium this could introduce noticeable contamination to the acid produced. To minimise this contamination all subsequent acids were produced in an argon glove box placed within a fume cupboard. A large argon flow was used to flush the box of the vapour produced by the reaction and the pot of P_4O_{10} was not opened until the box had been completely purged of air. The P_4O_{10} still formed a paste but with liquid condensed from the ^3H free solution in the box thus minimising contamination. A full description of the method is given in Appendix 5.

The strength of the acid produced and the amount needed to reprotonate the exchangeable hydrogens in a sample was determined by titrating against the ^3H free NaOH used for that particular exchange, with Phenolphthalein as an indicator. Again the acid was stored in argon filled bottles to minimise contamination.

Samples of both reagents were degassed for subsequent ^3H analysis as described in 3.3.9 to check their ^3H concentration and the results are shown in Table 3.4.

It is clear that both reagents have significantly higher ^3H concentrations than the ^3H free water, which has a mean concentration of 0.005TU. Contamination in the NaOH is likely due to ^3H from the paraffin that coats the Na pieces and from the ether layer that overlies the ^3H free water. Both of these are unavoidable but contamination is minimised by blotting each piece of Na on tissue paper to remove as much of the paraffin as possible immediately before addition to the reaction vessel. Producing H_3PO_4 in an argon glove box minimises contamination and the elevated ^3H concentration that remain are likely due to contaminants within the matrix of the P_4O_{10} which is again largely unavoidable. Both reagents will also be subject to atmospheric contamination every time they are opened and used and this probably explains much of the variability that is clearly evident in the concentrations in Table 3.4. NaOH sample 1 and H_3PO_4 samples 1,2 and 6 were used to exchange far fewer samples than the other reagents. They were therefore opened and exposed to the atmosphere far less than the other samples, which likely explains their anomalously low ^3H concentrations. Atmospheric contamination was minimised as much as possible by transferring reagents using positive pressure, as described in Appendix 4, rather than pouring and purging the bottles with argon before resealing. As the reagents were used and

transferred in a fume cupboard the protecting argon blanket will have been disturbed by the upward air flow. Clearly if the bottles were not then completely refilled contamination is likely. The results make it clear that this is an area that needs to be improved in the future, by opening reagent bottles as little as possible and purging them with argon for longer after each use.

Sample	Tritium (TU)	Comments
NaOH		
1	0.042 ± 0.0022	
2	0.57 ± 0.10	
3	0.40 ± 0.06	
4	0.35 ± 0.04	
5	0.53 ± 0.09	
6	0.51 ± 0.10	
Mean	0.40	
H_3PO_4		
1	0.086 ± 0.009	Made without an argon atmosphere
2	0.096 ± 0.008	Made without an argon atmosphere
3	0.37 ± 0.11	
4	0.38 ± 0.07	
5	0.78 ± 0.03	
6	<0.0096 ± 0.015	
7	<0.029 ± 0.053	
Mean	0.091	

Table 3.4. Tritium ratios measured by helium ingrowth for NaOH and H_3PO_4 made as described in 3.3.6.2 and 3.3.6.3 respectively. Where a sample is given a ratio preceded by a less than symbol then the ratio in the sample is lower than the detection limit, the number quoted

3.3.7 Carrying out the Exchange Reaction

To carry out an exchange, cellulose samples were first dried overnight in a 70° nitrogen oven to remove adsorbed water. Like other polysaccharides cellulose has a strong affinity for water and normally has a water content of 8-9% [*Whistler and Smart*, 1953]. The glassware used for the

exchange (a small Erlenmeyer flask and measuring cylinders) were also dried overnight in a 70°C nitrogen oven to minimise any ^3H contamination from water droplets.

One gram of cellulose sample was exchanged by adding the sample to 45ml of ~17% w/v ^3H free NaOH solution in an Erlenmeyer flask with stirring. The flask was stoppered and a gentle argon flow started to ensure there was no contamination from ambient air (Figure A6.1). After the flask had sat for 3-4 hours it was capped and taped to ensure that the headspace was full of argon. The sample was then left stirring overnight. After 24 hours the flask was unstoppered and neutralised (reprotonated) with ^3H free H_3PO_4. The sample was allowed to sit, while stirring for 30 minutes to allow all of the hydroxyl sites to reprotonate. The pH of the solution was then checked, to ensure that the sample was either neutral or slightly acidic and more acid was added if needed. A basic pH would indicate that not all of the sites had reprotonated. The sample was then centrifuged to separate the phases and placed in an argon filled glove box, where the supernatant was removed. The sample was then washed by adding ^3H free water and centrifuging again. This washing was repeated 4 times and the sample transferred to a pre-weighed 200ml alumino-silicate bulb for sealing and helium ingrowth. The sample bulbs were manufactured from Corning type-1720 glass which has an extremely low helium permeability [*Clarke et al.*, 1976] and then prepared by baking them at 625°C overnight in a helium free atmosphere. Headspace nitrogen from a liquid nitrogen tank was used as the low helium content gas to purge the bulbs in the oven. This procedure removes helium dissolved in the glass of the bulb which would otherwise have diffused into the sample during helium ingrowth reducing precision.

A more detailed description of the exchange method is given in Appendix 6.

Before the exchanged sample were flame sealed for helium ingrowth they were degassed and partially dried as described in 3.3.8.

3.3.8 Degassing of Samples for Helium Ingrowth

Once the exchanged cellulose samples have been transferred to alumino-silicate glass bulbs they are degassed and partially dried prior to sealing. Initially samples were freeze dried but this led to problems in the analysis of the samples on the mass spectrometer. As is discussed in 3.4.1 water vapour is needed as a 'carrier gas' to ensure there is good transfer of helium for analysis in the magnetic sector mass spectrometer. Therefore the following procedure was used where all gases were removed from the bulb prior to sealing but a small amount of water was left in the bulb to ensure there would be water vapour present to give a high draw down efficiency on the mass spectrometer.

The bulbs containing the wet cellulose samples were quickly transferred from the argon glove box to a dedicated vacuum system with a manifold for drying up to six samples simultaneously. The apparatus and procedure was designed to remove all gases and all but a few grams of the water from the exchanged cellulose samples. Before attaching samples the vacuum manifold was evacuated to at least $1x10^{-3}$ torr. Samples and flasks were then weighed and attached to the manifold using viton o-ring fittings as is shown in Figure 3.7. The samples were then opened to the vacuum using manual valves and the headspace was pumped through a liquid nitrogen cooled trap, both to aid water removal and to protect the vacuum pumps. Initially pumping was on a rough pump but once a pressure of 1×10^{-3} torr had been maintained for 30 minutes the system was moved onto a diffusion pump and left to evacuate overnight (at least 15 hours). When the pressure was low enough (less than $1x10^{-7}$ torr) the bulb was sealed off whilst still open to the diffusion pump to minimise helium contamination by heating the glass during sealing.

The bulbs were then reweighed to determine the weight of the wet sample. Samples were stored in a freezer to minimise helium permeation through the glass, which has a strong temperature dependence [*Clarke et al.*, 1976], for at least four months before analysis of the ^3He produced by ^3H decay.

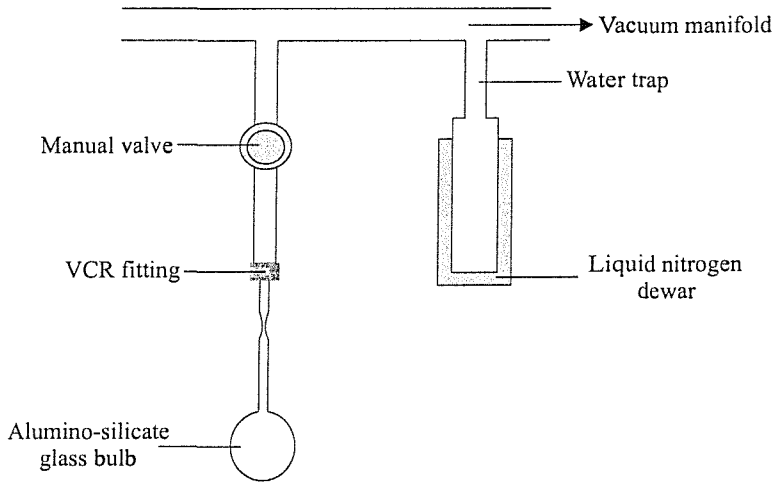

Figure 3.7. Schematic of the cellulose degassing and drying line.

When degassing samples containing a significant amount of water, drying was hastened by raising a 50°C water bath to submerge the sample bulbs for 30 minutes. This was not used routinely as it tended to completely freeze dry the cellulose leaving no water vapour to ensure good sample gas transfer on the mass spectrometer.

3.3.8.1 Air Correction

When the alumino-silicate sample bulbs were weighed prior to an exchange they contained air which was removed when the samples were degassed. The mass of the air removed was corrected for when the samples were reweighed after sealing, to give an accurate cellulose sample mass. The volume of the sample bulbs was determined by filling them with water and weighing. Filling three bulbs six times resulted in a mean volume of 210.43 ± 12.75 ml. Taking the density of air to be 1kg.m^{-3} this bulb volume was taken to be equivalent to 0.21 ± 0.01g of air and this correction was applied to all samples.

3.3.8.2 Fractionation During Degassing

The water that is left in the sample bulb upon sealing contributes to the tritium signal measured on the mass spectrometer and needs to be corrected for to get a true α-cellulose ^{3}H measurement. This was done by assuming that the water has a concentration of 0.002TU, the average of the degassed ^{3}H free water samples.

As water is lost from the cellulose samples during degassing evaporation causes the hydrogen in the water molecules to be slightly fractionated, with the lighter isotopes being preferentially evaporated. Therefore the ^{3}H signal seen in the water remaining in the bulb is slightly enriched compared to the original ^{3}H free water. In order to correct for this it is necessary to weigh the sample before and after degassing and record the amount of water removed.

The fractionation factor, α during this evaporation, is 1.15±0.02 [*Clarke et al.*, 1976] at 20°C which differs from the equilibrium value of 1.108 at the same temperature. The higher value is because the rapid removal of water vapour to the trap does not allow for the establishment of isotopic equilibrium. The correction factor to the samples is given by Equation 3.6, where W is the mass of the water in the bulb at the end of the degassing process and w_E is the mass of water removed from the sample.

$$\frac{W + \frac{w_E}{\alpha}}{W + w_E} \tag{3.6}$$

The mean amount of water removed from a sample in the Valentia time series was 30.82 ± 2.66g, with 0.5g water left in the bulb. This equates to a correction factor of 0.8716 ± 0.01458.

3.3.9 Degassing of Liquid Samples for Tritium Analysis

The tritium concentration of liquid samples was determined by initially removing any gases present in the solution, and then measuring the ingrowth of ^{3}He. Liquid samples were degassed on a separate vacuum manifold which allowed up to 7 samples to be degassed simultaneously (Figure 3.8). The entire system was diffusion pumped to a vacuum better than $5x10^{-7}$ torr to remove atmospheric gases and checked for leaks prior to starting a degassing procedure.

Approximately 100g of water or reagent was transferred from the glass bottles into pre-weighed, Corning type-1720 alumino-silicate glass bulbs under an argon blanket. The bulbs were prepared as described in 3.3.7. After sample introduction a flow restricting valve was closed and the headspace was pumped past a liquid nitrogen water trap for 5 minutes. The degassing section was then isolated and the bulb shaken using a speed controlled linear shaking table for 30 minutes. The motion of the shaker was enough to disturb the boundary between the sample and the headspace and hence enhance gas transfer but not so great that gases were re-entrained. This pump – shake cycle was repeated at least 7 times moving from pumping on the rough pump to the diffusion pump when the pressure surges were low enough. Once the pressure was below $1x10^{-7}$ torr the bulb was sealed whilst open to the diffusion pump to minimise contamination. The time of sealing was recorded and the bulbs re-weighed to determine the weight of the sample.

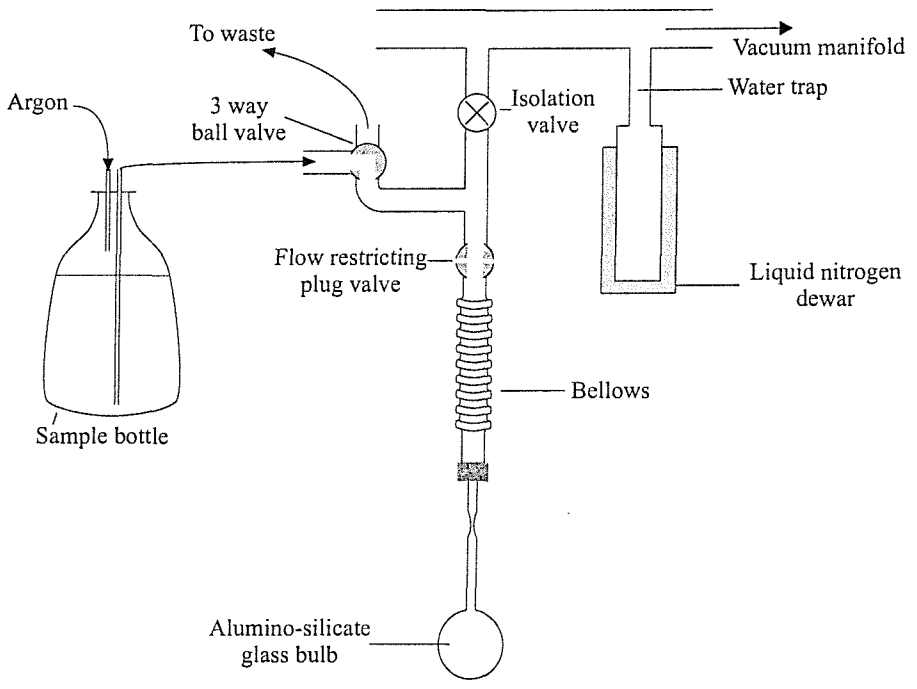

Figure 3.8. Schematic of the degassing line used for liquid samples

In order to correct for the fractionation associated with the degassing procedure (see 3.3.7) the volume of water or reagent transferred to the water trap following a degassing was recorded on several occasions. The mean mass of 2.33± 0.15g was used to calculate the correction factor for this fractionation and gives a value of 0.997±0.00346 for a 100g sample.

3.4 Sample Analysis

This section describes the methods and analytical procedures required for low level tritium measurements for both cellulose and liquid samples by mass spectrometric measurement of ingrown ^{3}He. The concentrations of ^{3}He, and hence ^{3}H in each sample were determined using the coupled statically operated, dual collector, magnetic sector and quadrupole mass spectrometer system in the Southampton University Noble Gas Laboratory. Sample gases were cryogenically separated using the method described by *Lott and Jenkins* [1984] with ^{3}H being measured by the helium ingrowth technique [*Clarke et al.*, 1976].

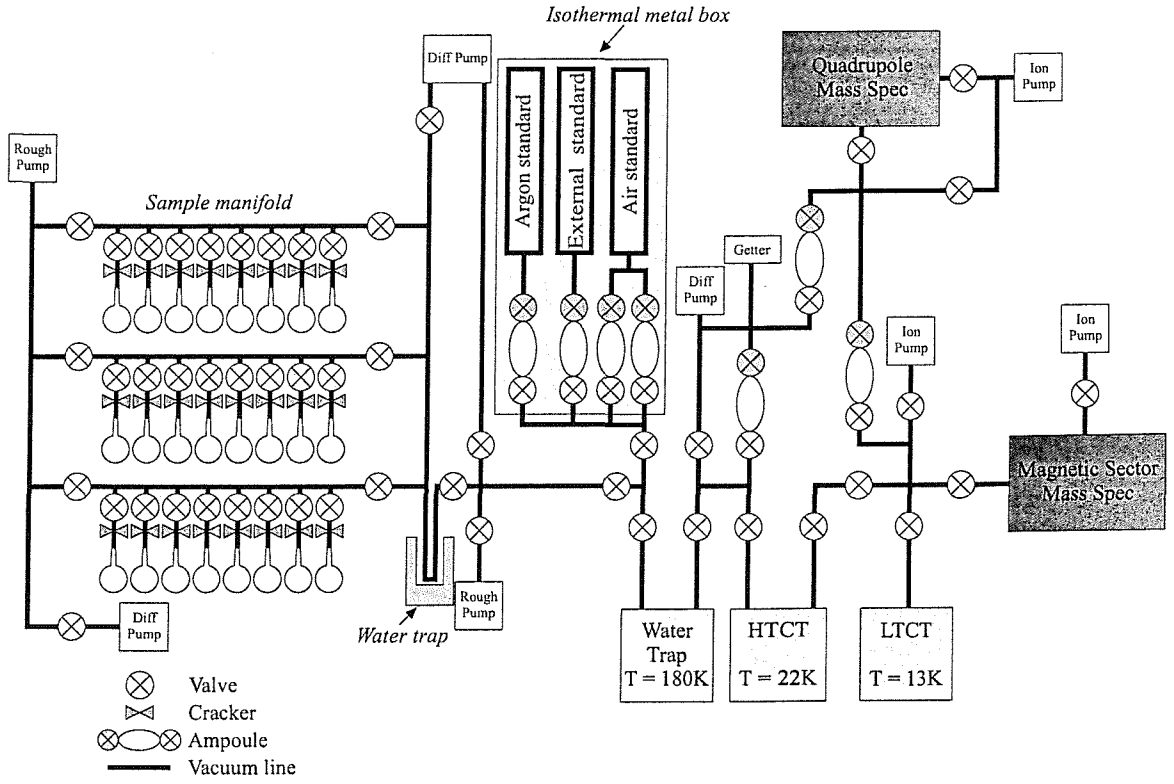

Figure 3.9. Schematic of the mass spectrometer sample processing line. HTCT and LTCT refer to the High Temperature Cryotrap and the Low Temperature Cryotrap respectively.

A schematic of the sample processing line is shown in Figure 3.9. All components of the line are made of stainless steel as the use of all metal valves and vacuum fittings wherever possible minimises the helium background in the system. The line was vacuum pumped using diffusion pumps to below $1x10^{-8}$ torr and valves are pneumatically operated Nupro valves which were

controlled by a solid state relay. Gases are progressively purified using four cryotraps at increasingly lower temperatures and the gases are exposed to SAES Zr-V-Fe getter granules to remove any unwanted reactive gases such as nitrogen and oxygen. The ultra high vacuum in the low temperature cryotrap, the magnetic sector mass spectrometer and the quadrupole mass spectrometer was maintained using ion pumps. The whole system was controlled using a Pentium based PC and an in house Visual Basic control programme.

The system has three fully automated manifolds, each with 8 ports which allows for continuous running of samples. The sample bulbs were scored with a glass knife near the sealing point and then carefully loaded onto the manifold using viton o-ring fittings. The narrow neck of the bulbs fits into the jaws of specially manufactured "crackers". These crackers are modified pneumatically activated, normally open Nupro valves, which when activated knock the top off the bulb releasing sample gas into the system. The 3 manifolds were vacuum pumped to less than $5x10^{-8}$ torr using dedicated rough and diffusion pumps. After all samples on a manifold had been analysed, the manifold was vented with laboratory grade nitrogen and the sections cleaned by removing all glass fragments, wiping with acetone and fitting fresh viton o-rings before loading more samples.

3.4.1 Sample Processing

When the top of a bulb is knocked off the sample gas in the headspace is released into the system and drawn down onto the High Temperature CryoTrap (HTCT) and the Low Temperature CryoTrap (LTCT) through two water traps. Originally the first water trap was cooled by a liquid nitrogen trap (T~77K) but this was found to lead to a significant under transfer of sample from the processing lines to the cryotraps. It appears that the geometry of the system means that cryopumping alone is not sufficient to pull down all the gases so water vapour is needed as a "carrier gas" to ensure a good draw down efficiency of the sample [*Postlethwaite*, 2002]. This problem was eliminated by replacing the liquid nitrogen trap with a higher temperature isopropanol refrigeration unit (T~243K) which pumps mechanically cooled fluid round the trap. The initial samples used to test the cellulose exchange technique were analysed with a liquid nitrogen trap but all other samples were run with the refrigeration unit.

The inlet to the second water trap is held at 250K and the outlet at 150K to ensure it doesn't become blocked, as this trap protects the HTCT (~22K) and LTCT (~13K) from any water vapour that may remain in the system. These three make up the cryogenic system which is cooled by a closed cycle, high purity helium gas refrigeration unit. During ^{3}H analysis samples were left open to the cryogenic system for three minutes, which has been shown to be sufficient time to transfer

the gases while minimising the amount of water vapour transferred from the bulb to the processing line [*Postlethwaite*, 2002].

The HTCT adsorbs all gases except neon and helium which are trapped on the low mass activated charcoal of the LTCT which needs to be below 14K to quantitatively adsorb helium with negligible fractionation [*Lott and Jenkins*, 1984]. The LTCT is then isolated and raised to 40K, the helium release temperature, ready for analysis. An aliquot (~1-2%) of the released helium is introduced into the quadrupole mass spectrometer and measured. If it is of suitable size the rest of the helium is introduced to the magnetic sector mass spectrometer for helium isotope analysis. The initial analysis in the quadrupole acts as a safety mechanism to protect the extremely sensitive helium mass spectrometer. The remaining gas is then flushed off the cryotraps as no other measurements are required (the system is also capable of measuring argon and neon isotopes). The total analysis time for a sample is 35 minutes.

3.4.2 Calculating Tritium from Measured Helium

The concentration of ^{3}He in a sample is made up of two parts, that due to ^{3}H decay and that due to air contamination. Measurement of the ^{3}He / ^{4}He ratio for every sample allowed this effect to be corrected for. All of the data from the two mass spectrometers was collated in a Visual Basic programme with the helium-3 signal recorded in counts per second (*cps*) and the helium-4 signal recorded in volts. The data was then calibrated against ^{3}He and ^{4}He measurements in an air standard and blank corrected, before being converted to concentrations as described in Equation 3.10.

The amount of ^{3}H in a sample was calculated from measured helium using the radioactive decay equation:

$$N = N_0 e^{-\lambda t} \tag{3.7}$$

where N_0 is the ^{3}H in the sample before decay, N is the ^{3}H left after decay, t is ingrowth time and λ is the decay constant. The ^{3}He signal measured by the instrument corresponds to $N_0 - N$ which means that the ^{3}H concentration of the sample can be calculated from Equation 3.8.

$$^3H = \frac{^3He}{1 - e^{-\lambda t}} \tag{3.8}$$

The amount of tritiugenic ^{3}He in a sample was calculated by subtracting that due to air contamination from the measured ^{3}He signal and multiplying by the ^{3}He sensitivity. The sensitivity of the machine is its response to the amount of gas g in the instrument. Knowing the sensitivity of the instrument at a gas pressure similar to that in the samples allowed the amount of gas in each sample to be calculated. The sensitivity of the machine when samples were run was determined by dividing the size of the air standard by the standard response at the time as follows:

$$^3He(sensitivity) = \frac{^3He(std)_{cc}}{^3He(std)_{cps} - ^3He(blank)_{cps}} \tag{3.9}$$

Therefore the tritiugenic ^{3}He sample is given by:

$$^3He(sample)_{cc} = \frac{^3He(std)_{cc}}{^3He(std)_{cps} - ^3He(blk)_{cps}} \cdot \left(^3He(sample)_{cps} - ^4He(sample)_V \cdot \frac{^3He(std)_{cps}}{^4He(std)_V} \right) \tag{3.10}$$

where *blk* and *std* refer to line blank and air standard responses respectively. The error in this measurement was calculated by converting the error in the ^{3}He measurement to cm^3. The measurement error was based on the Poisson counting statistics of the ^{3}He measurement such that:

$$\sigma^2_{^3He} = \left(\frac{\sqrt{N}}{T} \right)^2 + \left(\frac{\sqrt{n}}{t} \right)^2 \tag{3.11}$$

where N is the total number of ^{3}He ions counted during analysis, T is the length of time spent counting at the ^{3}He peak, n is the number of ^{3}He ions counted at baseline and t is the time spent measuring at baseline.

The calculated volume of tritiugenic helium (Equation 3.10) measured by the mass spectrometer in cm^3(STP) was first converted into cm^3(STP) of tritium using Equation 3.7 and then expressed as Tritium Units (TU). Although not a concentration, Tritium Units, which are defined as $^3H/^1H \times 10^{18}$ are a convenient way to examine low level ^{3}H measurements and have become the standard in oceanographic tracer studies. First the volume of ^{3}H in the sample was converted into moles by dividing by 22.4×10^3 (as 1 mole of gas occupies 22.4 litres at standard

temperature and pressure) and then this number was divided by the number of moles of hydrogen in the sample before multiplying by 10^{18} to give the sample measurement in TU.

In all calculations the revised ^3H half life of 4500 ± 8 days was used [*Lucas and Unterweger*, 2000] and the abundance of helium in the atmosphere was taken to be 5.24×10^{-6} (taken form the 81st edition of the CRC Handbook of Chemistry and Physics).

3.4.2.1 Cellulose Corrections

As explained in 3.4.1 water vapour is needed as a carrier gas to ensure that there is a good draw down of sample onto the cryotraps. Therefore wet cellulose samples were not completely freeze dried and some water was left behind. The contribution of this water to the final ^3H signal was taken into account by assuming that it had a concentration of 0.005 ± 0.004 TU, the average of the detectable Wrexham ^3H free water samples (see Table 3.3). However because of fractionation during degassing (see 3.3.8.2) the correction factor of 0.8716 ± 0.01458 was applied to all Valentia time series samples to account for the relative ^3H enrichment of the water due to evaporation. This relatively large correction factor, relative to that for liquid samples is due to a large amount of water being removed during the degassing procedure compared to the amount remaining in the sample. However it should be noted that the actual correction applied is small as the water has such a low ^3H concentration. The mass of dry cellulose and water in a sample was determined by removing all water from the sample after analysis by drying in a 70°C nitrogen oven and weighing.

3.4.2.2 Liquid Sample Corrections

When liquid samples were stored for ^3H analysis there was no heating or stirring so the gases were partitioned between the liquid and the headspace. To ensure there was equilibrium of helium between the two the sample bulbs were loaded onto a rotary shaker table and gently shaken for at least 8 hours prior to loading them on the mass spectrometer manifold.

Again a correction was applied to take into account fractionation during the degassing procedure (see 3.3.9). Using the mean mass of liquid removed a correction factor of 0.997 ± 0.0346 was applied to all liquid samples. As the isotopic fractionation factor, α is not known for NaOH or H_3PO_4 it was assumed to be the same as water and the same correction factor was applied.

3.4.3 Air Standards

As described in 3.4.2 the measurements of ^3He and ^4He peak heights in a sample are calibrated against those in a known quantity of air.

Samples of ambient air were collected from the dockside at the Southampton Oceanography Centre in stainless steel tanks fitted with Nupro valves. To collect a standard the tanks were first evacuated to less than $5x10^{-8}$ torr and sealed. They were then taken to the dockside and allowed to thermally equilibrate for 30 minutes after which the valve was opened and the tank allowed to fill with ambient air for 3 minutes. In order to make precise measurements of the amount of He in the standard a correction was applied to take into account deviations in conditions on the dockside from STP. Hence while the tank was filling barometric pressure was measured using a Vaisala PTB220 Class A Barometer (0.10hPa accuracy), relative humidity was measured with a Hanna Instruments HI93640 thermohygrometer (2% accuracy) and temperature was measured using a Digitron T600 precision thermometer (resolution of 0.01°C). The compounded error for the amount of dry air in an aliquot of air standard was 0.15% based on the accuracy of these instruments and the errors associated with the volumes of the standard tanks and aliquots [*Postlethwaite*, 2002].

3.4.3.1 Standard Expansion

For low level ^3H measurements very small amounts of helium were needed for standardisation so air standards were diluted by expanding them into a larger volume. An external standard, which was collected in exactly the same manner as the main air standard was regularly run against the main air standard to ensure there were no leaks or discrepancies in the system. The layout of standard collection tank and the main air standard and external standard tanks used is shown in Figure 3.10.

Aliquot volumes connect each of the standard tanks to the processing lines and the whole system is housed in an airtight metal box (Figure 3.10), in order to maintain an isothermal environment. Both the temperature within this box and the ambient air temperature in the laboratory were monitored to identify any temperature fluctuations that could affect the standard. The main air standard tank was used to provide standards to calibrate low level ^3H measurements. It has two aliquot volumes which are known as Large and Small, the volume ratio of which is approximately 10:1. These were usually used together as the running standard, which was optimised so that the amount of helium in the two aliquots matched that of the samples being run.

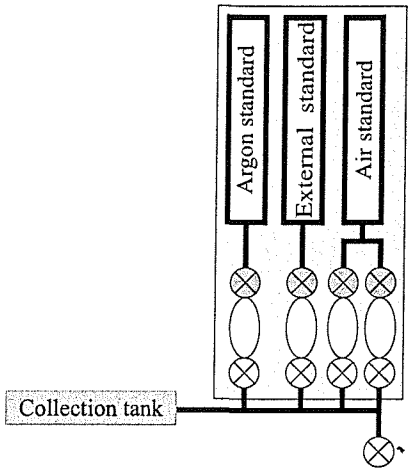

Figure 3.10. The layout of the volumes used to expand air standards in the isothermal metal box, showing how the collection tank is connected to the main and external standard tanks.

Accurately knowing the size of each air standard allows the sensitivity of the machine (Equation 3.9) and hence the concentration of all samples to be calculated (Equation 3.10). The volumes of all the tanks, aliquots and lines used in standard expansions must be known accurately to allow the size of the standard to be accurately determined. The volumes of all tanks and internal volumes used in air standard expansions were either measured gravimetrically or by comparison to stainless steel aliquot volumes, which had been calibrated against mercury calibrated glass volumes [*Postlethwaite*, 2002]. A range of tanks with different volumes to match the required standard size as closely as possible were available. Details of all of these volumes, calibrations and the full details of the standard size calculation are given in Appendix 7.

Expansion efficiency experiments were done when the system was set up to assess how well the gases equilibrated between the various volumes used in standard preparation and are described in Appendix 8. This was done as it has been seen that when an external standard is run against a main air standard a slightly different result is obtained than expected. The experiments reveal (see Table A8.1) that there was incomplete standard expansion which was monitored as samples were run by running air standards both before and after samples.

Air standards were run before, during and after the analysis of a manifold of samples. A cubic smoothing spline was fitted to this standard data and interpolated over the time of the sample analysis to allow the amount of tritiugenic helium in each sample to be calculated.

3.4.4 System Blanks

There is a blank signal in the machine for each gas. Line blanks were run approximately every three hours during sample analysis to determine the magnitude of these signals so they could be subtracted from all samples and standards. For example there is a blank signal due to interference

at the ^{3}He mid-peak position by ions from the low mass 'tail' of the HD+H_3 peak [*Clarke et al.*, 1976] as ^{3}He has a mass of 3.01603 AMU compared to 3.02193 AMU for HD and 3.02348 AMU for H_3. A blank signal also results from a 'memory effect' caused by embedded ions in the source slits being released during analysis.

A cubic smoothing spline was fitted to the line blanks and interpolated over the time of the data. All samples and standards were blank corrected using these interpolated line blank values.

3.4.4.1 Manifold Section Blanks

A blank, termed the "manifold blank" on each of three eight port manifolds was run before analysing a manifold of samples. If this blank was above a critical level suggesting there is a leak into the system, none of the samples were run until the leak had been found.

3.4.5 Limitations to the Accuracy of ^{3}H Measurements

Ultimately the precision of all tritium measurements depend on the ^{3}He detection limit of the mass spectrometer. The atom detection limit for a gas was calculated as the standard deviation of a series of line blanks. This detection limit is determined by background ion scattering of both hydrogen species (H_2, HD, H_3) and ^{4}He by the mass spectrometer [*Lott and Jenkins*, 1984]. This memory effect and consequently the detection limit were reduced by running a series of line blanks before any low level ^{3}H samples were introduced. With time the measured ^{3}He in the line blanks decreased as embedded ions were released, effectively cleaning the machine and reducing the detection limit. The detection limit was also minimised by retuning the instrument to give maximum sensitivity prior to running samples.

The ^{3}He detection limit of the mass spectrometer determines the minimum ^{3}H signal that can be seen in a sample and hence ultimately its precision. The smallest signal that can be seen is directly proportional to the ^{3}He detection limit of the instrument and inversely proportional to the mass of the sample and the storage time (see Appendix 9). Improving the ^{3}He detection limit from 800 to 500 atoms of ^{3}He improves the sample detection limit from 0.153TU to 0.096TU for a 5g cellulose sample sealed for 6 months. This highlights the importance of minimising the detection limit as much as possible for low level ^{3}H analyses.

Aside from the ultimate machine response the error in the ^{3}H concentration of a sample can be reduced by increasing its mass and storage time. For the same 5g cellulose sample either doubling its mass or ingrowth time will half the minimum ^{3}H which can be detected. Ideally the best results are obtained for large samples sealed for a long time, however both are limited in practise by time constraints. For cellulose samples the mass is limited by how long the samples take to prepare and must be balanced with time constraints and the expected ^{3}H signal. For the Valentia time series

approximately 1g cellulose samples were sealed and allowed to ingrow for as long as was practical (~5 months), resulting in a sample detection limit of approximately 0.8TU. As can be seen from Figure 3.11 this is good enough to resolve all but the pre-bomb samples, assuming that the precipitation signal is a good indicator of the ^3H concentration in the cellulose. As this was an initial test of whether the ^3H signal in tree ring cellulose reflects ambient precipitation the only measure of whether samples were ready for analysis was to compare the sample detection limit with the precipitation signal from Valentia. To improve precision a large sample (~4.5g) of 1940 wood was sealed to allow the pre-bomb signal to be resolved to 0.2TU.

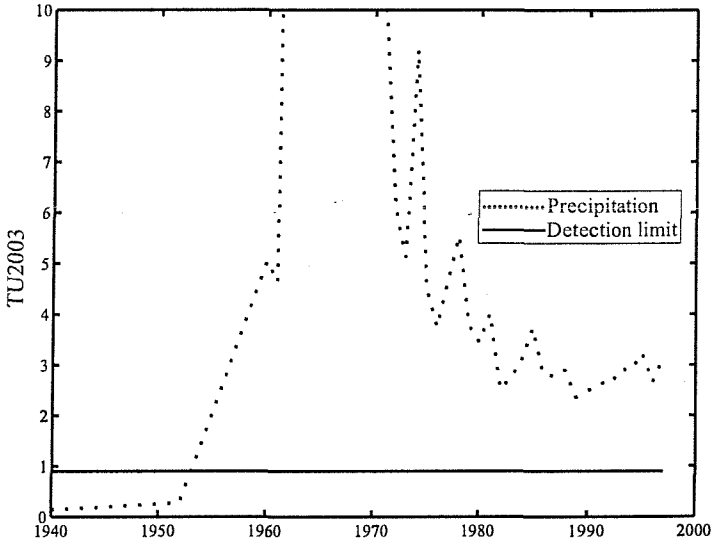

Figure 3.11. Comparison of the cellulose sample detection limit with the measured precipitation signal at Valentia, Ireland. Cellulose samples are unlikely to be a perfect reflection of precipitation but the graph indicates that 1g of cellulose sealed for 5 months will allow the signal to be resolved except for the years 1940-1953. Due to lack of data a pre-bomb concentration of 5TU is assumed during the 1940s, which gives a concentration of 0.14TU in 2003. Concentrations are given in TU decayed to January 1st 2003 (TU2003), though the scale only extends to 10TU for clarity. The maximum concentration is that for the bomb spike year of 1963 which is 102.55TU.

As well as reducing uncertainty by increasing sample size and storage time, error can be reduced by minimising the helium blank associated with sample preparation and analysis. According to Equation 3.13 this error is proportional to the square root of the number of ^3He atoms counted. This implies that a sample which has a significant atmospheric ^3He signal will have a larger error due to "Poisson statistical dilution" from this unwanted helium.

Atmospheric ^3He in a sample can be the result of incomplete degassing, diffusion through the glass walls of the sample bulb or diffusion through the o-ring fittings on the mass spectrometer manifold. Diffusion of ^3He through the glass of the sample bulb was minimised in several ways. Firstly the samples were kept open to the diffusion pump during sealing as the permeability of the glass increases with temperature so the pump was needed to minimise the amount of ^3He which entered the sample bulb. The increased permeability of the glass when hot also means that some

^{3}He is likely to enter the bulbs as they cool after sealing. Cooling the glass slowly after sealing ensures that the glass doesn't crack due to "thermal shock" which would lead to significant atmospheric contamination during storage. Secondly the atmospheric blank was minimised by using bulbs made from glass with a low helium permeability and storing samples at low temperatures after sealing.

Atmospheric contamination due to air diffusing through the o-ring on the manifold was enhanced if the crackers didn't break the bulb cleanly as this dislodged the o-ring allowing air to permeate the seal. This was minimised by carefully scoring the neck of the bulb to control where it breaks before inserting it in the manifold.

Finally, incomplete degassing was avoided by pumping on the cellulose samples for at least 18 hours prior to sealing and ensuring that the pressure reached at least $1x10^{-7}$ torr. Care was taken to ensure that the pressure reading reflected that in the sample bulbs. If the water trap became blocked with ice then despite continued degassing there was not a true pressure reading on the bulb side of the blockage. To avoid this the liquid nitrogen dewar was placed so as not to cool the top third of the trap and the trap was cleaned between each degassing to ensure it didn't fill with ice.

3.4.6 Results

As the NaOH exchange method has not been used before to measure ^{3}H concentrations in cellulose it was necessary to test it and confirm that the hydroxyl group contamination was being removed. To do this large samples of cellulose extracted from old wood, that should contain no appreciable ^{3}H, were exchanged and analysed.

3.4.7 Testing the Exchange

The exchange technique was tested using Irish oak wood from a tree felled in November 2000 twenty miles from the Valentia weather station. Examination of the rings revealed that the tree started to grow in 1839 and to allow large cellulose samples to be sealed, wood from 1839 to 1875 was combined and used in bulk. Ambient water from these years should contain no appreciable ^{3}H but the wood will have been subjected to both water and vapour with much higher concentrations during and after the weapons tests. If the exchange technique works any such contamination will have been removed and only the background pre-bomb concentration will be present. If all of the hydroxyl group contamination has been removed then the maximum ^{3}H concentration recorded in such a sample will be that from 1875.

Estimates of the natural ^3H concentration of precipitation vary from less than 1TU at equatorial latitudes to 6TU for Chicago precipitation [*Craig and Lal*, 1961]. Assuming a pre-bomb precipitation ^3H concentration of 5TU at Valentia the maximum signal that would be expected from 1875 is 0.004TU, for samples analysed in 2002. To get a sample detection limit for this low level, large samples of between 3 and 8g were allowed to ingrow ^3He for 6-8 months.

3.4.8 Initial Results from 1839-1875 Wood

Initially four samples were exchanged as described in 3.3.7 before being degassed and sealed for helium ingrowth. It should be noted that the sample size and time available meant that the detection limits for the sample varied from 0.04 to 0.14TU, which is significantly higher than the expected signal of 0.004TU. The ^3H concentration from each sample are compared with the sample detection limits in Table 3.5.

The results in Table 3.5 show that the exchanged cellulose samples consistently have a ^3H concentration of less than 1TU. Samples E1 and E2 have detectable concentrations, and all four have errors significantly larger than their detection limit. This extra ^3H could either be from ^3H or ^3He contamination.

Sample	NaOH (TU)	H_3PO_4 (TU)	Detection Limit (TU)	Tritium Ratio (TU)
E1	-	-	0.09	0.6 ± 0.2
E2	0.042 ± 0.022	0.086 ± 0.009	0.04	0.5 ± 0.2
E3	0.042 ± 0.022	0.086 ± 0.009	0.13	<0.13 ±0.3
E4	-	0.096 ± 0.008	0.15	<0.15 ±0.9

Table 3.5. A comparison of the ^3H ratios of the initial 4 samples used to test the exchange techniques with that of the reagents used for the exchange. Where a sample is given a ratio preceded by a less than symbol then the concentration in the sample is lower than the detection limit, the number quoted.

These four were the first cellulose samples prepared using the exchange method and the techniques required were still being refined. Critically, an efficient method to transfer wet cellulose into the glass sample bulbs had not been developed. At the time the bulbs being used had extremely narrow capillaries with an internal diameter of approximately 1mm at the narrowest point. Attempts to inject the cellulose using a large syringe or to guide it through the capillary failed, so the neck of the bulb was removed and the cellulose placed directly into the

bottom of it. To allow these samples to be degassed a new neck had to be glass blown onto the top of the bulb. To minimise contamination as much as possible nitrogen was blown over the glass as the new glass neck was attached and contamination from breath was removed by breathing through a plastic tube. Despite these precautions contamination from ambient air and the torch were inevitable and will have been compounded by the extensive heating of the glass required to successfully attach a new neck. Further contamination will also have been introduced from the new glass attached to the base of the bulb. This glass was not baked to remove dissolved helium as described in 3.3.7, so helium within this portion of glass will have diffused into the sample during storage. Once a neck had been successfully reattached the samples were degassed as normal removing much of the ambient air and torch gases from the sample. However contaminated vapours may have exchanged with the wet cellulose during the glass blowing or degassing and will not have been removed before sealing.

It is also possible that some of the ^{3}H signal in the four samples is from the reagents used for the exchange. The reagents used for the first exchange were not degassed and analysed but the concentrations of those used for the other three are shown in Table 3.5. The NaOH used to exchange sample E4 was degassed but the sample was aborted on the line as the pressure in the manifold was too high and it seems likely that it was incompletely degassed. *Feng et al.* [1993] reported that three to four washes of cellulose which had been soaked overnight in NaOH with water was enough to remove the isotopic signal of the base. It is therefore unlikely that any of the ^{3}H from either the acid or base remains as the exchanged cellulose was washed 4 times in a huge excess of ^{3}H free water before being transferred to the sample bulb. However as this has not been tested for the conditions used here it should be considered a potential source of ^{3}H.

The large error in sample E4 is believed to be due to atmospheric ^{3}He contamination. The ^{4}He signal from this sample was an order of magnitude larger than for the other three samples. "Left behinds", where a sample is analysed again, were also run for all of the samples to check that all of the helium in the sample has been extracted and measured. If the sample had been incompletely degassed, but not sufficiently to abort on the manifold, then the sample would be expected to be high in ^{4}He but the subsequent left behind would be low in ^{4}He. The left behind from E4 also had high ^{4}He so it is unlikely that incomplete degassing is the source of the uncertainty. High ^{4}He in a left behind is likely due to air diffusing through the o-ring on the mass spectrometer manifold.

Overall the results of these initial exchanges appear favourable as the ^{3}H concentrations measured are less than 1TU. Since the wood has been formed it will have been in contact with waters that had ^{3}H concentrations of several hundred times this value. As glass blowing is likely to have introduced significant contamination to the bulb such low ^{3}H measurements give a first indication that the exchange is working.

3.4.9 Improvements to Initial Procedures

The initial experiments highlight the importance of eliminating contamination for low level ^3H measurements. To eliminate the uncertainty introduced by glass blowing all subsequent samples were sealed in bulbs with an internal diameter of approximately 3mm at the narrowest point. This allowed wet cellulose to be easily transferred to the bulbs in an argon glove box by carefully guiding the cellulose down the neck using a long needle. By quickly transferring the bulbs from the argon atmosphere to the degassing manifold they should not be contaminated prior to sealing.

As an improved test of the exchange technique a further six large samples were sealed and allowed to ingrow for almost a year to allow for optimum precision. The same Irish oak wood was used and again the maximum ^3H signal that should be seen is 0.004TU, that estimated for 1875 precipitation. Contamination was minimised by not glass blowing, making H_3PO_4 under argon and using a better quality glove box for preparing exchanged samples. Precision was improved by reducing the helium blank by sealing the cellulose in 200cc rather than 1 litre glass bulbs. These modifications should minimise contamination sufficiently to allow the results to definitively test the efficiency of the exchange at removing hydroxyl group contamination. The results from this experiment are shown in Table 3.6.

Sample	NaOH (TU)	H_3PO_4 (TU)	Detection Limit (TU)	Tritium Ratio (TU)
OAK001	0.57 ± 0.10	<0.029 ± 0.053	0.14	2.01 ± 0.60
OAK002	0.57 ± 0.10	<0.029 ± 0.053	0.15	< 0.15 ± 0.78
OAK004	0.51 ± 0.10	<0.0096 ± 0.015	0.14	0.37 ± 0.43
OAK003	*Aborted during analysis due to high ^4He*			
OAK005	*Sample bulb cracked in storage*			
OAK006	*Sample bulb cracked in storage*			

Table3.6. Results from the second round of exchange tests. Again where a sample is given a ratio preceded by a less than symbol then the ratio in the sample is lower than the detection limit, the number quoted.

Unfortunately, of the six samples sealed only three yielded results. All six of these samples were sealed with between 5g and 15g of tritium free water in the bulb to ensure there was water vapour present to give good sample transfer on the mass spectrometer (see 3.4.1). When samples OAK005 and OAK006 were removed from the freezer the necks of the bulbs had cracked. It appeared that the water in the bulb had filled the neck and expanded on freezing causing cracks. These two sample bulbs contained in excess of 12g of water highlighting the importance of storing the bulbs vertically so the water cannot drain into the neck. The loss of these samples led

to the conclusion that it was unwise to leave such a large amount of water in the bulbs and only 0.5-1g of water was left in subsequent samples.

Sample OAK003 was aborted on the mass spectrometer as the ^4He pressure in the manifold was too high to allow the sample to be analysed. Such a high ^4He signal is indicative of atmospheric contamination, which in this case is likely to have occurred when the sample was sealed. As this bulb was sealed a small crack appeared and although the bulb was subsequently sealed successfully it was open to contamination through the crack.

The remaining three samples presented in Table 3.6 had lower ^4He concentrations than sample OAK003 but still higher than would be expected when the data is compared with line blanks. So it appears that there is still a problem with atmospheric helium contamination during analysis. When the sample bulbs were removed from the mass spectrometer manifold and examined it was clearly evident that the bulb necks had not broken cleanly. The manifold and crackers on the system were originally designed for use with the narrow necked sample bulbs which are used for liquid samples. However the difficulties associated with transferring exchanged cellulose to the bulbs necessitated a wider capillary, which has slightly changed the overall dimensions of the neck of the bulbs, even away from the sealing constriction. When these samples were run the bulbs were watched as they cracked and they were seen to move slightly, indicating that the crackers were not cleanly breaking the neck, which was confirmed when the bulbs were examined. It appears that the cracking may be dislodging the o-ring in some way, allowing for atmospheric helium to enter the bulbs. This atmospheric contamination contributes to the large error in the measurements presented in Table 3.6. This contribution is particularly important for sample OAK002 which was seen to move significantly during cracking and had a markedly elevated ^4He signal. This resulted in a large error in the sample concentration.

As with the results from the initial exchange tests (Table 3.5) these three samples have concentrations significantly greater than both their detection limits and the expected 1875 signal of 0.004TU. Again the uncertainties in the ^3H ratios for the three samples are also larger than the detection limits and the expected signal. These large errors are in part due to the poisson counting statistics from the atmospheric contamination but also reflect the sample masses and storage time. To significantly reduce the uncertainty in these measurements either much larger samples are needed or a longer ingrowth time is necessary, both of which are limited by the time involved to prepare cellulose samples. These samples were exchanged and prepared as cleanly as possible, with no glass blowing and H_3PO_4 that was synthesised under an argon blanket so the results indicate that not all of the contamination from the exchangeable hydrogen atoms is being removed.

The tritium ratio of sample OAK001 (2.01 ± 0.60TU) is an order of magnitude greater than that from any of the other samples, including those from the original exchange tests (see Table 3.5). This sample has a slightly elevated ^{4}He signal but even with the atmospheric correction it appears that this sample has been contaminated at some point. As OAK001 contains far more ^{3}H than the samples which were subjected to the significant contamination of glass blowing (E1-E4) it appears that this sample contains 'excess' ^{3}H. This extra ^{3}H could reflect a very poor degree of exchange in this sample and the ^{3}H being bomb ^{3}H contamination that has not been removed. This seems unlikely as the signal is much larger than that in samples which have been open to contamination. Therefore the additional ^{3}H signal has most probably been added during sample preparation. Contamination may be from the reagents used in the exchange or the result of contact with a luminous dial watch or water vapour in the laboratory as the sample was transferred to and from the argon glove box and to the freeze drying line. There are many possible sources of contamination, what can be said from the data is that for sample OAK001 the extraneous contamination is substantial and is unlikely a reflection of the performance of the exchange technique.

The results from the remaining two samples OAK002 and OAK004 confirm the favourable results of the initial tests. As there are only two samples to compare with the original tests it is not possible to comment statistically on any improvement in the results due to improved sample preparation. However the below detection limit result for OAK002 and the low level of that for OAK004 (0.37 ± 0.43TU) indicate that much of the potential bomb spike ^{3}H contamination is being removed by the exchange technique. The results also highlight the importance of carrying out the procedure as cleanly as possible to try and reduce the errors in the measurement.

3.5 Discussion of the Exchange Technique

3.5.1 Assumption About the Degree of Exchange

The results of the exchange tests indicate that the technique is removing potential hydroxyl group contamination from the cellulose molecule. However the results obtained are of the order 0.5TU which is significantly larger than the expected precipitation signal of 0.004TU. Although some of the discrepancy is likely to be from atmospheric helium contamination or the reagents used, as described above, it is clear that not all of the hydroxyl group contamination is being removed. Knowledge of the degree of exchange is critical when the results are being quoted in Tritium Units. These units are a ratio ($^{3}H/^{1}H \times 10^{18}$) so the amount of hydrogen in each sample needs to be accurately known. If the exchange was removing all of the hydroxyl group hydrogen's and replacing them with 'dead' hydrogen's, the amount of hydrogen used to get a measurement in Tritium Units would be that of the carbon bound fraction alone. As 70% of the hydrogen's on the

cellulose molecule ($C_6H_{10}O_5$) are carbon bound, the amount of hydrogen in the sample would be taken to be 7 moles per mole of cellulose. However, it is clear that this is not valid as the tests of the exchange technique indicate that not all of the hydroxyl group contamination is being removed.

From a single set of exchange tests it is not possible to ascertain the degree of exchange that is being achieved. To do so requires either a direct comparison with nitrated samples or doing a series of exchanges with solutions of differing ^3H concentrations. *Feng et al.* [1993] illustrated that the degree of exchange, x_e can be calculated by doing such a series of deuterium exchanges. A plot of cellulose deuterium against that of the water used for the exchange will yield a straight line from which x_e can be calculated (see Equation 3.4). By independently determining δD_U, that of the carbon bound fraction, for example by nitration, x_e can be calculated. *Feng et al.* [1993] carried out such experiments for cellulose samples from a commercial source and from six different tree species, comparing the results with nitration (the extent of which was determined using C/N ratios). These tests yielded an average degree of exchange of 0.255, which equated to 25.5% of the total hydrogens in cellulose being removed.

As the experiments carried out for the exchange described in this chapter provide no information on x_e, this average value of 25.5% of total hydrogens was used as an estimate of the degree of exchange being achieved. The exchange technique of *Feng et al.* [1993] uses a NaOH pre-treatment which improved the degree of exchange compared with earlier work (see discussion in 3.3.4) and is the most similar technique to that presented here. Therefore all cellulose results are quoted in TU, where the amount of hydrogen contributing to the signal is assumed to be 7.45 ± 0.45 moles per mole of cellulose. It should also be stressed that it was also assumed in these calculations that the extraction of cellulose from the raw wood has been 100% successful and that there is no hydrogen contributing to the signal from other oils, resins or sugars.

3.5.2 Error Analysis

For extremely low level tritium analyses such as these it is important to consider all errors. For each sample errors from sample weighing, degassing corrections (3.3.8.2), the air correction (3.3.8.1), the degree of exchange and the assumed concentration of ^3H free water were included, along with the analytical error due to Poisson counting statistics (Equation 3.11). Propagating these errors highlights that the contribution to the overall sample uncertainty is minimal from each term apart from the counting error, as is shown by Table 3.7. This error is proportional to the square root of the number of ^3He atoms counted and has two implications. Firstly, larger ^3H signal will have a larger absolute error but a smaller relative error. Secondly, when a sample has been significantly contaminated with atmospheric helium the error will be inflated by these counts.

This serves to highlight the difficulty of obtaining good precision for small low level samples and the importance of minimising atmospheric contamination.

Source of Error	Error Contribution
Counting	0.43 TU
Mass (weighing + air correction)	0.02 TU
Degree of exchange	0.02 TU
Tritium free water concentration (including fractionation)	0.004 TU

Table 3.7. An examination of the contribution to the total error from each of the individual sources for sample OAK004.

In the next chapter the exchange technique is used to construct a time series of ^{3}H concentrations in an Irish cedar tree to compare with the Valentia weather station precipitation record. This provides a first indication of whether the methods outlined in this chapter can be used to reconstruct past ^{3}H concentration in precipitation.

4. Climatic Significance of Hydrogen Isotope Reconstructions from an Irish Tree

4.1 Introduction

Having described a method to measure tritium concentrations in tree ring cellulose in the preceding chapter the validity of this technique and its potential for precipitation ^{3}H reconstructions will now be explored.

There have been many studies of isotopic ratios in plant matter with much work focusing on deuterium, hydrogen (D/H) and oxygen isotope ($^{18}O/^{16}O$) ratios. These ratios have been shown to vary in response to seasonal, geographic and long term climatic temperature changes such as those associated with glacial and inter-glacial cycles [*Epstein et al.*, 1976]. Also, deuterium reconstructions from tree ring cellulose have been shown to correlate with the isotopic signal in precipitation [*Epstein and Yapp*, 1976], humidity [*Yapp and Epstein*, 1982b] and the amount of precipitation [*Yapp and Epstein*, 1985]. Despite the positive correlations found, there remains substantial uncertainty as to what biological and environmental information is contained in tree ring isotopic signals [*DeNiro and Cooper*, 1990]. For example some studies [*DeNiro and Cooper*, 1990; *White et al.*, 1994] have found no evidence for a humidity signal but the deuterium signal of cellulose is thought to reflect precipitation only to a first approximation [*Roden and Ehleringer*, 2000].

4.1.1 The Hydrogen Isotope Signal in Precipitation

The precipitation process begins with the condensation of water molecules on nuclei such as smoke, dust or sea salt particles, after which the growth of droplets is by collision and coalescence [*Jouzel*, 1986]. Precipitation is the result of cooling of an air mass [*Friedman et al.*, 1964], for example by adiabatic cooling as an air mass rises over mountains, at warm or cold fronts or because of convection. It may also be caused by radiative cooling in the deposit of frost and dew and by relatively warm, moist air flowing over cool surfaces [*Friedman et al.*, 1964]. As clouds cool the amount of condensed water increases and precipitation occurs when the water droplets reach a size that causes them to fall. Some droplets will collect more condensed water vapour as they fall while others may evaporate and return to the atmosphere. As air ascends the condensate formed at any stage falls through the foregoing ones [*Dansgaard*, 1964] leading to mixing with other droplets and the taking up of new vapour. It is seen that there is less exchange between droplets and water vapour in areas of high humidity.

The condensed phase of clouds is enriched in heavy isotopes versus the surrounding water vapour as there is rapid exchange between the two phases [*Gat*, 1980]. The lower vapour pressures of the heavier water species, HDO, HTO and $H_2{}^{18}O$ compared with H_2O mean that as air cools there is a preferred condensation of the heavier species which are subsequently removed faster by precipitation [*Zahn et al.*, 1998]. Only hail and snow, which are frozen, are immune to exchange and are able to carry high tritium and deuterium levels all the way to the ground.

There are seasonal variations in the distribution of isotopes in precipitation [*Gat*, 1980], that are generally correlated with temperature. This results in winter precipitation being depleted in heavy species relative to summer rains. Isotopic depletions are also related to latitude, altitude, distance from the coast and the amount of precipitation [*Dansgaard*, 1964]. At low latitudes net evaporation of water from the ocean produces vapour which is depleted in heavy isotopes. As this vapour is transported poleward the decreasing temperature causes the vapour to condense on route. As the heavier species are more likely to condense first the vapour becomes progressively more depleted in these isotopes. This is a *Rayleigh Distillation* which results in the δD and δT of any further condensates also being lower as the vapour becomes increasingly depleted in the heavier species. This "amount" effect is related to the volume of precipitation that occurs. It is seen that there are low δD values in rainy months with higher values being seen in dry periods [*Dansgaard*, 1964].

The δD and δT composition of precipitation at any location results from the condensation temperature, the degree of evaporation and exchange in falling drops, and seasonal changes in the source area of the vapour. The exact signal recorded is strongly affected by local climate and micro-meteorological processes associated with rain formation [*Taylor*, 1966].

4.1.2 The Hydrogen Isotope Signal Recorded in Tree Ring Cellulose

The growth of a tree is controlled more by the movement of water than by any other substance [*Fritts*, 1976] and is the only source of hydrogen available to them [*Dawson and Ehleringer*, 1993]. The majority of water that a tree receives reaches it through its root system and is then carried to the leaves through the xylem. For most trees the root system extends well beyond the reach of the branches and is densest in soil layers where both oxygen and soil moisture are plentiful. A continuous hydrostatic system is formed by the water in a tree [*Fritts*, 1976], so that as water molecules diffuse out of leaf cells additional molecules take their place. Trees and plants act as intermediaries in the large scale hydrological cycle [*Yapp and Epstein*, 1982a] as water that is drawn from soil by their roots passes up through the stems and transpires from the leaves, often in large quantities.

4.1.2.1 Sources of Water to Trees

There are three sources of water available to trees [*White et al.*, 1985]; precipitation, groundwater and soil moisture. Growing season precipitation (summer) is generally enriched in heavy isotopes relative to groundwater and soil moisture which are both integrations of precipitation over time. *White et al.* [1985] identified three main water source scenarios for trees:

1. A *groundwater extreme* to describe sites with a very high water table where trees will have a large supply of groundwater to draw on even during periods of heavy summer rainfall. In this case $\delta D_{\text{SOURCE WATER}} = \delta D_{\text{GROUNDWATER}}$.

2. An *intermediate case* where groundwater is available to deep roots and summer rain is available to roots near the soil surface. At such sites trees will use both water sources and the δD value of the source water will reflect the relative contributions of the two.

3. A *summer rain extreme* to describe sites with poor soil development, minimal water content and groundwater that is inaccessible to even the deepest roots. At such locations the only water available to trees is summer, growing season rainfall and $\delta D_{\text{SOURCE WATER}} = \delta D_{\text{SUMMER RAIN}}$.

As most temperate trees tend to be best described by the intermediate case it is important to quantify the relative contributions of each source of water to allow precipitation reconstructions to be made from cellulose data. A study by *Woods and O'Neal* [1965] introduced tritiated water to three different soil depths. Within four hours elevated ^3H levels had been detected in the transpired water from surrounding small trees. Three days after the tracer injection 38 times more ^3H (per unit volume) was present in transpired water drawn from the upper 30.5 cm of soil than from soil at depths from 61-91.5 cm. From these results summer rain can be expected to make a significant contribution to tree source water, even when there is a steady supply of groundwater from greater depths. However the results will vary with tree species and soil type and shouldn't be considered universally applicable.

4.1.2.2 Evapotranspiration

It is known that the moisture in leaves is considerably enriched in heavy isotopes with respect to ambient precipitation. This is caused by fractionations that occur during evapotranspiration and can vary for different species. During evapotranspiration within the leaves complicated isotopic interactions occur between atmospheric water vapour and water taken up from the soil [*Schiegl*,

1974]. The isotopic enrichment of sap in leaf tissues occurs when there is evaporative gas exchange between the atmosphere which has a humidity of less than 100% and the inside of the leaf, which has a humidity close to 100% [*Dawson and Ehleringer*, 1993]. The heavy isotope enrichment in plant leaf water is proportional to relative humidity, atmospheric vapour composition and to both kinetic and equilibrium factors that are a function of temperature and the airflow dynamics in the leaf boundary layer [*Buhay et al.*, 1996]. Typically evapotranspiration causes leaf water to be enriched in deuterium by 40-50 ‰ [*Engel and Macko*, 1993].

Gas exchange in leaves occurs via stomata, which are pores that permit the rapid exchange of gases with the atmosphere and which are largely responsible for leaf water isotopic enrichments. Stomata can occur in all arboreal organs [*DeNiro and Cooper*, 1990], including trunks and stems but they are most widely distributed in leaves. Gas exchange can occur in tree trunks through lenticels, pores that connect the intercellular spaces in the bark to the atmosphere. Both the rings of the cambium and sapwood inside the bark are relatively impermeable to gas [*DeNiro and Cooper*, 1990] meaning that sap water cannot evaporate into intercellular spaces as is seen in leaves. Water can only reach the atmosphere from the trunk by diffusing into the bark before being lost to the atmosphere by widely spaced lenticels, which are not present in all trees.

Soil surface evaporation can lead to an enrichment of deuterium in water greater than would be seen from transpiration alone, which means trees incorporate water with a more positive δD than the annual average [*Yapp and Epstein*, 1982b]. This can occur if the infiltration rate of water into the soil is slow enough to cause increases in the δD value of precipitation due to evaporation while on the soil surface. Generally however soils are a caplillary system so they allow little mixing or fractionation of precipitated water [*Eriksson*, 1965] so the isotopic signal of the water evaporated from them is equivalent to precipitation.

4.1.2.3 Cellulose Synthesis and Fractionations

Water enters a tree, via the roots, with no apparent fractionation [*Engel and Macko*, 1993] and travels to the chloroplasts, which are the site of photosynthesis. The pathway of water through the trunk is enclosed by suberised and lignified tissues that prevent gaseous exchange with the atmosphere, therefore enrichment of xylem sap should not occur until the onset of evapotranspiration [*Dawson and Ehleringer*, 1993].

Cellulose synthesis begins with the production of glucose within the chloroplasts of tree leaves [*DeNiro and Cooper*, 1989] but as is illustrated by Figure 4.1 sucrose is the form in which fixed carbon is translocated through the phloem to other parts of the plant. Neither cellulose or lignin,

which make up the bulk of wood, are formed from glucose produced directly by photosynthesis but from sucrose which has been translocated from the leaves or from reserve carbohydrate storage elsewhere in the plant. Therefore the synthesis of cellulose that leads to the formation of annual tree rings is formed in the presence of sap, not leaf water. Critically, cambial growth typically occurs during the warmer months of the year during net photosynthesis so that the relative contribution of newly formed glucose and long term storage starch depends on species and the time of year [*DeNiro and Cooper*, 1989].

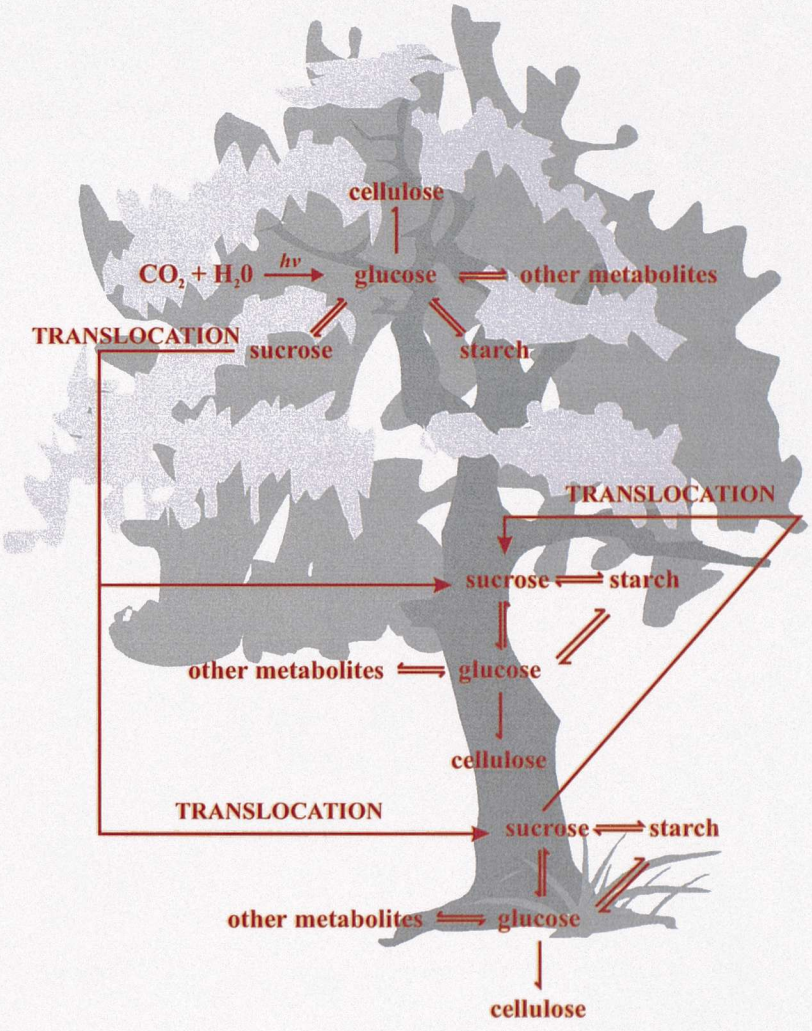

Figure 4.1. Schematic representing the biochemical and physical processes linking, glucose, sucrose, starch and cellulose in leaves (top), the shoot or trunk (middle) and the roots of a tree. Adapted from DeNiro and Cooper [1989].

As well as evapotranspiration leading to deuterium enrichment in leaves, the final isotopic signature of wood cellulose is also the result of fractionation between the carbohydrates being synthesised in the leaves and the water passing through them. The transfer of hydrogen from water molecules in the leaf to carbon-bound hydrogen in cellulose involves many biochemical

steps in which the bonding of the hydrogen atom is changed, all of which introduce the possibility of fractionation. Photosynthesis has a major affect on the deuterium content of organic matter [*Yakir*, 1992] and acts to deplete cellulose relative to the metabolic water used. However post-photosynthetic modification in an isotopically different water fraction in the stem enriches cellulose in heavy isotopes. Within the trunk sugars that have been translocated from the leaves are metabolised while being exposed to groundwater that has not been fractionated. It is thought [*Yakir*, 1992] that such enrichments may be the result of carbon bound hydrogens exchanging during metabolism via complex enzyme catalysed reactions. Such processes could enrich cellulose by an equilibrium fractionation due to rapid exchange or a kinetic effect associated with breaking the C-H bond. These fractionation factors are not well known but this effect may partly account for the good correlation that is seen between the δD value of cellulose and that of groundwater.

The final stable isotope concentration of cellulose is dependent on the interaction of three processes as is outlined in Figure 4.2 [*Dawson and Ehleringer*, 1993]:

1. The magnitude of evaporative enrichment in leaf water which is directly involved in photosynthesis (carbohydrate formation). If there has been an isotopic enrichment in the leaf water the carbohydrates would be expected to be enriched in the heavier isotopes relative to the tree's source water.

2. The fractionations associated with the process of photosynthesis, as it is capable of producing carbohydrates with carbon bound hydrogens that have δD values depleted by 150 to 200‰ relative to the source water.

3. Post photosynthetic metabolism can also lead to isotopic fractionations. For example when glucose is β-linked to form cellulose there can be an enrichment in δD of 140 to 180‰ relative to the source water.

Isotope studies indicate that there appears to be a "balance" between enrichment and depletion such that the δD measurement of cellulose correlates well with that of source water [*Dawson and Ehleringer*, 1993]. This relationship may be due to the cellulose being synthesised in the presence

of water that has not been subject to any biological or biophysical fractionation processes rather than a fine balance between the described processes.

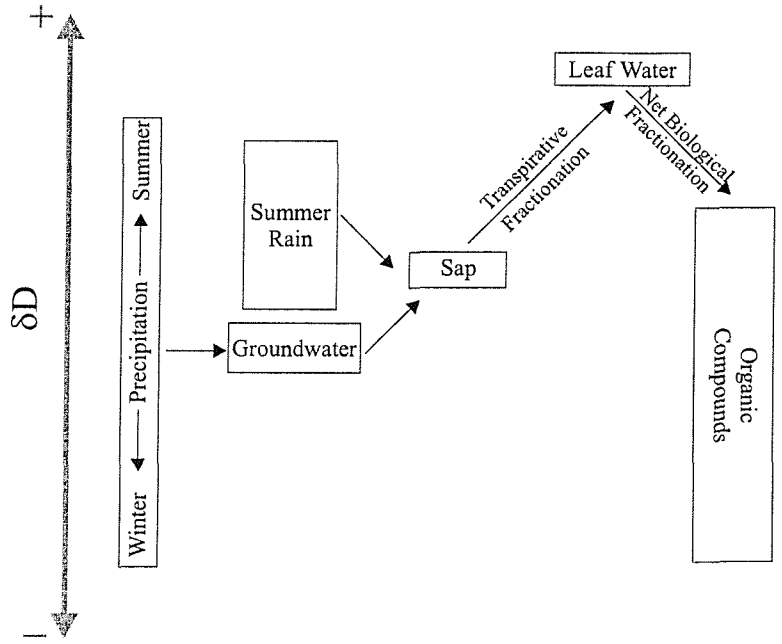

Figure 4.2. A simplified diagram of the changes in the hydrogen isotopic ratio in the pathway of hydrogen into plant organic matter. The heavy isotope, deuterium is enriched in leaf water due to evapotranspiration and depleted in fixed organic matter. Adapted from Engel and Macko [1993].

4.2 The Tree Sample

Time series of tritium and deuterium were constructed from an Irish tree and compared with the weather station data from Valentia, Ireland which is the only Irish station to collect precipitation samples for ^{3}H analysis. The sample used was a cross section of cedar tree donated by Professor Mike Baillie from the Queens University Belfast.

The tree died naturally when it was blown over during the Boxing Day storm of 1998. The tree grew in Tollymore Forest Park, Northern Ireland, close to the Irish Sea (Figure 4.3) at an altitude of approximately 100m on granitic bedrock. Originally, an oak sample from a tree felled close to Valentia was going to be used but the rings were found to be too narrow to sample over the critical bomb spike period. This was seen to be typical of oak samples from the area and the large amount of wood material needed for ^{3}H measurements made finding an alternative necessary. For the ^{3}H time series 1-2g cellulose samples were prepared, which necessitated approximately 5g of raw wood from each annual ring. Although the cedar sample is somewhat distant from Valentia

(see Figure 4.3) it had consistently wide rings (~9-10mm) from 1935-1998, which gave sufficient material to make the measurements.

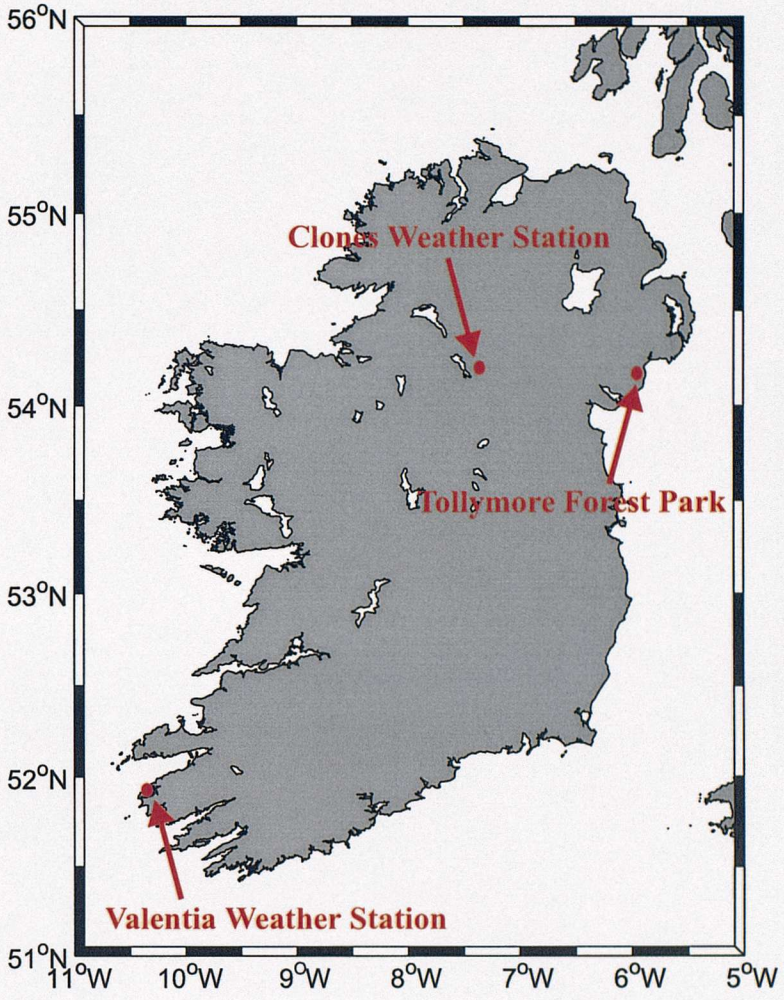

Figure 4.3. Map of Ireland showing the location of the Valentia weather station (51.9°N, 10.25°W) and Tollymore Forest Park (54.21°N, 5.93°W) from where the cedar tree sample was collected.

A tree ring is usually the result of a yearly flush of growth [*Fritts*, 1976] which begins in the spring and ends in summer or early autumn, so that only one layer is produced per year. The sharp boundaries between rings occur because the cells along the inner boundaries of a ring are larger and have thinner walls than those along the outer boundary. However not all rings are distinct annual increments of growth [*Fritts*, 1976]. Limiting factors such as water, temperature, light and oxygen can cause no growth to begin so no ring is produced. Also a period of stress during the growing season can cause two or more growth rings to form within the year. The cedar cross section showed no evidence of double or missing rings and was therefore suitable for time series work.

The wood of an annual ring is composed of *late* wood, which is formed in late summer and early autumn and *early* wood which is that formed in spring [*Epstein and Yapp*, 1976]. Late wood is less porous, more dense, darker in colour and isotopically distinct from the early wood portion of the same ring. *Epstein and Yapp* [1976] found that the late wood portion of annual rings is consistently depleted in deuterium relative to that in the early wood portion of the sample. The isotopic difference between the two fractions was attributed to either the tree using stored starch from the previous summer to form early wood or the spring water source being a mixture of rain and isotopically lighter melted snow. However the magnitude of the depletion was seen to vary from ring to ring with a difference of 52‰ measured in 1964 compared to 7‰ in 1962.

In this study wood from the whole ring has been used to give the amount of material required for the analyses. Following *Epstein et al.* [1976] it has been assumed that the signal from a total growth ring will suffice to evaluate isotopic records in terms of climatic trends, and will reflect an average of the conditions during the growth year.

4.3 An Irish Tree Ring Deuterium Reconstruction

A time series of deuterium measurements was made as a precursor to the tritium work to provide information on the likely water sources available to the tree. Also the apparent fractionation between precipitation and the cellulose samples evident from deuterium will be a useful indicator of the likely fractionation to be expected for ^{3}H. As there has been no work done on low level ^{3}H analyses in tree rings the deuterium record will provide a means to compare results from this tree to earlier work relating cellulose stable isotope signatures to climatic variables.

The time series was measured in the Stable Isotope Laboratory at the Institute of Arctic and Alpine Research in Boulder, Colorado by Mark Drier and Professor Jim White. Prior to this, cellulose was extracted from the cedar tree rings as described in Chapter 3 (microwaving to remove lipids, oils and other resinous material followed by lignin removal as described by *Loader et al.* [1997]). Between three and five measurements were made for each sample, depending on the amount of cellulose available, and the data shown represents the mean of the data for that year.

The measurements were made on cellulose nitrate as this is the standard technique for stable isotope analyses where small quantities of cellulose are used. A full description of the nitration method used can be found in *White* [1983]. To make measurements of stable isotopes in cellulose nitrate it was necessary to convert the carbon bound hydrogen atoms to hydrogen gas prior to

analysis on a mass spectrometer. First the samples were combusted in quartz tubes that contained copper (II) oxide, to provide a source of oxygen, at 900°C. Water was then separated from the other combustion products (CO_2 and N_2) on a dedicated vacuum line before being reduced to hydrogen gas by contact with hot zinc. It has been found [*Schimmelmann and DeNiro*, 1993] that the combustion process yields less than the theoretical amount of water, due to the hydration of glass and quartz but that this does not affect the determination of stable hydrogen isotope ratios. The techniques used are described in detail in *Schimmelmann and DeNiro* [1993] and *Coleman et al.* [1982]. The isotopic ratio of the gas produced was then measured on a dual inlet stable isotope mass spectrometer (Fisons VG Optima).

All of the deuterium measurements are expressed relative to Standard Mean Ocean Water (SMOW) using the formula:

$$\delta D = \left(\frac{(D/H)_{sample}}{(D/H)_{SMOW}} - 1 \right) \times 1000 \qquad (4.1)$$

4.3.1 Importance of Removing Hydroxyl Group Contamination

When the deuterium composition of cellulose nitrate was measured samples of untreated cellulose were also run. The results of this experiment are shown in Table 4.1.

Year	Nitrated (δD)	Raw Cellulose (δD)	Difference
1966	-67.97	-52.74	-15.23
1976	-62.41	-35.53	-26.88

Table 4.1. Comparison of the δD values of nitrated and untreated cellulose samples from the same year. The difference between the two highlights the importance of removing hydroxyl group contamination prior to doing isotopic analyses that reflect conditions the year that the cellulose was formed.

It is clear that the untreated cellulose samples are systematically enriched in deuterium compared to the nitrated cellulose from the same year. The cellulose has evidently been in contact with water or vapour with a higher δD than the year it was formed after synthesis, emphasising the importance of nitrating or exchanging samples prior to doing isotopic analyses as discussed in Chapter 3. The difference between nitrated and raw cellulose values differs for each year highlighting the many water and vapour interactions a sample will have been subjected to since it was formed.

4.3.2 Comparison to Precipitation

The deuterium concentrations measured in the cellulose nitrate samples (δD_{CELL}) were compared with those in annual precipitation at the Valentia weather station. Two comparisons were made, one with mean annual precipitation and one with a weighted annual mean which was defined as:

$$\delta_m{}^w = \frac{1}{P}\sum_{i=1}^{12} p_i \delta_i \tag{4.2}$$

where P denotes the amount of annual precipitation, p_i is the amount of monthly precipitation and δ_i is the monthly isotopic ratio of deuterium in precipitation [*Dansgaard*, 1964]. This weighted mean value is determined by conditions during rainy periods whereas the mean value of annual precipitation reflects the gross climatic conditions year round. In areas where the amount of precipitation varies significantly the unweighted mean may be heavily influenced by a few months that are extremely different from the norm. The weighted mean is also useful when there is not deuterium data for every month of the year, as is the case at Valentia when the unweighted mean is again likely to be biased.

4.3.2.1 Irish Climate

The climate of Ireland, like the rest of Northern Europe is influenced by the warm waters of the Gulf Stream and is in the path of prevailing south westerly winds coming from the Atlantic Ocean. This results in the country having an equable climate with no extremes, with January and February being the coldest months and July and August the warmest. Ireland is renowned for its rain which occurs mostly in the west of the country in the winter. This is illustrated by Figure 4.4 which shows that twice as much rain falls at Valentia in December and January than in April and July. This significant variability again makes a comparison of δD_{CELL} with the weighted mean defined in Equation 4.2 a useful tool to ensure the results aren't biased by wet or dry months.

However the map in Figure 4.3 illustrates that Tollymore Forest Park is further east than the Valentia weather station and is therefore likely to have a drier climate, assuming that the mean transport of water vapour is from the west. A comparison of precipitation at Valentia with that at the Clones weather station, that closest to the tree location, shows that this is indeed the case. The average annual rainfall, averaged over the period 1961 to 1996 is 1430.1mm at Valentia compared

to 928.4mm at Clones (source *Weather Ireland*). As expected, locations further away from the Atlantic Ocean have a drier climate.

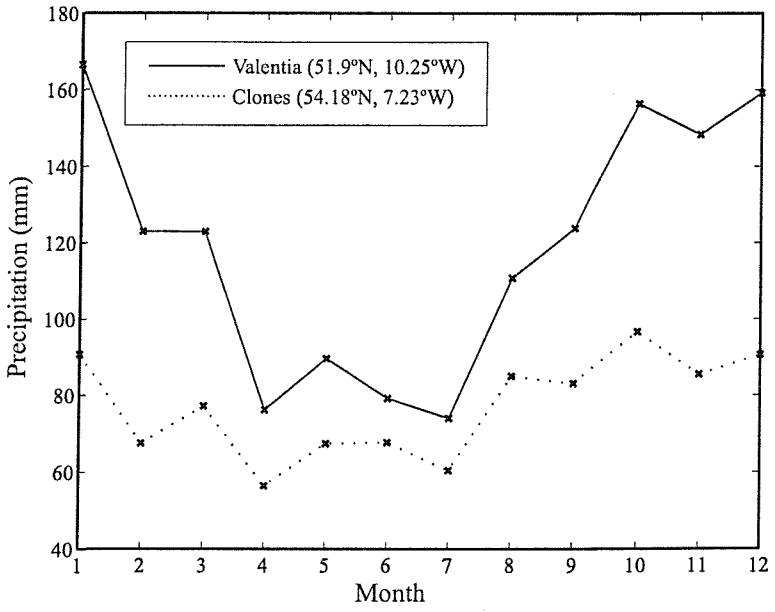

Figure 4.4. Comparison of the monthly amount of precipitation at the Valentia and Clones weather stations, Northern Ireland, averaged over the time period 1961-1996. The Clones weather station is that closest to Tollymore Forest Park from where the cedar tree sample originated. The drier climate of the more easterly Clones station is clearly evident which will affect the δD content of precipitation there, making it isotopically lighter.

4.3.2.2 Correcting for the Continental Effect

Atmospheric circulation over the European continent has an essentially zonal character [*Rozanski et al.*, 1982] and the isotopic composition of precipitation can be considered as a flux across the western boundary. Consequently precipitation at Tollymore Forest Park can be expected to be isotopically lighter than at either the Valentia or Clones weather station, both of which are located further west.

As air masses move across Ireland from the Atlantic Ocean the heavy isotopes will condense first so that the vapour becomes increasingly depleted in heavy isotopes. The decrease in the amount of precipitation further east in Ireland will result in later condensates being depleted in deuterium. *Rozanski et al.* [1982] studied the continental effect on the stable isotope composition of European precipitation, assuming that the meridional component of the water vapour transport is minimal. The work was based on IAEA data from 10 stations across Europe from Valentia to

Kraków (50.05°N, 19.48°E). The deuterium composition of precipitation at these sites was seen to correlate with surface air temperature and the δD was seen to deplete with increasing distance from the Atlantic coast. This continental effect was seen in both summer and winter precipitation and the resulting gradients were –3.3‰ per 100km in winter and –1.3‰ per 100km in summer.

A correction has been applied to all of the Valentia weather station precipitation δD values to take into account this continental effect. The correction applied was –2.3‰ per 100km, the average of the *Rozanski et al.* [1982] winter and summer values. As the zonal distance between Valentia and Tollymore Forest Park is 295 km a correction of –6.8‰ was applied to the precipitation δD values.

4.3.2.3 Comparison to Annual Precipitation

The time series of measured cellulose nitrate deuterium concentrations are compared with both mean annual and weighted mean annual precipitation from the Valentia weather station in Figure 4.5.

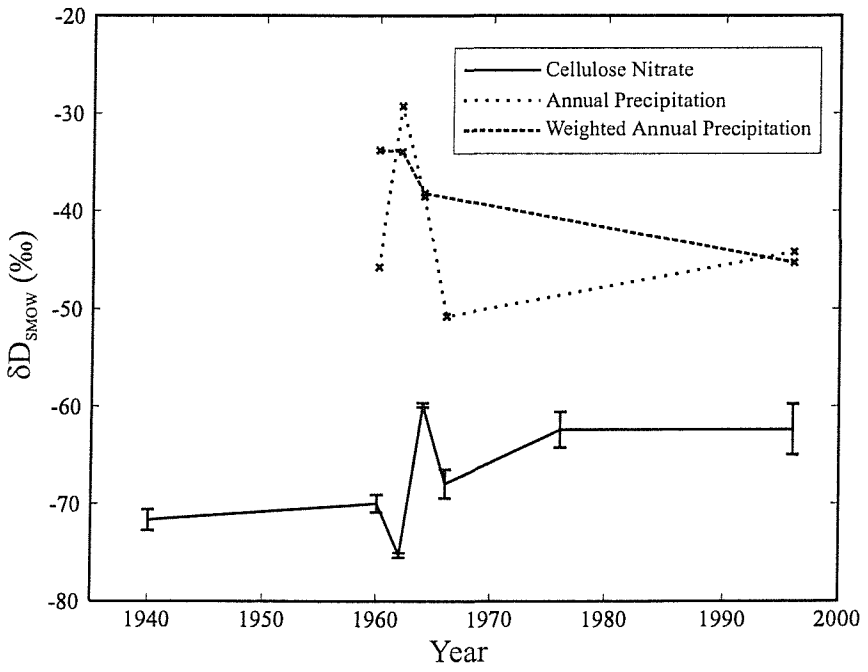

Figure 4.5. A comparison of δD_{CELL} from a Northern Ireland cedar tree with mean annual and weighted mean annual precipitation δD from the Valentia weather station. All precipitation values have been corrected for the continental effect (-6.8‰).

It is clear from Figure 4.5 that the δD_{CELL} values are significantly lighter than precipitation. This agrees with other studies [*Gray and Song*, 1984; *Epstein and Yapp,* 1976; *Yapp and Epstein*, 1982a], though *Pendall* [2000] found δD_{CELL} values for piñon pine cellulose to be enriched by 30-50‰ on average, illustrating the importance of leaf water in some cases. Unfortunately the sparsity of deuterium data at the Valentia weather station makes it hard to statistically correlate the δD_{CELL} values and those of precipitation.

Comparing the cellulose nitrate deuterium content with mean annual precipitation shows the same overall pattern with a clear spike being seen in 1964 after which the values decrease before increasing again. However not all of the years had 12 months worth of δD measurements at the Valentia weather station, for example only 1964 and 1996 have complete data sets with 1960, 1962 and 1966 having 10, 7 and 1 months respectively. This means that the annual means may be biased so a better comparison may be with the weighted annual mean, though there are only 4 data points available. However Figure 4.6 shows that although there is only a poor correlation between weighted annual precipitation and δD_{CELL} ($r^2 = 0.51$) it is a significantly better correlation than is seen with the annual mean ($r^2 = 0.13$). Although the annual precipitation signal is reflected in the cellulose deuterium concentrations there are other factors and processes involved as well.

4.3.2.4 Comparison to Seasonal Precipitation

The δD_{CELL} values were also compared with seasonal precipitation signals as tree ring δD values are not always a reflection of annual precipitation averages. Whether a tree reflects annual precipitation or seasonal components of the signal depends on local growth site conditions such as slope angle, soil drainage, root geometry and the seasonality of climate [*Yapp and Epstein*, 1985].

The cellulose deuterium values were compared with summer precipitation, which was defined here as between May and August and winter precipitation, from November to February. No correlation was found between δD_{CELL} and winter precipitation ($r^2 = 0.08$, N = 5) but there was a correlation with summer, growing season precipitation, though the lack of data means that the results have no statistical significance. The slope of the linear regression with summer precipitation is very close to 1 suggesting that this signal is the primary factor controlling δD_{CELL} for this tree.

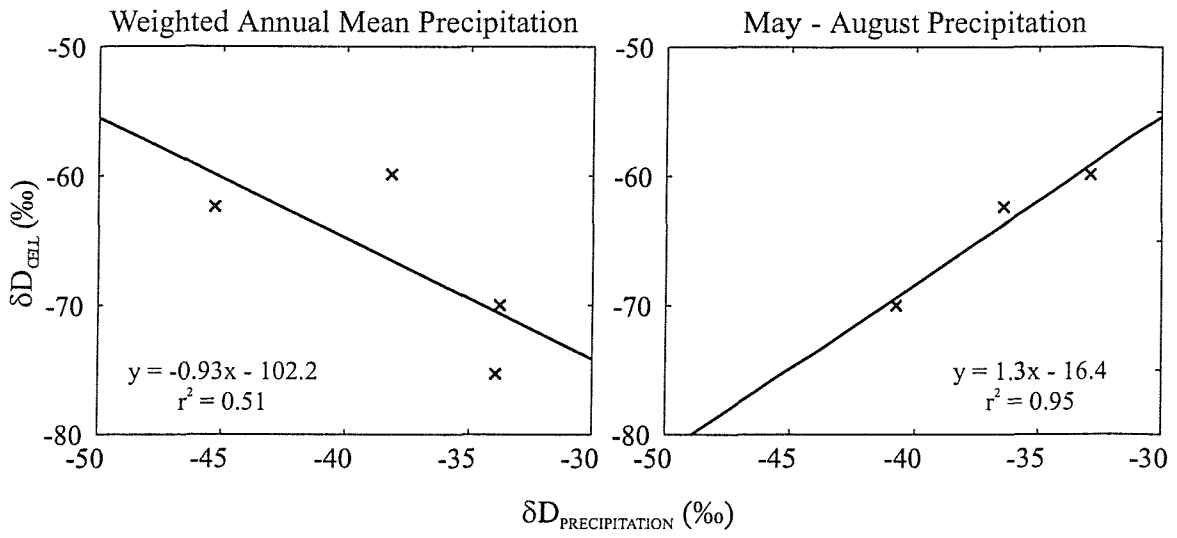

Figure 4.6. Correlation of the cellulose nitrate values with weighted annual, May-August and November-February precipitation. All of the precipitation values have been corrected by –6.8‰ to account for the distance between the Valentia weather station and the tree sample.

Overall lack of data makes it hard to elucidate water sources for this tree but the trends indicate that the cellulose does reflect precipitation and that the signal may be that of summer precipitation. This indicates that the major water source for the tree is precipitation and that it is not using a large amount of isotopically lighter groundwater or stored starch.

4.4 An Irish Tree Ring Tritium Reconstruction

A time series of tritium concentrations in cellulose was constructed from the same tree sample described in 4.2 for δD analysis. For these samples the exchange technique described in 3.3.7 and Appendix 6 was used to remove hydroxyl group contamination thus avoiding the dangers of flame sealing 1-2g samples of cellulose nitrate. The samples were then degassed as described in 3.3.8 and stored in a freezer for between 4 and 5 months prior to analyses of the ingrown helium (see 3.4). The ^{3}H concentrations of the time series samples is shown in Table 4.2.

Year	Tritium (TU2003)	Comment
1940	< 0.35	Applying fractionation correction described in the text to account for significant atmospheric ^{3}He.
1952	3.46 ± 2.97	
1960	*Aborted due to high ^{4}He – probably a leak in the bulb seal*	
1961	5.87 ± 2.09	
1963a	81.39 ± 7.08	
1963b		*Hole in the seal*
1966	19.65 ± 3.29	
1976	< 1.01 ± 2.36	
1996	< 0.92 ± 2.73	

Table 4.2. The tritium concentrations measured in exchanged cellulose samples from Tollymore Forest Park, Northern Ireland. Where a sample is given a ratio preceded by a less than symbol then the ratio in the sample is lower than the detection limit, the number quoted. All values presented are TU2003, the tritium in each sample on January 1st 2003.

4.4.1 Correcting for Atmospheric Contamination of the 1940 Sample

The tritium concentration measured in the 1940 cellulose sample, calculated as described in 3.4.2 was significantly higher than would be expected from pre-bomb ^{3}H levels. A measurement of 6.35 ± 2.90 TU2003 was found which corresponds to a 219 TU signal in 1940. This is significantly higher than pre-bomb estimates of the ^{3}H concentration of precipitation (1-6TU, *Craig and Lal* [1961]). As there is no evidence from the other samples that the tree sample itself, or the sample preparation has exposed the cellulose to this level of contamination the elevated measurement appears to be associated with fractionated atmospheric helium contamination during storage or analysis.

When the cellulose sample from 1940 was analysed on the mass spectrometer the cracking of the sample was observed to be extremely violent. When the pneumatically operated cracker (see Section 3.4) activated, the glass sample bulb was seen to move significantly, which is not usually the case. As was discussed in Section 3.4.9 the crackers were not designed to be used with the wide necked bulbs used for cellulose analysis and this has led to contamination in some of the exchange test samples. However the magnitude of the movement seen with the 1940 sample was significantly larger than had been witnessed before, presumably compromising the seal, and the subsequent contamination was evident in the results. The measured ^{4}He signal from 1940 (2.56 x

10^{-13} moles) was larger by approximately an order of magnitude compared with the other time series samples (3.20 x 10^{-14} moles for 1996, 1.98 x 10^{-14} moles for 1952) indicating that the sample had undergone significant helium contamination. It is probable that as the bulb moved during cracking air rushed into the sample as the o-ring, which provides the seal, was dislodged. Experience with a large number of seawater ^{3}H measurements has shown that results characterised by such high degrees of contamination are usually unreliable due to a significant degree of isotopic fractionation in the added helium.

Atmospheric contamination due to incomplete degassing or diffusion of helium through glass sample bulbs during storage is usually corrected for using Equation 3.10 and the measured ^{4}He signal for a sample, assuming an atmospheric isotopic ratio. Such an approach is unlikely to be appropriate in this case. Although air in an incompletely degassed sample will exhibit an atmospheric ratio it is unlikely to be the case for an o-ring leak such as this, which will be fractionated and enriched in the lighter isotope ^{3}He.

To attempt to account for this fractionation it has been assumed that the leak rate is limited by the molecular diffusivity of the species. In lieu of suitable molecular diffusivity data, a kinetic argument is used to explain the fractionation . The fractionation factor between ^{3}He and ^{4}He will be defined as:

$$\alpha = \frac{D_{^3He}}{D_{^4He}} \tag{4.3}$$

where D is the molecular diffusivity. The kinetic theory of gases states that the molecular diffusivity of a gas is related to its modal velocity, which is in turn related to the mass of the isotope under study. As all isotopes have the same kinetic energy at a given temperature $\left(\frac{1}{2}mv^2\right)$ the molecular diffusivity is proportional to $\frac{1}{\sqrt{m}}$ where m is the reduced mass. The reduced mass of a monatomic molecule is simply its atomic mass so the fractionation factor α for such a molecular leak is given by:

$$\alpha = \frac{\sqrt{m_{^4He}}}{\sqrt{m_{^3He}}} \tag{4.4}$$

Taking the atomic masses of ^3He and ^4He to be 3.01603 and 4.00260 amu respectively a fractionation factor of 1.15 was found.

The amount of ^3H in the 1940 cellulose sample was then recalculated assuming that the o-ring leak had fractionated the air so that its ^3He content was enriched by a factor of 0.075 ± 0.075 compared to the atmospheric ratio. This yielded a sub-detection limit tritium concentration which is more representative of pre-bomb conditions. However two things should be noted, firstly that it is virtually impossible to have confidence in the actual ^3H content of a sample which has been compromised in this way, and second diffusion may not be an appropriate model to use for a leak that may be better represented as a mass transfer process.

4.4.2 Comparison to Annual Precipitation

To compare the cellulose tritium concentrations ($^3H_{CELL}$) with those in precipitation it is again necessary to apply a continental correction to take into account the different locations of the tree sample and the Valentia weather station. As there is no suitable data from which to estimate the continental effect for ^3H an estimation of the fractionation is made by comparison to deuterium.

It is assumed that the fractionation of ^3H relative to deuterium is purely mass dependent and that the two can be related using Equation 4.5. This equation, which was determined for sulphur isotopes and has been shown to hold for the three isotopes of oxygen [*Thiemens and Bhattacharya*, 1990] relates fractionation effects ignoring mass independent terms.

$$\delta T/\delta D = \frac{1 - m_H/m_T}{1 - m_H/m_D} \tag{4.5}$$

By taking the mass of hydrogen (m_H) to be 1.00783 amu, the mass of deuterium (m_D) to be 2.0140 amu and that of tritium (m_T) to be 3.01605 amu the fractionation factors for ^3H should be 1.3328 larger than that for deuterium. The correction factor applied to all of the Valentia precipitation deuterium measurements was –2.3‰ per 100km (see 4.3.2.2) which translates to a correction of –3.1‰ per 100km for ^3H. Therefore all Valentia weather station ^3H concentrations were depleted by 0.9% for comparison with $^3H_{CELL}$.

Again the cellulose ^{3}H values were compared with both the annual mean ^{3}H in precipitation and the weighted annual mean (Equation 4.2) to take into account climatic variability. It is evident in Figure 4.7 that the cellulose tritium concentrations are reflecting precipitation, with a clear bomb spike in 1963. It appears that, as is seen with deuterium, the cellulose is depleted in ^{3}H with respect to ambient precipitation, though the lack of Valentia data prior to 1960 makes a complete comparison impossible.

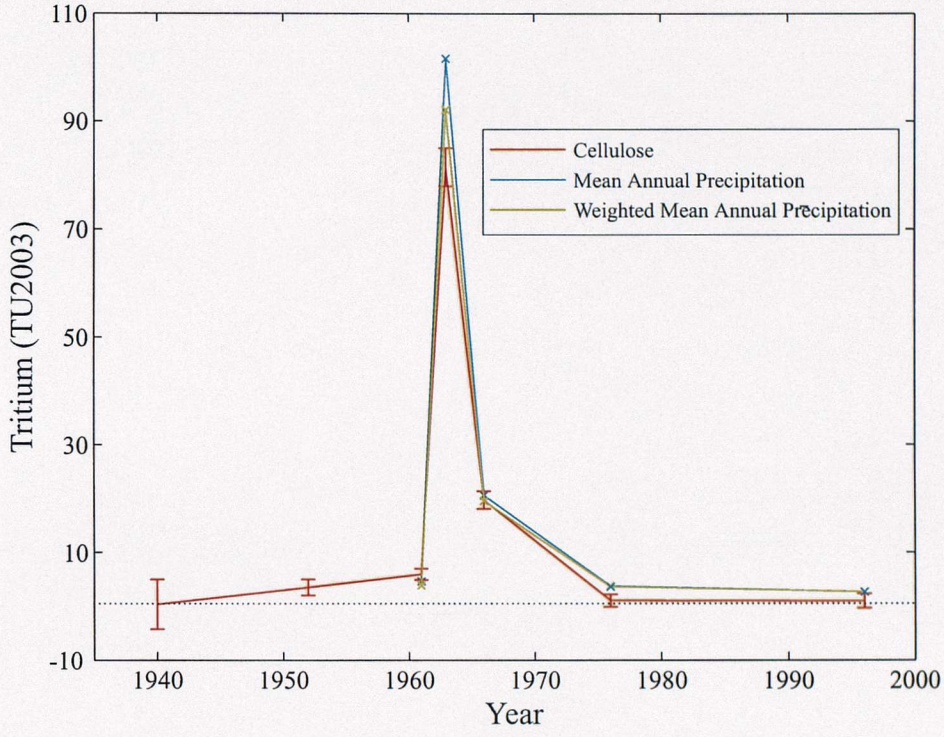

Figure 4.7. Comparison of $^{3}H_{CELL}$ from a Northern Ireland cedar tree with mean annual and weighted mean annual ^{3}H in precipitation from the Valentia weather station. All precipitation values have been corrected for the continental effect and all tritium concentrations have been decay corrected to January 1st 2003 (TU2003). For the cellulose measurements which were sub-detection limit (1976 and 1996) the number plotted is the detection limit for the sample at the time of analysis.

This good reflection of both annual mean and weighted annual mean precipitation indicates that precipitation is an important water source for the cedar tree under study and that stored starch from a previous year is not an important factor. As there appears to be no smearing of the 1963 bomb spike signal we must conclude that the cellulose ^{3}H signal reflects conditions the year that the material was synthesised. This good reflection of precipitation may result from the consistently wet climate of Ireland with even the driest months having in excess of 50mm of rain at the Clones weather station (Figure 4.4). These results indicate that groundwater does not seem to be an important water source for this tree, though better resolution would be needed to confirm that the signal is not smeared. It should be noted that a second cellulose sample from the 1963

ring, which could have confirmed the presence of a strong bomb spike was prepared but failed on the mass spectrometer because of atmospheric contamination. However confidence in the bomb spike measurements comes from comparing the mass spectrometer output for these samples with water samples (of which the laboratory has a long record of), standards and line blanks. The ^4He levels in the 1961, 1963 and 1966 samples were extremely low compared with standards and were comparable to those seen in water samples, making it unlikely that the observed tritium signals are due to atmospheric helium contamination. Therefore it seems fair to concluded that the tritium measured in these samples is an accurate record of that in the carbon bound hydrogen's of the cellulose itself.

The cellulose ^3H concentrations are directly compared with annual precipitation in Figure 4.8, which shows that there is a very good correlation between the two. There is an equally good correlation ($r^2 = 0.99$, N = 5) between $^3H_{CELL}$ and both annual mean and the weighted annual mean precipitation. However the slope of the regression with the weighted annual mean is closer to unity so there is a better quantitative agreement between the cellulose results and the seasonally weighted values, indicating that there are fewer complicating factors in the relationship.

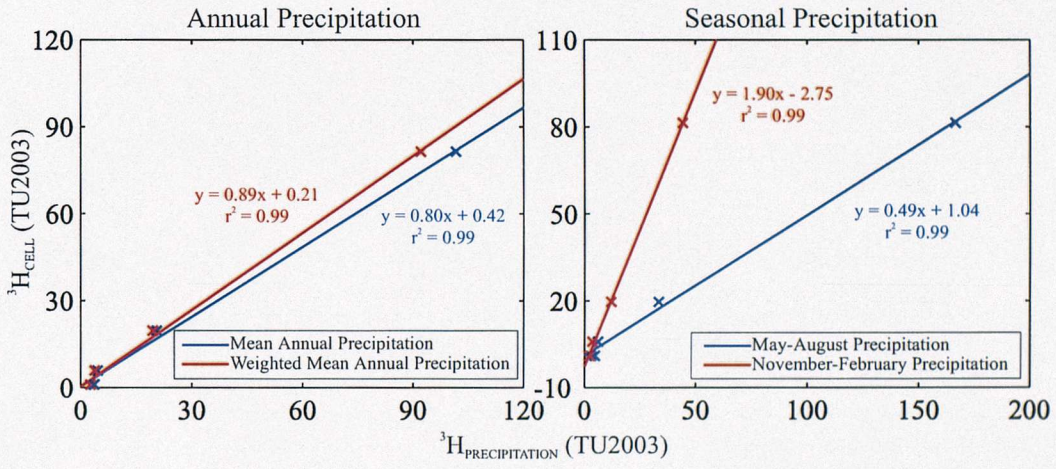

Figure 4.8. Correlation of the cellulose ^3H concentrations with annual and seasonal precipitation indices from the Valentia weather station. All of the values have been decay corrected to January 1st 2003 (TU2003) and the precipitation values have been corrected for the continental effect as described in the text.

4.4.3 Comparison to Seasonally Weighted Precipitation

There is a strong seasonal cycle to the concentration of tritium in precipitation as is illustrated by Figure 4.9. This seasonality is strongly related to the timing of stratospheric-tropospheric exchange [*Enhlat*, 1971] as it determines when tritiated water is rained out. In the northern

hemisphere stratospheric mass is at its maximum in late winter [*Danielsen*, 1968] and inflow to the troposphere occurs mainly in late winter and early spring. However the maximum ^3H in precipitation is seen in June and July which reflects the re-evaporation of soil moisture in summer and the time taken to pump HTO from the tropopause to the lowest levels. In summer, when evaporation exceeds precipitation, HTO stored in soils is re-evaporated providing the atmosphere with another ^3H source. The relatively sharp peak in the Valentia record (Figure 4.9) can be attributed to the effect of soil ^3H which is superimposed on the period of stratospheric input [*Enhlat*, 1971].

As with deuterium, $^3H_{CELL}$ values were compared with both summer (May – August) and winter (November – February) precipitation, using the monthly ^3H in precipitation data from the Valentia weather station. A good correlation is seen with both parameters (Figure 4.8) and it is not possible to statistically distinguish between the two. However as neither relationship is 1:1 it appears that other processes affect the relationships between $^3H_{CELL}$ and seasonal precipitation. Overall the ^3H results do not make it possible to determine whether the ^3H signal from cellulose is a better refection of summer or winter precipitation and it appears that the tree is reflecting annual conditions better. This is somewhat in contrast to the deuterium results which show a better correlation with summer precipitation. However the sparsity of both the deuterium and ^3H data make it hard to elucidate true relationships.

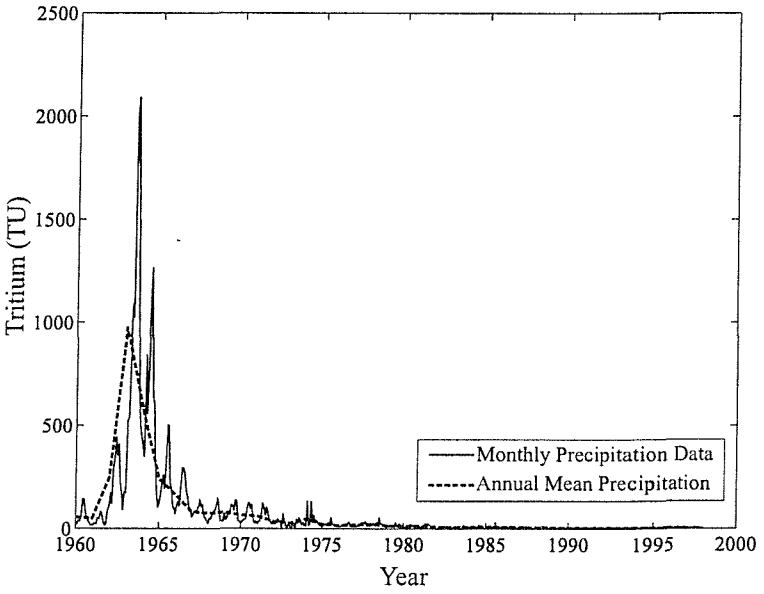

Figure 4.9. Comparison of the monthly ^3H in precipitation data from the Valentia weather station with the annual mean. There is a strong seasonal signal about the inter-annual trend. The data has not been decay corrected.

4.5 Discussion

The deuterium and tritium data presented above suggest that the Irish cedar tree from Tollymore Forest Park is reflecting ambient precipitation. However, as there is so little data available, it is virtually impossible to elucidate the importance of different water sources to the tree or the magnitude of the individual fractionation steps involved in cellulose synthesis.

4.5.1 Apparent Fractionation

The results presented in 4.3.1 indicate that the deuterium composition of the Irish cedar tree cellulose is related to that in ambient precipitation and it appears that the net effect is to deplete the cellulose compared with precipitation. Using the relationships presented in Figure 4.6 the cellulose is depleted by –16.4‰ when compared with growing season precipitation and –102.2‰ when compared with the weighted annual mean. As there is a much stronger correlation with summer precipitation it is assumed that a depletion of –16.4‰ is a more likely representation of the net fractionation between ambient precipitation and cellulose for this tree. Again it should be noted that the lack of statistical significance of the data makes it hard to attach great significance to these numbers.

Epstein et al. [1976] measured the δD of cellulose nitrate from 20 land and aquatic plants over a wide geographical range, from the Yukon Territories to Florida. In addition the δD of the environmental waters associated with the plants were also measured. Waters samples were taken from large bodies of water such as lakes as it was felt that they gave a more integrated representation of plant water source over a growing season. Plant and tree samples were chosen which either had their roots in water saturated soil at the edge of the water source or were growing directly in the water. The samples were then reanalysed by *Yapp and Epstein* [1982a] using an improved nitration technique and an average offset of –22 ± 0.4‰ was determined. The linear regression had a slope of 0.97 and a correlation coefficient of 0.978 indicating that the source water was the primary factor controlling the D/H ratio of the cellulose carbon bound hydrogen. *Gray and Song* [1984] also reported a linear relationship between cellulose nitrate and environmental water with deuterium being depleted by 30‰ and they attributed the discrepancy with the earlier results to the use of different nitration techniques. The net fractionation of –16.4‰ for the δD_{CELL} values presented here is similar to these values considering the large uncertainty in this result due to lack of data.

Looking at the ^3H results there is evidence of a strong correlation between $^3H_{CELL}$ and ambient annual precipitation. The less than 1:1 relationship between cellulose and weighted annual mean

precipitation indicates that there are other factors involved. To assess this the cellulose results were corrected for net biological fractionation during cellulose synthesis and compared again with precipitation. To do this the apparent biological fractionation of deuterium was assumed to be –22 ± 10‰, which encompasses the available deuterium fractionations from literature and the value from the δD_{CELL}, summer precipitation relationship presented above. To translate this into a net ^3H fractionation Equation 4.6 was used and yielded a value of –29 ± 13 ‰, and this value was assumed to represent the net fractionation of ^3H between precipitation and cellulose. Therefore all of the $^3H_{CELL}$ values were recalculated with an enrichment by 2.9 ± 1.3%, thus assuming that the relative fractionation is simply mass dependent, and compared again with weighted annual mean precipitation. Again a good correlation was seen ($r^2 = 0.99$) between the two and the relationship was closer to 1:1 (slope=0.91 compared to 0.89 in Figure 4.8) but it is clear that even correcting for net biological fractionation there are factors other than precipitation which determine the ^3H concentration of cellulose for this tree.

4.5.2 Humidity

Models which relate the δD of cellulose and precipitation have typically taken the form

$$\frac{\delta D_{CELL}+1000}{\delta D_{MW}+1000} = \alpha_B \alpha_E \alpha_K - \alpha_B (\alpha_E \alpha_K - 1) RH \qquad (4.6)$$

where the subscript *MW* refers to meteoric water, *RH* is the relative humidity and α_B, α_E and α_K are the net biochemical, equilibrium and kinetic fractionation factors respectively [*Pendall*, 2000]. This relationship was derived from a model of evaporation from a terminal lake and accounts for enrichment of leaf water by steady state evapotranspiration [*Pendall et al.*, 1999]. The model derivation treats leaf water as a closed system with water only entering through the stem and leaving via transpiration. It assumes that only leaf water is used for cellulose synthesis and that atmospheric water vapour is in isotopic equilibrium with meteoric water. The fractionation factors are temperature dependent and vary from species to species and with climatic regime [*DeNiro and Cooper*, 1989]. Net biochemical fractionation between leaf water and cellulose represents the largest source of uncertainty in the model [*Pendall et al.*, 1999] and must be evaluated for each species and assumed to be constant through time. The kinetic and equilibrium fractionation factors α_E and α_K are reasonably well known with α_E representing the phase change between liquid and vapour [*Pendall et al.*, 1999] and α_K being based on the kinetics of the diffusion of water species through the leaf stomata and the air boundary layer [*Yakir*, 1992]. The biochemical

fractionation term α_B may include fractionation both during photosynthesis as well as post photosynthetic exchanges between cellulose precursors and stored starch.

The importance of relative humidity in the above model was confirmed by *Yapp and Epstein* [1982a] who found that a lower relative humidity results in a more positive value of δD_{CELL}. Lower humidity will lead to more evapotranspiration because of the larger water vapour gradient between the leaf and the atmosphere, thus enriching leaf water and hence δD_{CELL}. *Tang et al.* [2000] concluded that the offset (or apparent biological fractionation) between δD_{CELL} and the δD of the tree source water is most strongly influenced by the humidity term which is more variable than the fractionation factors. It therefore seems likely that some of the scatter that is evident in the precipitation-cellulose relationships for the Irish cedar tree can be partly attributed to differences in relative humidity. However *White et al.* [1994] showed that for Eastern White Pine in the New York area the effect of changing relative humidity was effectively cancelled by changes in air vapour δD, as it was also lower when humidity decreased.

A comparison between the isotopic enrichment predicted by Equation 4.6 and measured leaf water was made by *Flanagan and Ehleringer* [1991] who studied leaf water in a controlled gas chamber, a greenhouse and in the field. They found that the model overestimated the degree of enrichment observed. This was attributed to two processes, first that vacuum distillation of leaf water will sample vein water which should be isotopically indistinct from stem water as well as leaf bulk tissue water, though this effect was not large enough to explain the discrepancy seen with the model predictions. Secondly the model assumes that leaf water has reached a steady state isotopically which is often not the case in the field when environmental conditions change rapidly during the course of a day and over a season. Also as is shown by Figure 4.1 wood cellulose is not formed directly by photosynthetically produced glucose but from sucrose that has been translocated from the leaves or from reserve carbohydrate storage in other parts of the plant. Therefore cellulose synthesis in tree trunks occurs in the presence of sap water, which is isotopically indistinct from the water taken up by the roots, not isotopically enriched leaf water [*DeNiro and Cooper*, 1989]. This process will effectively erase leaf water effects, particularly humidity but will likely yield a much simpler system where cellulose δD is simply related to the isotopic composition of source water [*White et al.*, 1994].

Based on these findings *Roden et al.* [2000] developed a mechanistic model on the premise that the hydrogen isotopic signature of organic molecules is related to that of leaf water during photosynthesis and that a fraction of these hydrogen atoms will subsequently exchange with medium water during cellulose synthesis. The model has two major components, a leaf water model (based on Equation 4.6) that predicts the extent of evaporative enrichment for a given

source water and atmospheric vapour, and a biochemical model (Equation 4.7) that predicts cellulose δD based on the extent of exchange during cellulose synthesis. It is expected that initial photosynthetic products will be enriched reflecting leaf water and that further biochemical fractionation occurs during sugar synthesis. The sugars are then exported to other parts of the plant or stored as starch in the chloroplast. It is assumed in the model that there is no fractionation associated with starch formation or degradation, since all of the product is consumed. The biochemical model predicts that the isotopic composition of cellulose is a function of both the isotopic ratio of the substrate sucrose and of the water in the cell, which could be that of a leaf, a root or a stem xylem cell of a tree ring. It takes the form:

$$\delta D_{CX} = f_H(\delta D_{WX} + \varepsilon_{HH}) + (1 - f_H)(\delta D_{WL} + \varepsilon_{HA}) \tag{4.7}$$

where the subscripts *CX, WX* and *WL* refer to xylem cellulose, xylem water and leaf water respectively, f_H is the fraction of carbon bound hydrogen atoms which undergo exchange with medium water at the site of cellulose synthesis, ε_{HH} is the heterotrophic fractionation factor for enzyme mediated exchange and ε_{HA} is the fractionation factor for autotrophic carbohydrate synthesis (that associated with photosynthesis).

This model shows that both humidity and meteoric water signals are incorporated into tree ring cellulose and is confirmed by results from field and greenhouse experiments. Greenhouse experiments yielded values of f_H of 0.36 [*Roden et al.*, 2000] in contrast to the work of *DeNiro and Cooper* [1989] and *Terwilliger and DeNiro* [1995] who found a value of 1, which would eradicate any leaf water signal from cellulose. The accuracy of the model was also tested to see if it could predict the composition of leaf water and tree ring cellulose for trees growing naturally in the field [*Roden and Ehleringer*, 2000]. Streamside trees were chosen so that the source water could be easily sampled and cottonwood, alder and birch trees were sampled in Arizona, Oregon and Utah, to allow the effect of different relative humdidities to be studied. The results of this study corroborate the model and again do not support complete isotopic exchange with stem water as cellulose is formed ($f_H = 0.31$).

In the light of this new model, which ties together the conflicting results of earlier studies it seems safe to conclude that humidity will contribute to the isotopic signal of tree ring cellulose. It is therefore likely that humidity contributes to the lack of a 1:1 relationship between δD_{CELL} and precipitation (Figure 4.6) and $^3H_{CELL}$ and precipitation (Figure 4.8) seen in this study. To quantitatively account for such effects for ^3H a comprehensive study of air temperature, humidity,

atmospheric water vapour, source water and leaf water during the growing season of the tree under study would be needed.

4.5.3 Groundwater

As Ireland has a temperate climate it seems likely that the intermediate tree water source case of *White et al.* [1985] may be the most appropriate (see 4.1.2.1). If this is the case then the tree will have groundwater available to it as well as growing season precipitation, though the effect should be minimised by the tree growing on granitic bedrock. As the tritium signal of groundwater will be a reflection of many years of precipitation this signal may affect the simple 1:1 relationship between $^{3}H_{CELL}$ and precipitation that might be expected.

Before the onset of the thermonuclear weapons testing program in 1952 groundwater will have been essentially ^{3}H free. In the early bomb years the groundwater contribution would therefore have diluted the increasingly tritiated precipitation signal. Over time as groundwater ^{3}H levels increased the relative importance of this ^{3}H source would also have increased, particularly in later years when the precipitation signal relaxed towards its pre-bomb state. If this were the case, and the groundwater contribution was important for this tree, this effect should be seen in the results as a larger offset between $^{3}H_{CELL}$ and precipitation in the early years of bomb testing compared with later in the record. Unfortunately the lack of both cellulose and precipitation data and the large errors in the $^{3}H_{CELL}$ values make it impossible to see if groundwater is a major water source for this tree.

4.5.4 Reservoir Renewal Model

The effect of soil water residence time on the tritium signal of the water used by the cedar tree to synthesis cellulose was explored using a simple reservoir renewal model for Valentia precipitation. The model assumed that the tree forms cellulose in the presence of trunk water, isotopic enrichment due to evapotranspiration in the leaves was ignored. The calculation was based on the water used by the tree having a characteristic residence time (τ in years) in the soil-tree system before being used to synthesise carbohydrates in the trunk. The reservoir size was defined as:

$$\text{Reservoir Size} = \tau \times \text{Annual Average Precipitation Rate} \qquad (4.8)$$

Monthly precipitation ^3H concentrations and precipitation rates were taken from the WMO / IAEA data set. Steady state was assumed as was a pre-bomb precipitation ^3H concentration of 5 TU. Twelve integrations of the model were done with residence times ranging from 2 months to 2 years. The model ignores groundwater from deep aquifers, which is reasonable for this particular tree as it grew on granitic bedrock and was therefore unlikely to have access to deep water sources. The results of the model, which predicts the concentration of water used by the tree, for 6 different residence time are shown in Figure 4.10.

The graphs in Figure 2.10 indicate that the cellulose data diverges from the model for residence times in excess of 10 months and that for timescales longer than a year there is significant smearing of the ^3H signal. Therefore it can be concluded that the tree is using precipitation that is less than a year old, which is to be expected given the good correlation between $^3H_{CELL}$ and annual precipitation (Figure 4.7) but also presents the possibility that during the summer growing season a fraction of the water used may reflect conditions at the end of the previous year. The apparent offset between the model and cellulose concentrations will be due to the effect of the other contributing factors already discussed, namely humidity and fractionation. However the reservoir model emphasises that the large part of the cellulose ^3H signal can be explained by precipitation alone.

The model also highlights the importance of careful site selection for doing tritium reconstructions. For values of τ in excess of a year there is significant smearing of the model water ^3H signal, and the values deviate significantly from the measured $^3H_{CELL}$ values. This carries the implication that a tree from a location where residence times are high will be a poor choice for ^3H in precipitation time series work. If the model is run with a much longer residence time, from 10 to 100 years, radioactive decay is the dominant factor determining the model water concentration and it is seen to diverge further from the data with time, becoming a flat line after 50 years. This illustrates that if a tree did have access to a deep aquifer whose water was essentially ^3H free then this could have a significant impact on its hydrogen isotopic composition, making it less suitable for time series work.

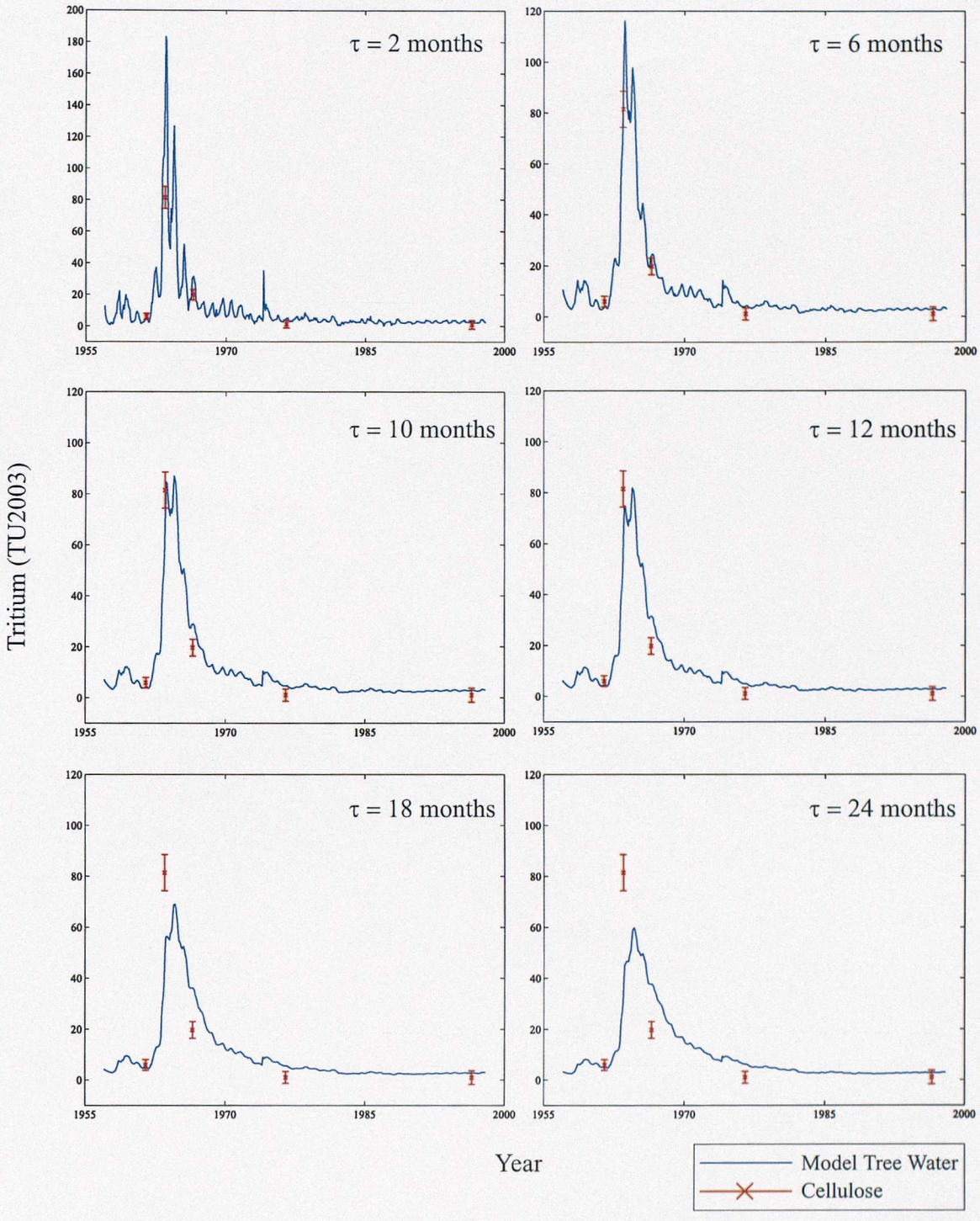

Figure 4.10. Comparison of the source water ^{3}H concentrations used by the cedar tree predicted by the reservoir renewal model with the measured cellulose concentrations. For clarity note the different scale used on the 2 month residence time plot. All the results have been decay corrected to January 1st 2003.

The cedar tree used in this study was an optimal choice for looking at precipitation because it is unlikely to have had access to groundwater with a different ^{3}H concentration. Future studies should involve careful tree selection to ensure that the signal measured is likely to be a good

reflection of ambient precipitation. In conclusion the main water source for this tree has been ambient precipitation and it is likely that the main factors contributing to the deviation from a 1:1 relationship with $^{3}H_{CELL}$ (Figure 4.8) are humidity and fractionation effects as groundwater is unlikely to be an important factor in this case.

4.6 Conclusions

The hydrogen isotope composition of the carbon bound fraction of cellulose relative to that of the source water is related to three main factors, isotopic enrichment of leaf water because of evapotranspiration, fractionations associated with photosynthesis and post photosynthetic metabolism. The relative importance of these three for a particular tree which grew under a specific set of environmental conditions determines whether the cellulose hydrogen reflects ambient precipitation.

The cellulose of the cedar tree sampled, from Tollymore Forest Park, appears to be recording precipitation though it is isotopically depleted in both deuterium and tritium relative to ambient precipitation. The lack of a 1:1 relationship between the two isotopes and precipitation indicates that other factors, namely groundwater and humidity are important in determining the measured isotopic signal. Some of the scatter evident in the isotopic results is also likely to be due to incomplete removal of the exchangeable hydroxyl groups on the cellulose molecule. Neither the nitration procedure used for the deuterium analyses or the exchange technique for ^{3}H will have been 100% complete so small levels of contamination are likely in the results (see Chapter 3).

Although the tritium measurements presented here are too few to understand the mechanism of fractionation and water uptake they do confirm that the cellulose ^{3}H signal is recording precipitation. Figure 4.7 is extremely encouraging as it shows that the shape of the $^{3}H_{CELL}$ curve mirrors that of annual precipitation, though a direct relationship has not been found. To be convinced that precipitation is a major source of ^{3}H for a particular tree a comprehensive study comparable to that by *White et al.* [1994] for deuterium and oxygen needs to be done. In such a study measurements of the isotopic composition of groundwater, sap, leaf water, humidity, atmospheric vapour, precipitation and temperature would be made in parallel to measurements of $^{3}H_{CELL}$. This would make the relative importance of different water sources and other climatic parameters clear and allow estimates of net biochemical fractionation to be made.

In conclusion the work presented in this chapter shows that the tritium signal in precipitation is recorded in the carbon bound fraction of tree ring cellulose. This illustrates the potential for improving knowledge of the input of ^{3}H to the oceans by reconstructing ^{3}H in precipitation from

trees. Improved cellulose sampling with a cleaner exchange technique to reduce hydroxyl group contamination and a reduction in the large errors in sample ^3H measurement will further improve the usefulness of this technique. Sealing larger cellulose samples for longer time periods and improving mass spectrometer precision will both allow smaller ^3H signals to be measured and reduce the error in each sample measurement. This will become extremely important if ^3H reconstructions are to be made at oceanic locales or in the southern hemisphere where ^3H levels are significantly lower than in the continental northern hemisphere. In many ways Ireland was an ideal location for an initial test of whether $^3H_{CELL}$ reflected ambient precipitation as its location in the northern hemisphere ensures there is a large and relatively easy signal to detect and the area's wet climate makes it more likely that precipitation will be a dominant source of water for a tree. To confirm the validity of the technique at a less optimal location it would be useful to measure ^3H at an ocean island. Bermuda would be a good choice for such an experiment as there is some precipitation ^3H data available (WMO/IAEA) which could be used to determine how important precipitation is to the sampled tree.

As a first study of low level tritium measurements in tree ring cellulose this work is a significant step forward from earlier studies. Two papers published in the 1980s [*Kozák*, 1982, *Kozák et al.*, 1989] measured ^3H in Hungarian tree ring cellulose after equilibration with ^3H free water or acid, by liquid scintillation counting. The uncertainties in the measurements were significant (41-177TU) but the results of *Kozák et al.* [1989] were shown to be within experimental errors of ambient precipitation and those of *Kozák* [1982] highlighted the usefulness of cellulose reconstructions to investigate ^3H releases from industrial sources. Here the use of helium ingrowth allows much lower ^3H signals to be measured and the results presented in this study would not have been detected using the techniques presented in the earlier papers.

The extraction and exchange technique described in Chapter 3 and tritium measurement by helium ingrowth allows ^3H in precipitation signals to be measured in tree ring cellulose. The Valentia time series presented, though essentially qualitative in nature, highlights the potential of this technique to improve knowledge of the ^3H input function.

5. Synthesis and Future Work

5.1 Introduction

In this thesis the possibility of using tritium as a tracer in circulation and modelling studies has been explored, the limitations highlighted and the potential of a new technique to further constrain the isotope's input function presented. The first was achieved by constructing a simple multi-box model of the shallow circulation of the North Pacific Ocean to evaluate the inventory and distribution of ^{3}H in the basin for comparison with observations. The model highlighted the significance of uncertainties in the ^{3}H input function, particularly over the oceans, which has important implications for the isotopes use in constraining high resolution general circulation models. In the laboratory, a technique was developed to measure ^{3}H concentrations in tree rings, which were assumed to reflect ambient precipitation the year that the wood was laid down. An initial test of both this hypothesis and the method itself was done on an Irish tree, for comparison with the comprehensive record of ^{3}H in precipitation from the Valentia weather station.

In this chapter the results of this method development are discussed in the context of further improving the technique to allow the ultimate goal of improving tritium's usefulness as a tracer to be achieved.

5.2 Main Achievements of the Thesis

In Chapter 2 an improved model function of the tritium distribution in precipitation was presented and its limitations discussed. The major result of this was the emergence of a third factor which was not seen in the earlier *Doney et al.* [1992] analysis that was attributed to direct ^{3}H deposition during the thermonuclear era. The resulting precipitation ^{3}H distribution was then used to calculate the total atmospheric deposition of ^{3}H to the North Pacific, as part of a model to study the recirculation and inventory of the isotope in this basin.

A North Pacific tritium inventory was calculated from the WOCE cruise dataset, which was in line with the earlier estimates of *Broecker et al.* [1986] and *Van Scoy et al.* [1991]. The inventory of 23.4 ± 2.0 kg presented here is the best constrained estimate so far, as both the spatial and depth coverage of the WOCE cruises were more extensive than those for either the GEOSECS or the Long Lines cruises, which were used to construct the earlier estimates. By comparing the results of this inventory with GEOSECS data it became evident that there has been an increased homogenisation of the ^{3}H distribution in the years between the two surveys as a result of

circulation and mixing. The changing depth distribution shows that there has been an overall increase in the depth penetration of ^{3}H, in line with radiocarbon data [*Peng et al.*, 1998]. The distribution in the tropics and subtropics also agrees with bomb radiocarbon work, with the shift in ^{3}H from intermediate to low latitudes being indicative of a Hadley cell circulation. This improved estimate of the North Pacific ^{3}H inventory was used to constrain the advective and atmospheric terms in the North Pacific box model.

The North Pacific tritium budget model presented in Chapter 2 showed that the main source of bomb ^{3}H to the basin has been atmospheric deposition, with vapour deposition exceeding precipitation by a factor of two. The Indonesian Throughflow was shown to be the most important advective term to the basins ^{3}H budget and it was seen to be comparable in importance to atmospheric deposition after 1975. A sensitivity study yielded inventories in good agreement with the WOCE data though the model struggled to reproduce the ^{3}H depth distribution at high latitudes, which may be a reflection of the lack of intermediate depth circulation further south in the model. The optimal values of the model parameters give a C_V / C_P ratio of 0.67 confirming the importance of vapour deposition to the oceans, and an Indonesian Throughflow at the upper end of observational estimates. Overall the modelling work highlights the potential of ^{3}H to constrain circulation and GCMs in the future.

The second half of this thesis has been concerned with the development of a new technique to measure ^{3}H in tree rings, as a way to make historical reconstructions of the isotope in precipitation. For this, the work presented in Chapters 3 and 4 represents a significant advance. The microwave extraction method gives a fast, effective way to extract cellulose from softwoods and is considerably faster and cheaper than more conventional approaches. The results in Chapter 3 show that the NaOH exchange technique developed gives a safe way to prepare large cellulose samples for ^{3}H measurement, and the time series presented in Chapter 4 shows the considerable potential of tree ring reconstructions to reflect precipitation the year the wood was formed.

Overall this thesis has achieved the following:

1. Presented an improved global model function to compute the concentration of ^{3}H in precipitation at any location.

2. Highlighted the importance of direct ^{3}H deposition in the 1960s to the distribution of the isotope in precipitation.

3. Used ^{3}H data to provide direct evidence of intermediate depth ventilation in the North Pacific.

4. Showed that vapour deposition is the dominant mechanism for ^{3}H reaching the North Pacific.

5. Illustrated that the magnitude of the Indonesian Throughflow is very important to the ^{3}H budget of the North Pacific basin and that a simple multi-box model indicates its magnitude may be at the upper end of other observational estimates.

6. Shown the potential of ^{3}H to be used to constrain models and circulation.

7. Presented a new rapid technique to extract oils, lipids and resins from softwoods.

8. Offered an alternative to nitration to remove hydroxyl group contamination from the cellulose molecule for dendroclimatological work.

9. Shown, for the first time that ^{3}H from tree rings provides an accurate record of the isotope's concentration in precipitation.

5.3 Future Work to Improve the Method

The work presented in Chapter 4 illustrates the potential of ^{3}H measurements in tree rings to improve historical knowledge of ^{3}H deposition to the earth's surface via precipitation. However the limitations imposed by both the time taken to develop the method coupled with the that for helium ingrowth severely limited the number of samples that could be prepared and hence the comprehensiveness of the test of the technique. Therefore further work, which was beyond the scope of this thesis is needed to refine the technique and allow confident precipitation time histories to be made.

5.3.1 Cellulose Extraction

During the course of the laboratory work few difficulties were encountered in the extraction of α-cellulose from hard woods and the sodium chlorite delignification procedure of *Loader et al.* [1997] was successfully scaled up to 4-5g samples. However the difficulty in getting sufficient wood from an Irish oak due to narrow rings necessitated the use of a cedar tree for the time series work presented in Chapter 4. As a softwood, it required an extra solvent extraction stage to

successfully extract α-cellulose for ^3H measurement. The microwave extraction procedure that was developed (see 3.2) was successful in giving a relatively fast way to produce cellulose. However the procedure was not tried on other softwood types and it is likely that some modifications would be needed to take into account the significant chemical heterogeneity among the wood of different tree species [*Epstein et al.*, 1976; *Loader et al.*, 1997]. Longer or shorter extraction times will likely be needed depending on the wood being used and it is likely that some experimentation will always be needed to get the optimal procedure whenever a new tree species is encountered, but the success here indicates that microwave extraction will offer a more efficient option than traditional soxhlet extraction.

The purity of the α-cellulose product yielded by microwave extraction and subsequent delignification was not comprehensively assessed in this thesis. Product purity is critical for ^3H reconstructions when results are presented in TU, as the ratio requires knowledge of the total amount of hydrogen present in a sample, which was assumed to be pure cellulose. The presence of even trace amounts of lignin, oils or other residues will affect the accuracy of the data. Although colour has been the standard way to assess product purity [*Sheu and Chiu*, 1995] with white being indicative of pure α-cellulose, spectroscopic analysis of the product would provide a more convincing argument for ^3H work.

5.3.2 The Exchange Technique

The success of the exchange technique at removing hydroxyl group contamination from the cellulose molecule was demonstrated in 3.4, though it is clear from the results that some contamination remains. To eliminate the contamination and improve the technique several tests are needed.

5.3.2.1 Reagent Purity

The acid and base used in the exchange reaction consistently contained more tritium than the water from which they were produced and are therefore a potential source of contamination. One way to minimise the contamination may be to allow argon to flow in to the separating funnel while the NaOH is being synthesised. However the inherent dangers of adding sodium to water make further minimisation of contamination difficult. By making the H_3PO_4 in a glove box contamination is being minimised as much as possible and it appears that it is material in the phosphorous pentoxide matrix that is causing the problem. The purpose of the acid is to reprotonate the hydroxyl sites after reaction with NaOH, however it would be worth exploring the

necessity of this stage as flushing samples with an excess of ^3H free water will reprotonate the sites without contamination, and may represent a more efficient way to carry out an exchange.

5.3.2.2 *Extent of Exchange*

Knowledge of the extent of exchange achieved is critical for two reasons. Firstly, as described in 3.5.1, to present results in TU it is necessary to know what percentage of the cellulose hydrogens are contributing to the measured ^3H signal. Secondly to compare tree ring ^3H time series with precipitation it is important to be aware how much of the signal may represent conditions outside of the year that the wood was formed. To assess the degree of exchange being achieved a comprehensive comparison with nitration would be needed. By subjecting cellulose samples from the same ring to both nitration and exchange a direct comparison could be made. To do this the degree of nitration would need to be calculated by measuring the products nitrogen content, with a 14.2% nitrogen content representing complete substitution.

It is possible that carrying out the exchange reaction at different temperatures may affect the degree of substitution achieved. Exchange at higher temperatures should offer a kinetic advantage but as the reaction may be being prohibited by the accessibility of the hydroxyl sites the increased swelling of cellulose at low temperatures may be of more benefit. Both possibilities should be explored to optimise the exchange, an area which will be critical for ocean island and southern hemisphere tree ring time series as the precipitation signal will be much smaller than at Valentia.

5.3.3 Tritium in Tree Rings as a Reflection of Precipitation

The results presented in Figure 4.7 and discussed in 4.4 show that the cellulose from the Irish cedar tree exhibits the bomb tritium spike that is evident in precipitation. However the small amount of data in this thesis only provides an initial test of the hypothesis and more work, which includes sample replicates is needed to confirm reproducibility.

The lack of a 1:1 relationship between the measured tritium concentration of cellulose ($^3H_{CELL}$) and precipitation indicates that other factors, such as groundwater usage and humidity are also important. To make ^3H in precipitation reconstructions with a sufficient accuracy to better constrain the isotopes input function the importance of the other factors has to be quantified. This will allow $^3H_{CELL}$ measurements to be easily translated into precipitation concentrations. To this end a comprehensive study of ^3H concentrations in groundwater, vapour, sap, leaf water and cellulose at a location with some precipitation data, such as Bermuda or Hawaii would be useful.

Also, in this work whole wood has been used and a comparison of both early and late wood $^3H_{CELL}$ values with ambient precipitation will confirm whether the tree sampled is incorporating the isotopic signal from the previous growing season in the wood it lays down in the spring. The ease of such a study will be limited by the amount of wood needed to measure low levels of ^3H to a good degree of accuracy.

5.4 Improving the Tritium Input Function

The WMO / IAEA tritium in precipitation database provides a valuable tool to constrain the deposition of ^3H to the earths surface. The large number of long duration records on the continents allows the deposition over land to be well constrained. However the few sampling stations at truly oceanic locations, those that are out of the marine boundary layer, are very few. The work presented in this thesis illustrates for the first time the potential of tree ring ^3H concentrations at oceanic islands to fill in the gaps in the knowledge of ^3H deposition over the oceans. In practise the major difficulties will be associated with finding suitable trees, both to provide enough ring material for low level ^3H measurement and those that have annual rings. In tropical oceanic climates many islands may exhibit few tree species apart from palms, which do not form annual rings, or the climate will be consistently warm and wet leading to annual growth rings being absent.

As discussed in Chapter 2, to further improve the tritium input function the assumption of isotopic equilibrium between rain and vapour needs to be tested. This could either be achieved with comprehensive sampling in the field of the ^3H concentration of both marine vapour and precipitation, though sampling vapour is notoriously difficult. In lieu of such data, information on the C_V / C_P ratio could be gleaned from a comprehensive atmospheric modelling simulation of the pathways of ^3H in the atmosphere. This would require knowledge of the location and yields of as many as possible of the thermonuclear weapons tests and a model that could address the shortcomings of the *Koster et al.* [1989] analysis. Such a study could, if coupled to an ocean model also address the issue of the continent-marine transition length scale which is at present estimated from precipitable water data.

5.5 The Importance of the Input Function – Comparison to Other Tracers

The use of a chemical tracer to assess water masses and circulation in ocean models requires both knowledge of its input function and a realistic representation of its seawater chemistry [*England and Maier-Reimer*, 2001]. For tritium the seawater chemistry is well known but, as demonstrated by the modelling work in Chapter 2, the input function is a source of uncertainty.

Biochemical complications fundamentally limit the usefulness of tracers such as oxygen and phosphate to validate ocean models. In contrast, by simulating the $^{14}C/^{12}C$ ratio it is possible to use radiocarbon while avoiding the problems associated with biological consumption and remineralisation that limit the utility of nutrients as tracers.

The anthropogenic tracers tritium, chlorofluorocarbons (CFCs) and bomb ^{14}C are particularly well suited to studying decadal scale model ventilation. However, although the inter-hemispheric input differences of ^{3}H make it particularly useful as a tool to distinguish ventilation pathways it has been considered [*England and Maier-Reimer*, 2001] less useful than CFCs and bomb ^{14}C for decadal and inter-decadal model validation due to the problems with its input function.

The industrial release of CFCs started in the 1930s and accelerated markedly over the following thirty years following their widespread use as refrigerants and aerosol propellants, and the atmospheric concentration of these gases has continued to rise until very recently. The majority of CFC production occurs in the northern hemisphere but rapid mixing in the lower atmosphere and the chemical stability of CFCs has resulted in there being a relatively uniform distribution of these gases in the troposphere [*England and Maier-Reimer*, 2001]. Therefore they have a significant input function over the entire ocean, making them clearly distinct from ^{3}H and the precise knowledge of their input function and the ease of measurement makes CFCs a powerful tool for model validation [*Jean-Baptiste and Messias*, 1993]. However the improved knowledge of the tritium input function that could be produced by reconstructions of the isotopes concentration in precipitation over the ocean should make ^{3}H as powerful a tool in circulation studies as CFCs.

5.6 Summary

This thesis has successfully combined modelling and laboratory work to highlight the usefulness of tritium as a tracer and address the shortcomings of its input function.

The modelling work has highlighted the usefulness of tritium in such studies showing that it can be used to constrain circulation. The simple multi-box model of the North Pacific produced a realistic simulation of the ^{3}H distribution in this basin and showed that fluxes such as the Indonesian Throughflow can be constrained (here to 15.8 Sv), highlighting the usefulness of ^{3}H to studies of circulation and model validation. The work also showed that the usefulness of ^{3}H is at present limited by the lack of constraint on its atmospheric deposition over the oceans, which can make other tracers such as CFCs more attractive to modelling studies. This problem has been addressed in the second half of the thesis with the development of a technique to improve knowledge of ^{3}H deposition via precipitation over the oceans. The initial test of this technique

conducted here and described in Chapter 4 shows that the precipitation signal is recorded in annual tree rings, though further work is needed to allow the contribution to the signal from other factors, such as humidity and groundwater to be removed.

The primary aim of this work, to provide a tool to improve knowledge of tritium deposition has been achieved and it can be concluded that in the future ^{3}H will be a powerful tool for model validation efforts.

Appendix 1 – The Seasonal Cycle of Tritium in Precipitation

It is clear from Figure A1.1 that there is a strong seasonal precipitation tritium signal which is not incorporated into the global model function of ^3H in precipitation described in Chapter 2.

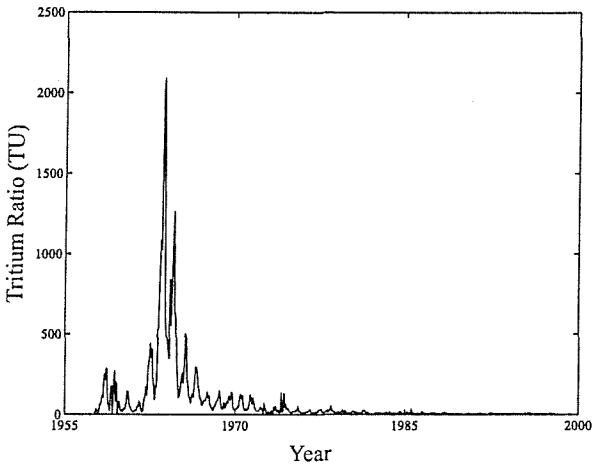

Figure A1.1. The ^3H in precipitation time history recorded on a monthly basis at Valentia, Ireland.

The timing of the seasonal cycle of ^3H in precipitation is closely linked with that of stratospheric-tropospheric exchange [*Gat*, 1980, *Enhlat*, 1971]. Stratospheric mass is at its greatest in late winter [*Danielsen*, 1968] and inflow to the troposphere occurs mainly in late winter and early spring. However the ^3H in precipitation peak is in summer (June and July) and this delay has been attributed to the time taken to pump HTO from the tropopause to the lowest levels and to the re-evaporation of soil moisture in summer [*Enhlat*, 1971]. Once evaporation begins to exceed precipitation in early summer HTO stored in soils is re-evaporated providing the atmosphere with an additional source of ^3H. As there is a relatively sharp peak in evapotranspiration in July this pulse only lasts for a few months and is superimposed on and extends beyond the period of stratospheric input [*Enhlat*, 1971]. This soil ^3H results in the relatively sharp ^3H in precipitation peak in June and July that is seen in the Valentia records. However it should also be noted that seasonal variations in the isotopic signal in precipitation are generally correlated with temperature [*Gat*, 1980] so that winter precipitation is depleted in heavy isotopes relative to that in summer.

Following the analysis of *Doney et al.*, [1992] the seasonal cycle of ^3H in precipitation is modelled as a simple sinusoidal cycle about the inter-annual trend by expanding Equation 2.3 such that:

$$C_{monthly}(t) = [1 + a_m \cos(2\pi(t - \phi))].[f_0 + f_1 \hat{c}_{pm}(t,1) + f_2 \hat{c}_{pm}(t,2) + f_3 \hat{c}_{pm}(t,3) + \varepsilon_m(t)] \quad (1)$$

where a_m and ϕ are the amplitude and phase respectively. To obtain the factor scores at a monthly resolution a cubic spline interpolation procedure was used from the annual data. Time t and phase ϕ are in decimal years and the value of ϕ corresponds to the peak in the annual cycle. Equation 1 was solved to give a_m and ϕ at each station using a non-linear, least squares routine and the results are given in the table below. The standard deviation of the residuals was calculated in the same manner as in the yearly case such that:

$$\sigma_m = \left(\frac{1}{N-3} \sum_{i=1}^{N} \varepsilon_m^2 \right)^{\frac{1}{2}} \quad (2)$$

where N is now the number of months rather than years. The performance of the model at two continental and two oceanic stations is shown in Figure A1.2.

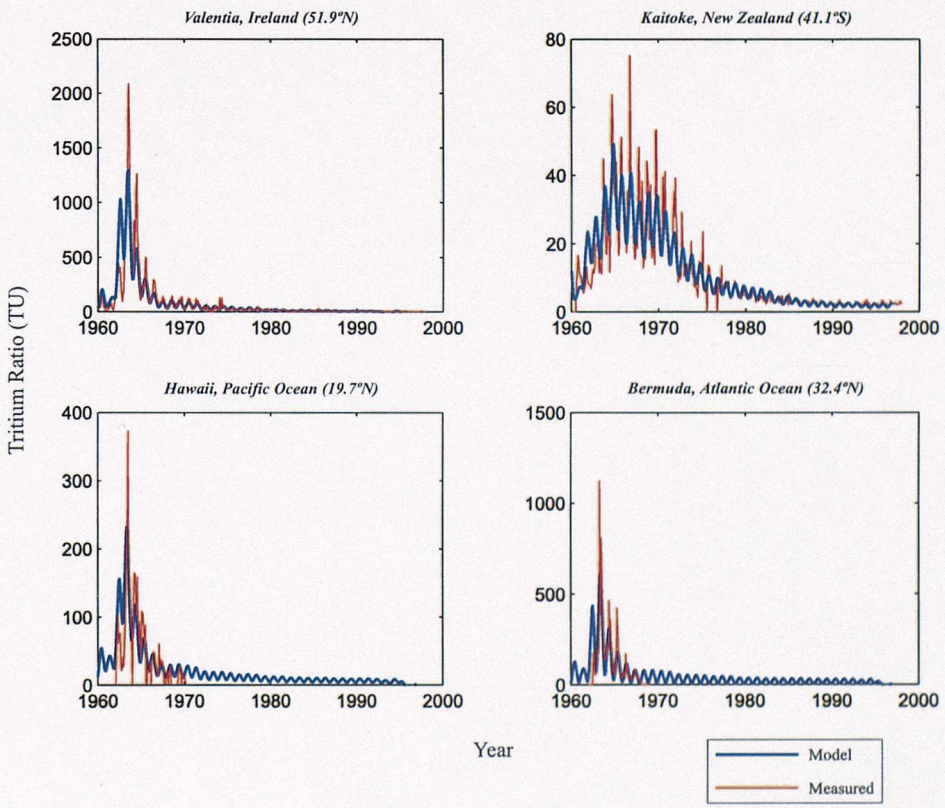

Figure A1.2. A comparison of the monthly ratios of ^3H in precipitation at 4 locations predicted by the least squares solution of Equation 1 compared with the raw data from each station. The scales vary with each plot as there are large differences in ^3H concentration with latitude.

It is clear that the seasonal cycle is reproduced well by the model function at the two continental stations, Valentia and Kaitoke, though the overall magnitude of the signal is underestimated particularly in the years surrounding the bomb spike. The shape of the predicted ^3H in precipitation curve at oceanic locations with sparse data such as Bermuda and Hawaii is realistic but the magnitude may be overestimated in later years. It appears that the signal does not decay as fast as it should after the bomb spike when there is no data to fit the model function to. It is clear that at all four stations the summer ^3H peak is significantly underestimated and that the peak is more poorly represented than the corresponding trough. Figure A1.3 highlights that the seasonal signal is not symmetrical about the annual average so using a simple sinusoidal function may not be appropriate. This asymmetry is likely due to the spike of ^3H evaporated from soils in June and July causing abnormally high precipitation concentration in these months.

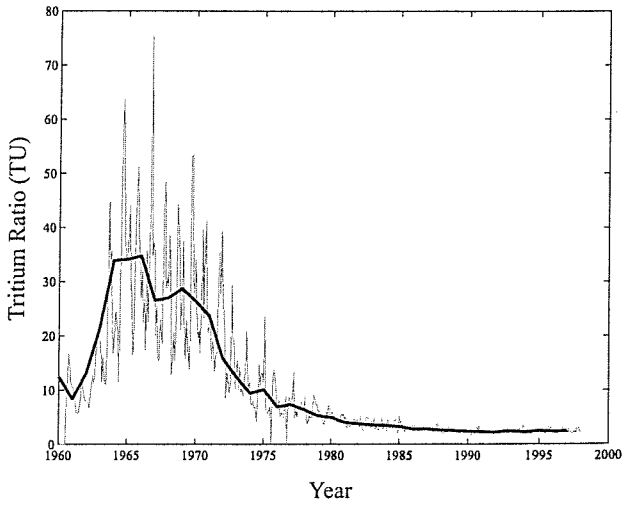

Figure A1.3. Comparison of the recorded monthly ^3H in precipitation ratios (grey line) with the annual average (black line) at Kaitoke, New Zealand. It is immediately obvious that the seasonal signal is not symmetrical about the annual average, with there being very distinct summer peaks.

Station	Latitude	Longitude	f_1	f_2	f_3	f_0	σ_a	a_m	ϕ	σ_m
Isfjord Radio, Norway	78.07	13.63	341.33	107.88	83.35	172.09	116.18	0.68	-0.42	525.76
Tana, Norway	70.40	28.20	307.94	132.48	57.33	247.99	122.51	0.89	-0.49	618.11
Gjermundnas, Norway	62.62	7.17	289.38	58.12	64.09	150.74	94.91	1.00	-0.47	396.37
Fanaraken, Norway	61.52	7.90	284.64	102.34	75.90	186.56	91.07	0.60	0.46	612.02
Trysil, Norway	61.33	12.25	508.39	131.29	126.46	292.88	135.16	0.61	0.47	680.04
Lista, Norway	58.10	6.57	256.77	65.21	55.97	157.65	65.62	0.61	-0.44	303.10
As, Norway	59.67	10.68	421.27	92.33	105.79	230.34	162.42	0.68	0.48	577.91
Forshult, Sweden	60.17	13.78	459.81	105.79	109.12	249.37	135.31	0.64	0.46	558.30
Kvarntorp, Sweden	59.20	15.50	440.34	108.03	160.89	276.90	112.74	0.66	0.48	633.75
Flahult, Sweden	57.70	14.20	446.13	107.16	102.04	263.62	138.41	0.84	0.47	464.56
Plonninge, Sweden	56.70	12.70	406.52	81.90	100.35	218.40	130.47	0.68	0.50	729.31
Smedby, Sweden	56.70	16.20	418.97	107.71	94.39	240.47	108.90	0.73	0.47	762.14
Kiruna, Sweden	67.87	20.23	570.96	130.58	130.32	378.66	401.24	0.56	0.44	823.42
Arjeplog, Sweden	66.05	17.90	492.97	168.21	104.68	373.29	185.06	0.66	0.45	604.62
Robacksdalen, Sweden	63.80	20.20	390.34	123.46	101.90	295.95	233.35	0.62	0.47	611.26
Huddinge, Sweden	59.23	17.98	357.50	102.93	97.04	211.13	74.18	0.61	0.49	434.89
Goteborg, Sweden	57.70	11.97	358.04	89.90	80.30	191.63	67.39	0.78	0.45	498.39
Bredkalen, Sweden	63.90	15.30	471.07	111.75	97.77	274.51	200.75	0.82	-0.47	531.71
Skurup, Sweden	55.47	13.50	405.32	97.43	86.81	221.82	89.48	0.85	0.44	615.42
Pelkosenniemi, Finland	67.10	27.50	432.79	248.33	162.33	607.55	417.26	0.48	0.45	943.28
Valentia, Ireland	51.93	-10.25	170.25	45.94	44.04	78.88	9.62	0.49	-0.49	116.20
Reykjavik, Iceland	64.13	-21.93	245.82	79.21	54.18	161.78	55.11	0.38	0.49	391.18
Groennedal, Greenland	61.22	-48.12	400.99	97.23	120.16	227.06	105.53	0.76	-0.48	538.05
Nord, Greenland	81.60	-16.67	991.26	194.75	401.81	480.10	173.39	0.38	0.45	1277.52
Odum, Denmark	56.30	10.13	355.25	84.91	90.77	200.89	101.65	0.84	0.49	468.36
Askov, Denmark	55.50	9.13	299.27	80.04	80.25	196.79	93.59	0.82	0.50	404.34
Tystofte, Denmark	55.20	11.17	381.60	71.06	81.60	190.41	154.72	1.00	0.50	426.30
Gibraltar, UK	36.15	-5.35	101.91	33.77	32.43	69.70	37.19	0.38	0.37	103.12
Punta Delgada, Azores	37.77	-25.65	75.35	22.32	32.15	45.79	10.54	0.35	0.46	90.43
Hof-Hohensaas, Germany	50.32	11.88	527.36	98.19	150.97	236.75	96.27	0.49	-0.50	322.73
Stuttgart, Germany	48.83	9.20	511.53	133.75	113.77	252.03	80.46	0.39	-0.48	422.68

Station	Latitude	Longitude	f_1	f_2	f_3	f_0	σ_a	a_m	ϕ	σ_m
Vienna, Austria	48.25	16.37	507.94	147.19	134.86	242.76	48.40	0.54	0.50	309.74
Genoa, Italy	44.42	8.85	252.63	72.23	77.44	129.30	45.78	0.54	0.50	173.55
Athens, Greece	37.90	23.73	208.62	79.79	51.41	111.19	52.67	0.44	0.39	255.89
Har Kna'an, Israel	32.97	35.50	280.02	44.12	201.21	152.65	71.91	0.32	0.28	286.40
Bet Dagan, Israel	32.00	34.82	123.63	40.79	53.15	75.14	20.22	0.23	0.36	96.32
Teheran, Iran	35.68	51.32	532.73	106.98	161.78	224.41	110.83	0.32	0.43	445.16
Kabul, Afghanistan	34.67	69.08	728.22	341.20	224.72	386.85	263.87	0.87	-0.27	532.87
Bahrain, Bahrain	26.27	50.62	133.92	45.16	86.55	83.62	46.38	0.70	-0.38	155.70
Karachi, Pakistan	24.90	67.13	0.89	-35.49	447.01	148.94	298.24	2.00	-0.11	967.06
New Delhi, India	28.58	77.20	129.27	63.35	58.35	93.73	60.66	0.78	0.25	87.77
Bombay, India	18.90	72.82	59.81	16.82	12.44	35.77	21.48	0.29	-0.43	77.16
Hong Kong, China	22.32	114.17	45.37	19.52	26.88	35.64	28.21	0.15	0.06	36.69
Pohang, Korea	36.03	129.38	204.93	72.23	57.07	101.58	33.23	0.41	0.37	177.22
Tokyo, Japan	35.68	139.77	153.72	49.64	43.78	77.31	23.71	0.43	0.39	147.79
St Helena, Atlantic Ocean	-15.97	-5.70	0.23	1.73	0.14	5.64	1.16	0.22	-0.17	2.55
Diego Garcia, Indian Ocean	-7.32	72.40	6.14	21.97	6.01	17.16	26.94	0.24	0.36	51.14
Alexandra, Egypt	31.20	29.95	139.30	43.00	42.30	79.89	18.54	0.21	0.21	119.61
Khartoum, Sudan	15.60	32.55	245.22	74.62	61.77	129.95	24.08	0.15	0.48	285.47
Entebbe, Uganda	0.05	32.45	23.17	9.79	2.76	20.00	11.72	6.03	0.45	184.73
Dar Es Salaam, Tanzania	-6.88	39.20	4.22	5.39	1.66	10.64	8.09	0.21	0.10	17.70
Kinshasa, Dem. Rep. Congo	-4.37	15.25	15.05	12.13	3.98	27.72	10.68	0.29	0.16	23.67
Antananarivo, Madagascar	-18.90	47.53	6.27	5.84	8.69	19.23	9.96	0.24	-0.06	15.79
Harare, Zimbabwe	-17.83	31.02	4.68	8.85	3.66	13.16	2.76	0.13	-0.32	8.57
Windhoek, Namibia	-22.57	17.10	8.05	14.71	5.32	20.54	6.09	0.21	-0.07	10.96
Pretoria, South Africa	-25.73	28.18	7.01	15.52	3.75	20.05	6.07	0.27	-0.16	11.12
Malan, Soouth Africa	-33.97	18.60	2.08	6.59	1.38	10.30	3.76	0.13	0.01	7.12
Gough Island, Atlantic Ocean	-40.35	-9.88	2.44	7.40	0.85	10.12	4.39	0.22	-0.16	7.01
Bethel, Alaska	60.78	-161.80	340.13	94.97	115.19	224.38	91.87	0.74	-0.49	562.00
Palmer, Alaska	61.62	-149.10	404.12	192.59	70.11	432.55	346.16	0.65	0.48	835.47
Adak, Alaska	51.88	-176.65	254.21	48.74	78.82	116.56	99.88	0.96	0.49	379.76
Ottowa, Canada	45.32	-75.67	499.42	146.82	157.98	255.68	59.45	0.31	-0.47	318.45

Station	Latitude	Longitude	f_1	f_2	f_3	f_0	σ_a	a_m	ϕ	σ_m
Goose Bay, Canada	53.32	-60.42	531.80	154.63	139.53	315.52	114.80	0.64	-0.50	704.64
Edmonton, Canada	53.57	-113.52	706.36	251.82	194.57	476.83	193.12	0.44	0.48	982.66
Fort Smith, Canada	60.02	-111.97	702.06	252.89	195.21	462.82	227.89	0.56	0.47	868.79
Whitehorse, Canada	60.72	-135.07	756.23	178.90	206.31	359.06	162.92	0.59	0.48	835.98
Ocala, USA	29.18	-82.13	89.71	27.30	31.49	47.52	14.03	0.35	-0.48	70.70
Waco, USA	31.62	-97.22	131.05	31.37	106.83	83.53	28.48	0.31	0.49	121.83
Hatteras, USA	35.27	-75.55	141.60	36.30	60.31	75.49	15.65	0.57	0.49	119.35
Albuquerque, USA	35.05	-106.62	389.83	130.10	99.28	188.69	98.33	0.42	-0.17	484.33
Flagstaff, USA	35.13	-111.67	277.78	130.33	207.02	209.95	174.54	0.53	0.40	511.15
Santa Maria, USA	34.90	-120.45	117.87	29.98	53.09	62.83	18.01	0.41	0.43	130.75
Menlo Park, USA	37.45	-122.13	132.15	36.94	35.97	75.01	25.92	0.14	0.48	113.54
Chicago, USA	41.78	-87.75	412.55	111.19	190.63	216.10	70.72	0.43	0.46	357.89
Lincoln, USA	40.82	-96.70	355.56	133.20	136.68	194.06	84.08	0.43	0.42	268.41
Weathership, Atlantic Ocean	35.00	-48.00	64.77	21.64	23.91	41.37	9.43	0.49	0.45	73.96
Bermuda	32.37	-64.68	62.31	18.68	17.77	46.74	26.57	0.80	0.42	116.60
Stanley, Falkland Islands	-51.70	-57.87	3.83	12.76	3.96	18.17	5.76	0.30	-0.17	12.11
Weathership, Pacific Ocean	31.00	164.00	61.26	21.49	18.39	44.35	21.40	0.57	0.45	99.75
Midway Island, Pacific Ocean	28.22	-177.37	45.41	14.09	17.22	25.87	7.26	0.28	0.42	51.84
Taguac Guam, Pacific Ocean	13.55	144.83	12.47	3.89	18.23	14.86	4.37	0.30	0.46	19.18
Wake Island, Pacific Ocean	19.28	166.65	22.32	8.58	9.12	16.57	3.71	0.35	0.41	28.35
Johnston Island, Pacific Ocean	16.73	-169.52	17.17	5.74	9.52	15.37	4.75	0.38	0.38	24.05
Hawaii	19.72	-155.07	28.23	9.02	9.85	20.81	5.87	0.44	0.38	42.64
Christmas Island, Pacific Ocean	1.98	-157.46	2.73	2.54	0.87	7.09	5.89	0.56	0.19	7.48
Canton Island, Pacific Ocean	-2.77	-171.72	0.86	0.50	2.95	6.48	4.51	0.17	0.09	8.79
Kaitaia, New Zealand	-35.07	173.28	2.53	7.18	2.13	8.77	2.02	0.24	-0.19	3.80
Kaitoke, New Zealand	-41.10	175.17	2.89	9.90	1.63	10.96	2.42	0.32	-0.21	5.40
Invercargill, New Zealand	-46.42	168.32	3.52	10.96	2.76	12.37	3.05	0.25	-0.14	7.06
Brisbane, Australia	-27.43	153.08	4.34	6.76	12.19	13.58	7.00	0.42	-0.20	11.53
Adelaide, Australia	-34.93	138.58	7.48	15.72	13.65	21.17	11.52	0.33	-0.15	24.02
Melbourne, Australia	-37.82	144.97	6.12	15.38	3.45	18.98	4.45	0.32	-0.17	10.78
Jakarta, Indonesia	-6.18	106.83	9.35	3.88	22.27	14.46	12.30	0.08	0.14	21.49

The normalised factor scores that were used to predict the annual concentration of ^3H in precipitation are given below:

Year	$c_p(t,1)$	$c_p(t,2)$	$c_p(t,3)$
1960.5	-0.090	0.050	-0.142
1961.5	-1.085	-1.158	4.963
1962.5	0.035	0.476	2.949
1963.5	5.122	-0.520	0.706
1964.5	2.682	1.234	0.066
1965.5	0.424	2.549	0.048
1966.5	-0.132	1.749	0.273
1967.5	-0.573	2.258	-0.093
1968.5	-0.509	1.350	0.079
1969.5	-0.489	1.779	-0.255
1970.5	-0.560	1.539	-0.014
1971.5	-0.399	1.193	-0.132
1972.5	-0.354	0.696	-0.250
1973.5	-0.300	0.399	-0.282
1974.5	-0.338	0.246	-0.071
1975.5	-0.206	0.005	-0.263
1976.5	-0.205	-0.219	-0.254
1977.5	-0.233	-0.288	-0.098
1978.5	-0.152	-0.380	-0.257
1979.5	-0.202	-0.376	-0.250
1980.5	-0.213	-0.424	-0.269
1981.5	-0.174	-0.468	-0.297
1982.5	-0.215	-0.497	-0.280
1983.5	-0.183	-0.556	-0.305
1984.5	-0.125	-0.690	-0.375
1985.5	-0.140	-0.637	-0.408
1986.5	-0.102	-0.730	-0.394
1987.5	-0.101	-0.749	-0.434
1988.5	-0.122	-0.763	-0.386
1989.5	-0.122	-0.771	-0.403
1990.5	-0.093	-0.804	-0.415
1991.5	-0.108	-0.801	-0.394
1992.5	-0.117	-0.802	-0.394
1993.5	-0.129	-0.782	-0.399
1994.5	-0.106	-0.827	-0.401
1995.5	-0.111	-0.809	-0.401
1996.5	-0.162	-0.685	-0.336
1997.5	-0.115	-0.785	-0.433

Appendix 2: The Extraction of α-cellulose from Hard Woods Based on the Method of *Loader et al.*, [1997]

This method is a modification of the sodium chlorite oxidation method of *Green*, [1963] and allows the rapid batch processing of small wood samples.

1. Chop wood samples into slivers ~ 40μm thick using a chisel or scalpel.

Reagents are used in the ratios given in the table below which can be scaled for the mass of wood being processed.

Reagent	Quantity
Wood shavings	1g
Deionised water	175ml
Sodium chlorite	2.5g
Acetic acid	1.7ml
10% (w/v) NaOH	75ml
17% (w/v) NaOH	67ml

2. Place the wood sample in glass Erlenmeyer flask with the appropriate amount of water, acetic acid and sodium chlorite.

3. Cover the top of the flask with a watch glass and place in an ultrasonic bath at 70°C for 1 hour.

4. Repeat the additions of acetic acid and sodium chlorite 3 more times.

As there is a large amount of chemical heterogeneity between the wood of different tree species and between individuals of the same species modifications may be needed. Some species may need additional rounds of treatments with acetic acid and sodium chlorite. Good product was achieved with the 4 additions described for Irish oak samples. However to get a good white α-cellulose product from Irish cedar samples (a softwood) the samples were treated as above but were left sitting in the solution overnight before continuing.

5. Filter the sample using a No. 1 glass sinter.

6. Wash the sample with hot and then room temperature Q-water.

At this stage the resulting carbohydrate fraction (holocellulose) can be divided into alkali soluble hemicellulose and alkali insoluble α-cellulose using repeated caustic base treatments as follows.

7. Add the sample to a fresh Erlenmeyer flask containing the 10% NaOH, cover with a watch glass and place in an ultrasonic bath for 45 minutes at 80°C.
8. Filter the sample and wash with cold and then room temperature Q-water.
9. Return the sample to the Erlenmeyer flask adding the 17% NaOH, cover with a watch glass and place in a room temperature ultrasonic bath for 45 minutes.
10. Filter the sample and wash with Q-water.
11. Wash with 1% HCl followed by copious amounts of room temperature Q-water.
12. Dry the white α-cellulose in a 40°C nitrogen oven overnight.

Cleaning the Glass Sinters

The glass sinters used in each filtration stage must be thoroughly cleaned to remove all traces of cellulose. Sinters are first cleaned in deionised water before soaking them overnight in a chromic acid solution which is prepared as follows:

1. While heating and stirring dissolve 6g of potassium dichromate in 45ml of Q-water.
2. Cool the solution on a stir plate.
3. Using a pipette slowly add 195ml of concentrated H_2SO_4. Considerable heat is evolved so use a water bath.
4. Allow to cool and transfer the solution to glass pots.

Finally the chromic acid solution is removed from the sinters by washing in copious amounts of deionised water.

Appendix 3: A New Microwave Extraction Technique to Extract α-Cellulose from Soft Woods

This method is based on running 6 vessels at once with them evenly spaced in the rotating carousel of a 650W MDS-2000 microwave which has been shown to have an APO of 542.0 ± 24.2W.

For all stages in this extraction procedure set the maximum pressure to 110psi and the maximum temperature to 120°C.

1. Chop wood samples into ~40μm slivers using a chisel and scalpel.
2. Place 1g of wood in each PFA digestion vessel.
3. Carefully add 20ml of 2:1 chloroform-ethanol to each extraction vessel ensuring that all of the solid is submerged.
4. Fit each vessel cap with a new rupture membrane and secure the locking rings to hand tightness.
5. Place the vessels in the microwave with Teflon vent tubes connecting each exhaust port to a central Teflon containment vessel.
6. Extract the samples for 45 minutes as 3 cycles of 5 minutes heating at 70% power (380W) followed by a 10 minutes at 12% power (65W).
7. Cool the vessels for 30 minutes in a water bath before opening. Decant the supernatant and wash the wood slivers with a small volume of benzene-methanol azeotrope.
8. Add 20ml of fresh benzene-methanol azeotrope to each vessel.
9. Extract the samples for 45 minutes as 3 cycles of 5 minutes heating at 60% power (325W) followed by 10 minutes at 12% power (65W).
10. Again allow the vessels to cool before opening and removing the supernatant.
11. Remove all traces of benzeze by washing each sample with a small volume of acetone.
12. Add 20ml of fresh acetone to each vessel.
13. Run the samples for 5 minutes at 60% power followed by 10 minutes at 12% power.

14. Cool the vessels and remove the supernatant.

15. Transfer each sample to an Erlenmeyer flask.

16. Leave the samples to dry overnight in a fume cupboard.

17. Follow the procedure of *Loader et al.*, [1997], which is outlined in Appendix 2 to retrieve α-cellulose.

Appendix 4: Synthesis of ^3H free NaOH Following *Cornog* [1921]

To make 900ml of 17% NaOH approximately 87.9g of metallic sodium (Na) is needed. However this tends to yield NaOH with concentrations nearer 19% and experience indicates that 80% of this, or 70g of Na is sufficient. As Na tends to come in stick form the amount needed is worked out by volume using the density of Na ($0.971 g.cm^{-3}$). Therefore

$$\frac{70g}{0.971g.cm^{-3}} cm^3$$

of Na is needed, which equals $72.1 cm^3$. Typically the Na used has a surface area of $4.4 cm^2$ so a 16.4cm length is needed to make 900ml of 17% NaOH.

Sodium hydroxide was routinely synthesised in a fume cupboard as follows:

1. To minimise contamination transfer 900ml of ^3H free water to a glass separating funnel using positive pressure as described below.

2. Add enough anhydrous ether to form a ~4-5cm layer on top of the water as is shown below.

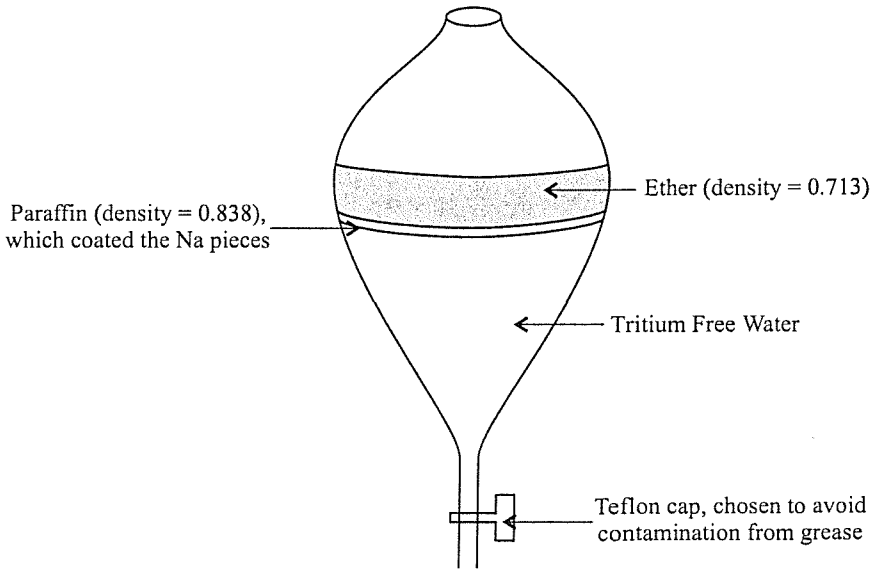

Figure A4.1. The apparatus used to synthesise ^3H free NaOH using metallic sodium. All densities are in g/cm^3.

3. Put a glass stopper on the flask and shake it to mix the 2 liquids. Release the cap a couple of times to vent the fumes. Remove the glass stopper.

4. Allow the liquids in the funnel to settle so the boundary between the water and ether can be clearly seen.

5. Cut the Na into ~0.5cm cubes and to prevent contact with air store them in a tray of paraffin ensuring they are all submerged.

6. Blot a piece of Na with tissue to minimise any ^3H contamination from the paraffin and carefully drop into the flask, taking care not to disturb the ether water boundary. Trace amounts of paraffin form a layer between the ether and the water.

7. Continue adding Na so there are no more than 3-4 pieces reacting at once.

The depth of the ether layer should be continuously monitored to ensure it is still 4-5cm deep. If it needs to be topped up pour some ether into a glass bottle and add a small amount of ^3H free water using positive pressure. Shake the bottle and pour the liquid into the top of the separating funnel.

8. Continue adding Na until it has all been added.

9. Allow all of the pieces to react completely.

10. Drain any solids from the bottom of the flask.

11. Drain the NaOH into a round bottomed flask.

12. Remove the last traces of ether by boiling the solution in a spark free heating mantle (usually takes 30-45 minutes). Use an argon atmosphere to prevent ^3H contamination and reaction with atmospheric CO_2.

13. Allow the solution to cool and settle, still under an argon blanket.

14. Calculate the strength of the solution by titrating against 1M HCl using a Phenolphthalein indicator which will change from colourless to pink when the end point is reached.

15. To minimise contamination store the NaOH in an argon filled bottle prepared as described in 3.3.6.

Transferring Liquids Using Positive Pressure

To minimise atmospheric contamination of ^3H free water and reagents they are transferred using positive pressure supplied by argon gas rather than pouring. The bottle (or measuring cylinder) containing the ^3H free liquid is fitted with a 2 hole bung. Tubing from 1 hole leads to the argon supply and to the bottle headspace, the other is submerged in the liquid to be transferred. When a gentle argon flow is started the pressure exerted by the gas forces the liquid from the bottle as is shown below.

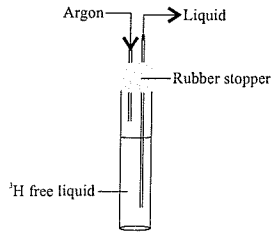

Appendix 5: Synthesis of ^3H free H_3PO_4

To make 800ml of ^3H free H_3PO_4 it is necessary to add 135g of P_4O_{10} to 800ml of ^3H free water. The strongly hydroscopic nature of P_4O_{10} makes it difficult to weigh this amount on a balance without introducing significant ^3H contamination from ambient water vapour. Therefore the solid is added to water using a steel measuring scoop. A teaspoon (5ml) measuring scoop was found to hold 3g of P_4O_{10} on average so 45 scoops were added to make 800ml of the acid.

Phosphoric acid was routinely synthesised in a glove box placed within a fume cupboard as follows:

1. Make sure that all necessary items are in the glove box before starting:
    - Unopened bottle of ^3H free water.
    - Pot of P_4O_{10}.
    - Large beaker.
    - Measuring scoop.
    - Crystallising dish.
    - Stir plate and stir-bar.
    - Tissue paper.
    - Argon filled bottle, prepared as described in 3.3.6.
    - Glass funnel.
2. Place the beaker, containing the stir-bar on the stir plate.
3. Start a large argon flow to the glove box.
4. Allow the box to purge (based on the flow rate used). Once purged the flow can be reduced a bit but needs to be sufficient to clear the box of the fumes produced by the reaction.
5. Transfer 800ml of ^3H free water to the beaker and start stirring.

6. Open the pot of P_4O_{10} and fill the crystallising dish with the powder. Firmly close the lid on the P_4O_{10} pot to minimise contamination.

7. Measure out a scoop of P_4O_{10} powder.

8. Quickly add the scoop of powder directly to the water and swirl to remove any paste stuck to the metal.

9. Dry the teaspoon with tissue paper.

10. Repeat the process monitoring how hot the beaker becomes, taking breaks if necessary.

11. Continue until 45 scoops of the P_4O_{10} has been added.

12. Allow the acid to cool while stirring.

13. Using the funnel carefully pour the acid into the argon filled bottle.

14. Remove the bottle from the glove box.

15. Stop argon flow to the box.

16. Fit the bottle containing the acid with a two holed bung. Fit one hole of the bung with tubing from the argon supply and purge the bottle with a gentle flow to ensure it is stored under an argon blanket.

17. Once purged cap and tape the bottle for storage.

18. The strength of the solution and the amount needed for the exchange can be calculated by titrating against the ^3H free NaOH produced as described in Appendix 4, using Phenolphthalein as an indicator.

Appendix 6: The Exchange Reaction

6.1 Calculating the volume of NaOH needed per gram of cellulose

Molar mass of cellulose ($C_6H_{10}O_5$) = 162.14 g.mol^{-1}

∴number of moles of exchangeable hydrogen in 1g cellulose =

$$\frac{1}{162.14} x10x0.3 = 0.0185$$

As 30% of the hydrogens in cellulose are

In 100ml of 17% w/v NaOH there are $\frac{17}{39.997} = 0.425$ moles of OH^-

∴ there are 4.25 x 10^{-3} moles of OH in 1 ml of 17% w/v NaOH.

∴to react with all of the exchangeable hydrogens in 1g cellulose need $\frac{0.0185}{4.25x10^{-3}}$ ml

= 4.4ml NaOH.

As a large excess is wanted 45ml of NaOH is used per gram of cellulose.

6.2 Carrying out an exchange

1. Dry the cellulose to be exchanged, a measuring cylinder and an Erlenmeyer flask in a 70°C N_2 oven overnight.

2. Remove the flask and measuring cylinder from the oven and purge with argon.

4. Weigh the cellulose and quickly transfer to the Erlenmeyer flask. Stopper the flask as is shown in Figure A6.1 and start a gentle argon flow.

5. Use positive pressure (Appendix 4) to transfer ^3H free NaOH to the measuring cylinder (45ml per gram of cellulose) and then to the Erlenmeyer flak.

6. Add a stir-bar to the flask and place it over a stir plate. Start the reaction stirring so that all of the cellulose is gently swirling in the solution. Do not allow the stirring to be

vigorous enough to splash cellulose up the sides of the flask where it will stick and not exchange.

7. Leave the cellulose and NaOH stirring under a gentle argon flow.

8. After 3-4 hours remove the argon flow from the flask. Cap and securely tape the flask to leave the cellulose solution sitting under an argon blanket.

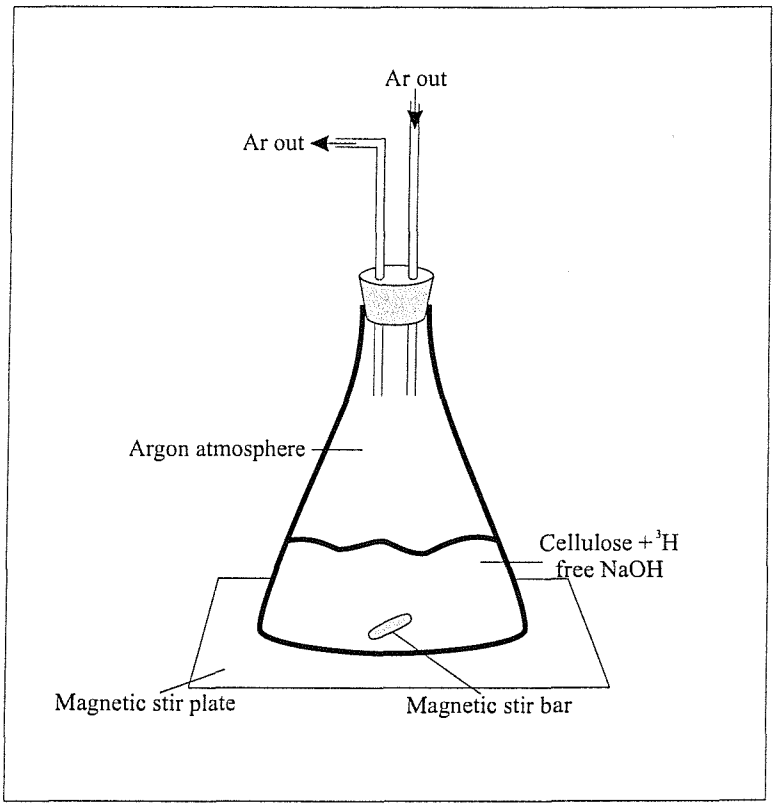

Figure A6.1. Apparatus for the exchange reaction. After 3 hours the flask can be capped and taped to minimise the use of argon gas.

9. Leave the solution overnight and place another measuring cylinder (for measuring out H_3PO_4) into a 70°C N_2 oven.

10. After 24 hours remove the measuring cylinder from the oven and purge with argon.

11. Start an argon flow to a glove box containing:

    a. A pre-weighed 200ml alumino-silicate sample bulb.

    b. Centrifuge bottles (with screw tops).

c. A long syringe needle, tweezers and spatula.

d. Supply of ^3H free water.

e. A glass filter assembly fitted with a number 1 glass sinter.

f. Glass beakers.

g. Parafilm.

Choose the flow rate to allow the box to purge within 1 hour.

12. Calculate the amount of H_3PO_4 needed to neutralise the base used to exchange the sample (by titrating the two). Experience shows that adding an extra 25% of the acid ensures that all of the hydroxyl group sites are reprotonated.

13. Remove the tape and cap from the reaction flask and re-stopper the flask with a gentle argon flow.

14. Use positive pressure to transfer the acid to a measuring cylinder and then to the reaction flask.

15. Leave the solution stirring under argon for 30 minutes to reprotonate.

16. Test the pH of the solution. If it is still basic then add more acid and allow to stir before testing the pH again. This step is rarely needed if an extra 25% of acid is added initially.

17. Take the reaction vessel to an argon filled glove box and pour the sample into a centrifuge bottle.

18. Centrifuge the sample for 5 minutes at 3500rpm.

19. Return the bottle to the glove box and remove the supernatant from the sample (for speed and ease this is done by having a Pasteur pipette connected to an external vacuum pump).

20. Wash the sample by filling the bottle with ^3H free water.

21. Centrifuge for 5 minutes at 3500rpm, before returning the bottle to the glove box and removing the supernatant.

22. Repeat steps 20 and 21 three more times to do a total of 4 washes.

23. After the final wash only remove 2/3 of the supernatant from the bottle.

24. Shake the solution and cellulose vigorously and pour through a filter assembly, without vacuum.

25. The wet cellulose can now be transferred to a labelled alumino-silicate glass bulb. Experience showed that this is best achieved by using tweezers to place cellulose into the end of the bulb and guiding it down the neck with a long syringe needle.

26. Once all of the cellulose has been transferred to the bulb wash the bulb down with a small amount of ^{3}H free water to ensure there is no material in the constriction, which could interfere with the flame sealing of the bulb.

27. Parafilm the top of the bulb to minimise contamination.

28. Degas the sample as described in 3.3.8.

Up to 4 samples were routinely exchanged at once. When step 24 is reached samples can be left sitting in solution while a sample is being transferred to a bulb.

Appendix 7: Standard Expansion and Calibrations

7.1 Volume Calibrations

As discussed in 3.4.3.1 there are a range of standard tanks available to match the required standard size as closely as possible. The volumes of both the standard collection tanks and the standard tanks used in the noble gas mass spectrometer system are shown in Table A7.1. These volumes were calculated by filling each tank with demineralised water at a known temperature and weighing [*Postlethwaite*, 2002].

Tank name	Tank + valve volume (cm^3)
Tank 2	19716 ± 6
Tank 3	19566 ± 6
Tank 4	19581 ± 6
Tank 5	19601 ± 6
Tank A	1846.18 ± 0.34
Tank B	27.251 ± 0.025

Table A7.1. The volumes of the standard collection tanks and standard tanks used at the Southampton University Noble Gas Laboratory. Tank B is generally used as the standard collection tank for low level ^3H measurements.

The volume of the Large and Small aliquots from the main standard tank and the aliquot connecting the external standard tank to the processing line were calibrated by comparing peak heights with glass aliquot volumes [*Postlethwaite*, 2002]. All of the aliquot volumes relevant to ^3H sample analysis are shown in Table A7.2.

Volume name	**Volume (cm^3)**	**% Error**
Primary Glass Aliquot (81/225)	0.8477 ± 0.00012	0.01%
Secondary Glass Aliquot (10/145)	0.7855 ± 0.00012	0.01%
Large Aliquot	0.74855 ± 0.0007	0.09%
Small Aliquot	0.07405 ± 0.0004	0.54%
External Aliquot	0.75282 ± 0.0008	0.11%

Table A7.2. The volumes of the aliquots routinely used for standard delivery to the noble gas mass spectrometer and the volume of the glass aliquots used for the aliquot volume calibrations.

The auxiliary volumes used in standard delivery and expansion were measured by expanding an aliquot of air, of a known size between the standard aliquot and the auxiliary volume [*Postlethwaite*, 2002]. The auxiliary volume was then isolated and the peak height measurement from the gas trapped in this volume was compared with a full standard aliquot. The resulting auxiliary volumes are shown in Table A7.3.

Volume name	Volume (cc)	How measured
Behind large and small aliquots	16.41 ± 0.07	Peak height comparison run against large aliquot
Behind external aliquot	8.81 ± 0.77	Length and internal diameter of volume measured.
From aliquots to processing section	36.44 ± 0.29	Peak height comparison run against large aliquot

Table A7.3. The auxiliary volumes used in standard expansion and delivery.

7.2 Calculating Standard Size

For ^{3}H analysis of low level cellulose and liquid samples the main air standard was made by expanding ambient air collected in Tank B into Tank 3.

Volume of Tank B = 27.251cm^3

Volume of Tank 3 = 19566cm^3

Conditions during standard collection:

Air temperature = 6.4°C

Pressure = 1031.4hPa

Relative humidity = 65.88%

Abundance of He in the atmosphere = 5.24 x 10^{-6}

7.2.1 Volume of dry air collected

Have to correct for the standard not being collected at STP.

$$V = \frac{273.15}{273.15+T} \times \frac{P - P_{H_2O}}{1013.25} . V_{col}$$

where:

T = the air temperature during standard collection in °C.

P = the barometric pressure during standard collection.

P_{H_2O} = the pressure of water vapour in the air during standard collection.

V_{col} = the volume of Tank B.

P_{H_2O} = *Vapour pressure of* H_2O *at* T°C x *relative humidity.*

$\therefore P_{H_2O}$ = 9.62062 x 0.6588 hPa

= 6.3381 hPa

$$\therefore \textit{volume of dry air collected, } V = \frac{273.15}{273.15+6.4} \times \frac{1031.4-6.3381}{1013.25} \times 27.251 \text{ cm}^3$$

$$V = 26.9375 \text{ cm}^3$$

7.2.2 Expansion volumes

The volumes that are filled with gas during an expansion and those that are retained after an expansion are highlighted in red below in Figure A7.1.

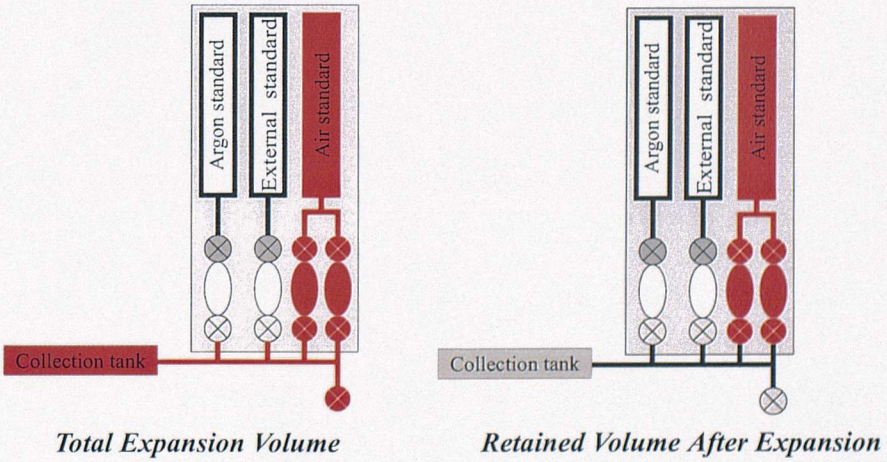

Figure A7.1. The volumes that were filled with gas during and after expansion of the main air standard for low level ^3H analysis.

7.2.3 Volume of dry air retained after expansion

$$V_{\exp} = V \times {}^{V_{retained}}\!/_{V_{\exp ansion}}$$

$$= V \times \frac{\left(V_{aliquots} + V_{Tank3} + V_{behindaliquots}\right)}{\left(V_{aliquots} + V_{Tank3} + V_{behindaliquots} + V_{line} + V_{valve} + V_{TankB}\right)}$$

$$= 26.9375 \times \frac{0.74885 + 0.07405 + 19566 + 16.41}{0.74885 + 0.07405 + 19566 + 16.41 + 36.44 + 1.78 + 27.251}\ \text{cm}^3$$

$$= 26.8477\ \text{cm}^3$$

7.2.4 Volume of He retained after expansion

$$V_{He} = V_{\exp} \times He_{atm}$$

$$= 26.8477 \times 5.24x10^{-6}\ \text{cm}^3$$

$$= 1.4068 \times 10^{-4}\ \text{cm}^3$$

7.2.5 Volume of He in first aliquot

$$S = V_{He} \times \frac{V_{aliquots}}{V_{retained}}$$

$$\text{S} = 1.4068 \times 10^{-4} \times \frac{0.74885 + 0.07405}{0.74885 + 0.07405 + 19566 + 16.41}$$

$$\underline{\text{S} = 5.911 \times 10^{-9}\ \text{cm}^3}$$

The size of the standard decreases over time as more aliquots are removed for analysis and is given at any time by:

$$S_{0,g} = S \times \left(1 - \alpha_L\right)^m \times \left(1 - \alpha_S\right)^n$$

where:

S is the size of the standard.

α_L is the ratio of the large aliquot volume to the total volume behind the two aliquots.

α_S is the ratio of the small aliquot volume to the total volume behind the two aliquots.

m is the number of large aliquots already removed from the air standard tank.

n is the number of small aliquots already removed from the main standard tank.

Appendix 8: Expansion Efficiency Experiments

Expansion efficiency experiments were carried out to assess how well gases equilibrated between the various volumes involved in standard preparation. A 20 litre standard tank was evacuated and filled with marine air before being placed on the vacuum system in the isothermal metal standard box, with two other evacuated 20 litre standard tanks as shown in Figure A6.1. The valves connecting the tanks were opened and the gases were left overnight to equilibrate between the three tanks. The tanks were then isolated and a series of mass spectrometric measurements were made of aliquots of gas from each standard.

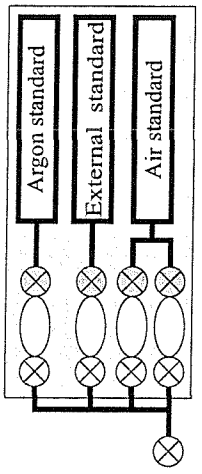

Figure A8.1. The layout of the volumes used in the expansion efficiency experiments.

Assuming that the expansion is complete the partial pressure of dry air in the main standard tank is given by:

$$P_i^0 = P^0 \frac{V_i}{V_T} \qquad (1)$$

where P_i^0 is the partial pressure of dry air in tank i directly following expansion, P_0 is the partial pressure of dry air in the tank that was filled with marine air before expansion, V_i is the volume of tank i and V_T is the total volume used in the expansion. However it has been show by inter-standard comparisons that this assumption may not be valid [*Postlethwaite*, 2002].

At time t the partial pressure behind aliquot i is given by:

$$P_i = P_i^0 (1-\alpha_i)^{N_i} \quad (2)$$

P_i: the number of aliquots taken from tank i at time t

$(1-\alpha_i)$: the ratio of aliquot i to the total volume behind it

The measured ion beam intensity of helium in an aliquot from tank i is proportional to the size of the gas in the aliquot:

$$I_i \propto P_i v_i \quad (3)$$

where v_i is the volume of the aliquot connected to tank i. Therefore combining (2) and (3):

$$\frac{I_2}{I_1} = \frac{P_2 v_2}{P_1 v_1} = \frac{P_2^0 (1-\alpha_2)^{N_2} v_2}{P_1^0 (1-\alpha_1)^{N_1} v_1} \quad (4)$$

and if R is defined such that:

$$P_i^0 = R_{1,i} P_1^0 \quad (5)$$

then substituting into (4) gives:

$$R_{1,i} = \frac{I_i (1-\alpha_1)^{N_1} v_1}{I_1 (1-\alpha_i)^{N_i} v_i} \quad (6)$$

Mass is conserved during the expansion such that:

$$P_0^0 V_1 = P_1^0 V_1 + P_2^0 V_2 + P_3^0 V_3 + P_r^0 V_r \quad (7)$$

where P_r and V_r refer to the pressure and volume in the vacuum lines that connect the tanks during the expansion. P_r^0 cannot be measured so it was estimated as the average of the partial pressures in the three tanks:

$$P_r^0 = \frac{1}{3}\left(P_1^0 + P_2^0 + P_3^0\right) = \frac{P_1^0}{3}\left(1 + R_{1,2} + R_{1,3}\right) \tag{8}$$

Hence by substituting we get:

$$P_0^0 V_1 = P_1^0 V_1 + R_{1,2} P_1^0 V_2 + R_{1,3} P_1^0 V_3 + \frac{P_1^0 V_r}{3}\left(1 + R_{1,2} + R_{1,3}\right) \tag{9}$$

and

$$P_1^0 = \frac{P_0^0 V_1}{f} \tag{10}$$

where

$$f = V_1 + R_{1,2}\left(V_2 + \frac{V_r}{3}\right) + R_{1,3}\left(V_3 + \frac{V_r}{3}\right) + \frac{V_r}{3}$$

The experiment was repeated with the expansion carried out on a separate vacuum system yielding the results shown in the table below.

	P_1^0	P_2^0	P_3^0
Experiment 1			
Assuming complete expansion	0.307832	0.305506	0.305903
Following correction	0.305506	0.308412	0.309608
Ratio	0.99244	1.00951	1.01211
Experiment 2			
Assuming complete expansion	0.308767	0.307842	0.307900
Following correction	0.305034	0.307454	0.310690
Ratio	0.98791	0.99874	1.00906

Table A8.1 – The partial pressure of air inside the three standard tanks used in the expansion efficiency experiments, adapted from Postlethwaite, *[2002].*

Appendix 9: Detection Limit Calculations

As the helium detection limit of the mass spectrometer is known the smallest possible signal which can be measured in a cellulose sample can be calculated as follows.

- Let the detection limit of the mass spectrometer = x

Considering 1g of cellulose with a concentration of 1TU:

- 1g cellulose = $\frac{1}{162.142}$ moles.

$= \frac{1}{162.142}$ x 10 moles hydrogen.

$= \frac{1}{162.142}$ x10 x 6.022×10^{23} atoms hydrogen.

$= \frac{1}{162.142}$ x 10 x 6.022×10^{23} x 1×10^{-18} atoms tritium.

∴ **<u>1g cellulose at 1TU ~ 37140 ^{3}H atoms</u>**

- If the mass spectrometer detection limit for ^{3}He is x atoms.

- So will detect $\frac{37140}{x}$ atoms per TU.g.

- ∴ have a $\frac{x}{37140} TUg$ detection limit for 1g of cellulose at 1TU.

- ∴ the TU detection limit for a sample of mass M(g) which is sealed for helium ingrowth for t days is equal to:

$$\frac{x}{37140} \cdot \frac{1}{M} \cdot \frac{1}{\lambda t}$$

as $\lambda = \frac{\ln 2}{t_{1/2}} = \frac{\ln 2}{4500}$ this equates to the detection limit for a cellulose sample of mass M(g) sealed for t days being:

$$\frac{x}{37140}.\frac{4500}{\ln 2.M.t}\,\mathbf{TU}$$

Therefore if the ^{3}H detection limit of the instrument is 600 atoms the smallest possible ^{3}H signal that can be measured in a 3g cellulose sample sealed for 150 days is 0.23TU, compared to 0.19TU for the same sample with a ^{3}He detection limit of 500 atoms.

Similarly the detection limit for a water sample of mass M(g) sealed for t days is:

$$\frac{x}{66855}.\frac{4500}{\ln 2.M.t}\,\mathbf{TU}$$

while that for Mg of NaOH sealed for t days is:

$$\frac{x}{15056}.\frac{4500}{\ln 2.M.t}\,\mathbf{TU}$$

and that for Mg of H_3PO_4 sealed for t days is:

$$\frac{x}{18436}.\frac{4500}{\ln 2.M.t}\,\mathbf{TU}$$

6. References

Barnabas, I.J., J.R. Dean, I.A. Fowlis, and S.P. Owen, Extraction of Polycyclic Aromatic Hydrocarbons From Highly Contaminated Soils Using Microwave Energy, *Analyst, 120*, 1897-1904, 1995.

Baumgartner, A., and E. Reichel, *The World Water Balance*, 179 pp., Elsevier, 1975.

Begemann, F., and W.F. Libby, Continental water balance, ground water inventory and storage times, surface ocean mixing rates and world-wide circulation patterns from cosmic-ray and bomb tritium, *Geochimica et Cosmochimica Acta, 12*, 277-296, 1957.

Broecker, W.S., T.H. Peng, and G. Östlund, The distribution of bomb tritium in the ocean, *Journal of Geophysical Research. 91*, 14,331-14,344, 1986.

Buhay, W.M., T.W.D. Edwards, and R. Aravena, Evaluating kinetic fractionation factors used for ecological and paleoclimatic reconstructions from oxygen and hydrogen isotope ratios in plant water and cellulose, *Geochimica et Cosmochimica Acta, 60*, 2209-2218, 1996.

Clarke, W.B., W.J. Jenkins, and Z. Top, Determination of Tritium by Mass Spectrometric Measurement of ^{3}He, *International Journal of Applied Radiation and Isotopes, 27*, 515-522, 1976.

Coleman, M.L., T.J. Shepherd, J.J. Durham, J.E. Rouse, and G.R. Moore, Reduction of Water with Zinc for Hydrogen Isotope Analysis, *Analytical Chemistry, 54*, 993-995, 1982.

Cornog, J., A Simple Method for the Production of Sodium Hydroxide Free from Carbon Dioxide, *Journal of the American Chemical Society, 43*, 2573-2574, 1921.

Craig, H., and D. Lal, The production rate of natural tritium, *Tellus, 13*, 85-105, 1961.

Da Silva, A., A.C. Young, and S. Levitus, Atlas of Surface Marine Data 1994, Volume 1: Algorithms and Procedures, NOAA Atlas NESDIS 6, U.S. Department of Commerce, Washington, D.C., 1994.

Danielsen, E.F., Stratospheric-Tropospheric Exchange Based on Radioactivity, Ozone and Potential Vorticity, *Journal of Atmospheric Science, 25*, 502-518, 1968.

Dansgaard, W., Stable isotopes in precipitation, *Tellus, 16*, 436-468, 1964.

Dawsey, T.R., and C.L. M^{C}Cormick, The Lithium Chloride / Dimethylacetamide Solvent for Cellulose: A Literature Review, *JMS-Rev. Macromolecular Chemistry and Physics, C30*, 405-440, 1990.

Dawson, T.E., and J.R. Ehleringer, Isotopic enrichment of water in 'woody' tissues of plants: Implications for plant water source, water uptake, and other studies which use the stable isotopic composition of cellulose, *Geochimica et Cosmochimica Acta, 57*, 3487-3492, 1993.

DeNiro, M.J., The effects of different methods of preparing cellulose nitrate on the determination of the D/H ratios of non-exchangeable hydrogen of cellulose, *Earth and Planetary Science Letters, 54*, 177-185, 1981.

DeNiro, M.J., and L.W. Cooper, Post-photosynthetic modification of oxygen isotope ratios of carbohydrates in the potato: Implications for paleoclimatic reconstruction based upon isotopic analysis of wood cellulose, *Geochimica et Cosmochimica Acta, 53*, 2573-2580, 1989.

DeNiro, M.J., and L.W. Cooper, Water is lost from leaves and trunks of trees by fundamentally different mechanisms, *Geochimica et Cosmochimica Acta, 54*, 1845-1846, 1990.

Doney, S.C., D.M. Glover, and W.J. Jenkins, A global model function of the tritium concentration in precipitation, 1960-1986., *Journal of Geophysical Research, 97* (5481-5492), 1992.

Doney, S.C., W.J. Jenkins, and J.L. Bullister, A comparison of ocean tracer dating techniques on a meridional section in the eastern North Atlantic, *Deep Sea Research, 44*, 603-626, 1997.

Doney, S.C., W.J. Jenkins, and H.G. Östlund, A tritium budget for the North Atlantic, *Journal of Geophysical Research, 98*, 18,069-18,081, 1993.

Dreisigacker, E., and W. Roether, Tritium and ^{90}Sr in North Atlantic Surface Waters, *Earth and Planetary Science Letters, 38*, 301-312, 1978.

Engel, M.H., and S.A. Macko, *Organic Geochemistry: Principles and Applications*, 861 pp., Plenum Press, 1993.

England, M.H., and E. Maier-Reimer, Using chemical tracers to assess ocean models, *Review of Geophysics, 39*, 29-70, 2001.

Enhlat, D.H., Vertical profiles and transport of HTO in the troposphere, *Journal of Geophysical Research, 76*, 7351-7367., 1971.

Epstein, S., and C.J. Yapp, Climatic Implications of the D/H Ratio of Hydrogen in C-H Groups in Tree Cellulose, *Earth and Planetary Science Letters, 30*, 252-261, 1976.

Epstein, S., C.J. Yapp, and J.H. Hall, The determination of the D/H ratio of non-exchangeable hydrogen in cellulose extracted from aquatic and land plants, *Earth and Planetary Science Letters, 30*, 214-251, 1976.

Eriksson, E., An account of the major pulses of tritium and their effects in the atmosphere, *Tellus, 17*, 118-130, 1965.

Feng, X., R.V. Krishnamurthy, and S. Epstein, Determination of D/H ratios of nonexchangeable hydrogen in cellulose: A method based on the cellulose-water exchange reaction, *Geochimica et Cosmochimica Acta, 57*, 4249-4256, 1993.

Fieux, M., R. Molcard, and A.G. Ilahude., Geostrophic transport of the Pacific-Indian Oceans throughflow, *Journal of Geophysical Research, 101*, 12,421-12,432, 1996.

Fine, R.A., Direct evidence using tritium data for throughflow from the Pacific into the Indian Ocean, *Nature, 315*, 478-480, 1985.

Fine, R.A., and H.G. Östlund, Source function for tritium transport models in the Pacific, *Geophysical Research Letters, 4*, 461-464, 1977.

Fine, R.A., W.H. Peterson, and H.G. Östlund, The Penetration of Tritium into the Tropical Pacific, *Journal of Physical Oceanography, 17*, 553-564, 1987.

Fine, R.A., J.L. Reid, and H.G. Östlund, Circulation of Tritium in the Pacific Ocean, *Journal of Physical Oceanography, 11*, 3-14, 1981.

Fischer, L.B., Microwave Dissolution of Geologic Material: Application to Isotope Dilution Analysis, *Analytical Chemistry, 58*, 261-263, 1986.

Flanagan, L.B., and J.R. Ehleringer, Stable isotope composition of stem and leaf water: applications to the study of plant water use, *Functional Ecology, 5*, 270-277, 1991.

Friedman, I., A.C. Redfield, B. Schoen, and J. Harris, The Variation of the Deuterium Content of Natural Waters in the Hydrologic Cycle, *Review of Geophysics, 2*, 177-224, 1964.

Frilette, V.J., J. Hanle, and H. Mark, Rate of Exchange of Cellulose with Heavy Water, *Journal of the American Chemical Society, 70*, 1107-1113, 1948.

Fritts, H.C., *Tree Rings and Climate*, 567 pp., Academic Press inc., London, 1976.

Ganzler, K., and A. Salgo, Microwave-extraction - a new method superseding traditional Soxhlet extraction, *Z Lebensm Unters Forsch, 184*, 274-276, 1987.

Ganzler, K., A. Salgo, and K. Valko, Microwave extraction : A novel sample preparation method for chromatography, *Journal of Chromatography, 371*, 299-306, 1986.

Gat, J.R., The Isotopes of Hydrogen and Oxygen in Precipitation, in *Handbook of Environmental Isotope Geochemistry, Vol 1 - The Terrestrial Environment A*, edited by P. Fritz, and J.C. Fontes, pp. 21-47, 1980.

Godfrey, J.S., The effect of the Indonesian throughflow on ocean circulation and heat exchange with the atmosphere: A review, *Journal of Geophysical Research, 101*, 12,217-12,237, 1996.

Gordon, A.L., Interocean Exchange of Thermocline Water, *Journal of Geophysical Research, 91*, 5037-5046, 1986.

Gray, J., and S.J. Song, Climatic implications of the natural variations of D/H ratios in tree ring cellulose, *Earth and Planetary Science Letters, 70*, 129-138, 1984.

Green, J.W., Methods of Carbohydrate Chemistry III, edited by R.L. Whistler, pp. 9-21, Academic Press, New York, 1963.

Grinsted, M.J., and A.T. Wilson, Hydrogen isotope chemistry of cellulose and other organic materials of geochemical interest, *New Zealand Journal of Science, 22*, 281-287, 1979.

Hall, I.R., Cycling of Trace Metals in Coastal Waters: Biogeochemical Processes Involving Suspended Particles, PhD Thesis, University of Southampton, 1993.

Hedges, J.L., The Chemistry of Archaeological Wood, in *Arid Wood: Properties, Chemistry and Preservation*, pp. 111-140, American Chemical Society, 1990.

Heinze, C., E. Maier-Reimer, and P. Schlosser, Transient tracers in a global OGCM: Source functions and simulated distributions, *Journal of Geophysical Research, 103*, 15,903-15,922, 1998.

Huang, R.X., and S. Russell, Ventilation of the Subtropical North Pacific, *Journal of Physical Oceanography, 24*, 2589-2605, 1994.

Jean-Baptiste, P., and M.J. Messias, Using tracers to study ocean circulation: What more can we learn by the year 2000?, *Annales de l'Institut océanographique, 69*, 283-305, 1993.

Jenkins, W.J., Studying subtropical thermocline ventilation and circulation using tritium and ^{3}He, *Journal of Geophysical Research, 103*, 15,817-15,831, 1998.

Jepsen, D., AGSO vigil traces nuclear testing, *AusGEO News, 59*, 6-8, 2000.

Jia, Y., and K.J. Richards, Tritium distributions in an isopycnic model of the North Atlantic, *Journal of Geophysical Research, 101*, 11,883-11,901, 1996.

Johnson, G.C., The Pacific Ocean subtropical cell surface limb, *Geophysical Research Letters, 28*, 1771-1774, 2001.

Jones Williams, M.A.J., Investigations into the Effects of Petroleum Hydrocarbons on the Immunocompetence of *Ostrea edulis* and the Potential Application for Biological Monitoring (with Preliminary Investigations on the Immunology of *Crassostrea rhizophrae)*, PhD thesis, University of Southampton, 1997.

Jouzel, J., Isotopes in Cloud Physics: Multiphase and Multistage Condensation Processes, in *Handbook of Environmental Isotope Geochemistry, Vol 2 - The Terrestrial Environment B*, edited by P. Fritz, and J.C. Fontes, pp. 61-112, Elsevier, 1986.

Jouzel, J., J.G. Russell, R. Suozzo, R. Koster, J.W.C. White, and W.S. Broecker., Simulations of the HDO and $H_2{}^{18}O$ Atmospheric Cycle Using the NASA/GISS General Circulation Model: The Seasonal Cycle for Present Day Conditions, *Journal of Geophysical Research, 92* (14,739-14,760), 1987.

Key, R.M., Changes in the Pacific Ocean Distribution of Radiocarbon, *US WOCE Implementation Report, 9*, 5-8, 1997.

Koster, R.D., W.S. Broecker, J. Jouzel, R.J. Suozzo, G.L. Russell, D. Rind, and J.W.C. White, The global geochemistry of bomb-produced tritium: general circulation model compared to available observations and traditional interpretations, *Journal of Geophysical Research, 94*, 18,305-18,326, 1989.

Kozák, K., Analysis of Tritium in Tree Rings, *Acta Physica Academiae Scientiarum Hungaricae, 52*, 429-434, 1982.

Kozák, K., B. Obelic, and N. Horvatincic, Tritium and ^{14}C in Tree Rings of the Last Three Decades, *Radiocarbon, 31*, 766-770, 1989.

Kozlowski, T.T., and S.G. Pallardy, *Physiology of Woody Plants, 2nd Edition*, Academic Press, 1997.

Kurahashi, T., T. Mizutani, and J. Yoshida, Effects of intramolecular hydrogen-bonding network on the relative reactivities of carbohydrate OH groups, *Journal of the Chemical Society, Perkin Transactions, 1*, 465-473, 1999.

Lawrence, J.R., and J.W.C. White, Growing season precipitation from D/H ratios of Eastern White Pine, *Nature, 311*, 558-560, 1984.

Leavitt, S.W., and S.R. Danzer, Method for Batch Processing Small Wood Samples to Holocellulose for Stable-Carbon Isotope Analysis, *Analytical Chemistry., 65*, 87-89, 1993.

Libby, W.F., Moratorium tritium geophysics, *Journal of Geophysical Research, 68*, 4485-4494, 1963.

Lipps, F.B., and R.S. Hemler, On the downward transfer of tritium to the ocean by a cloud model, *Journal of Geophysical Research, 97*, 12,889-12,900, 1992.

Liu, Z., and B. Huang, Why is There a Tritium Maximum in the Central Equatorial Pacific Thermocline?, *Journal of Physical Oceanography, 28*, 1527-1533, 1998.

Liu, Z., and S.G.H. Philander, Tropical-Extratropical Oceanic Exchange Pathways, in *Ocean Circulation and Climate*, edited by G. Siedler, J. Church, and J. Gould, pp. 247-257, Academic Press, 2001.

Loader, N.J., I. Robertson, A.C. Barker, V.R. Switsur, and J.S. Waterhouse, An improved technique for batch processing of small wholewood samples to α-cellulose, *Chemical Geology, 136*, 313-317, 1997.

Lopez-Avila, V., R. Young, and W.F. Beckert, Microwave-Assisted Extraction of Organic Compounds from Standard Reference Soils and Sediments, *Analytical Chemistry, 66*, 1097-1106, 1994.

Lott, D.E., and W.J. Jenkins, An automated cryogenic charcoal trap system for helium isotope mass spectrometry, *Review of Scientific Instruments, 55*, 1982-1988, 1984.

Lucas, L.L., and M.P. Unterweger, Comprehensive review and critical evaluation of the half-life of tritium, *Journal of Research of the National Institute of Standards and Technology, 105*, 541-549, 2000.

Mahadevan, A., An analysis of bomb radiocarbon trends in the Pacific, *Marine Chemistry, 73*, 273-290, 2001.

Mann, J., and H.J. Marrinan, The reaction between cellulose and heavy water. Parts 1, 2 and 3., *Transactions of the Faraday Society, 52*, 481-497, 1956.

Marsh, J.T., and F.C. Wood, *An Introduction to the Chemistry of Cellulose*, 431 pp., Chapman and Hall, 1938.

Matusiewicz, H., Development of a High-Pressure Asher Focused Microwave System for Sample Preparation, *Analytical Chemistry, 71*, 3145-3149, 1999.

M^{C}Creary, J.P., and P. Lu, Influence of the Indonesian Throughflow on the Circulation of Pacific Intermediate Water, *Journal of Physical Oceanography, 31*, 932-942, 2001.

McGuffie, K., and A. Henderson-Sellers, Forty years of numerical climate modelling, *International Journal of Climatology, 21*, 1067-1109, 2001.

M^{C}Phaden, M.J., and R.A. Fine, A Dynamical Interpretation of the Tritium Maximum in the Central Equatorial Pacific, *Journal of Physical Oceanography, 18*, 1454-1457, 1988.

Memery, L., and C. Wunsch, Constraining the North Atlantic Circulation with Tritium Data, *Journal of Geophysical Research, 95*, 5239-5256, 1990.

Michel, R.L., and H.E. Suess, Bomb Tritium in the Pacific Ocean, *Journal of Geophysical Research, 80*, 4139-4152, 1975.

Morey, S.L., J.F. Shriver, and J.J. O'Brien, The effects of Halmahera on the Indonesian Throughflow, *Journal of Geophysical Research, 104*, 23,281-23,296, 1999.

Östlund, H.G., The Residence Time of the Freshwater Component in the Arctic Ocean, *Journal of Geophysical Research, 87*, 2035-2043, 1982.

Östlund, H.G., and A.S. Mason, Atmospheric tritium, 1968-1984, in *Tritium Lab. Data Report,* 134pp, Rosenstiel School. of Marine. and Atmospheric. Science., Univ. of Miami, Miami, Florida., 1985.

Peixoto, J.P., and A.H. Oort, The atmospheric branch of the hydrological cycle and climate, in *Variations in the global water budget*, edited by A. Street-Perrott, M. Beran, and R. Ratcliffe, pp. 5-65, D. Reidel, 1983.

Pendall, E., Influence of precipitation seasonality on piñon pine cellulose δD values, *Global Change Biology, 6*, 1-15, 2000.

Pendall, E., J.L. Betancourt, and S.W. Leavitt, Paleoclimatic significance of δD and $d^{13}C$ values in piñon pine needles from packrat middens spanning the last 40,000 years., *Palaeogeography, Palaeoclimatology, Palaoecology, 147*, 53-72, 1999.

Peng, T.H., R.M. Key, and H.G. Östlund, Temporal variations of bomb radiocarbon inventory in the Pacific Ocean, *Marine Chemistry., 60*, 3-13, 1998.

Percival, E.G.V., *Structural Carbohydrate Chemistry (2nd Ed.)*, 360 pp., J. Garnet Miller LtD., 1962.

Postlethwaite, C.F., Developing a tool for evaluating the role of seasonal sea ice in deep-water formation, PhD Thesis, University of Southampton, 2002.

Potemra, J.T., R. Lukas, and G.T. Mitchum, Large-scale estimation of transport from the Pacific to the Indian Ocean, *Journal of Geophysical Research, 102*, 27,795-27,812, 1997.

Prabhakara, C., H.D. Chang, and A.T.C. Chang, Remote sensing of precipitable water over the oceans from Nimbus 7 microwave measurements, *Journal of Applied Meteorology, 21*, 59-68, 1982.

Qiu, B., and R.X. Huang, Ventilation of the North Atlantic and North Pacific: Subduction Versus Obduction, *Journal of Physical Oceanography, 25*, 2374-2390, 1995.

Reid, J.L., Intermediate Waters of the Pacific Ocean, *The Johns Hopkins Oceanographic Studies, 2*, 85, 1965.

Richter, R.C., D. Link, and H.M. Kingston, Microwave-Enhanced Chemistry, *Analytical Chemistry, 73*, 30A-37A, 2001.

Roden, J.S., and J.R. Ehleringer, Hydrogen and oxygen isotope ratios of tree ring cellulose for field-grown riparian trees, *Oecologia, 123*, 481-489, 2000.

Roden, J.S., G. Lin, and J.R. Ehleringer, A mechanistic model for interpretation of hydrogen and oxygen isotope ratios in tree-ring cellulose, *Geochimica et Cosmochimica Acta, 64*, 21-35, 2000.

Rodgers, K.B., M.A. Cane, N.H. Naik, and D.P. Schrag, The role of the Indonesian Throughflow in equatorial Pacific thermocline ventilation, *Journal of Geophysical Research, 104*, 20,551-20,570, 1999.

Roether, W., An account of tritium in the ocean, IAEA Special Report 21pp, 1989.

Rozanski, K., C. Sonntag, and K.O. Munnich, Factors controlling stable isotope composition of European precipitation, *Tellus, 34*, 142-150, 1982.

Sarmiento, J.L., A Simulation of Bomb Tritium Entry into the Atlantic Ocean, *Journal of Physical Oceanography, 13*, 1924-1939, 1983.

Schiegl, W.E., Climatic significance of deuterium abundance in growth rings of *Picea*, *Nature, 251*, 582-584, 1974.

Schiegl, W.E., and J.C. Vogel, Deuterium Content of Organic Matter, *Earth and Planetary Science Letters, 7*, 307-313, 1970.

Schimmelmann, A., Determination of the Concentration Stable Isotope Composition of Nonexchangeable Hydrogen in Organic Matter, *Analytical Chemistry, 63*, 2456-2459, 1991.

Schimmelmann, A., and M.J. DeNiro, Preparation of Organic and Water Hydrogen for Stable Isotope Analysis: Effects Due to Reaction Vessels and Zinc Reagent, *Analytical Chemistry, 65*, 789-792, 1993.

Sheu, D.D., and C.H. Chiu, Evaluation of cellulose extraction procedures for stable carbon isotope measurement in tree ring research, *International Journal of Environmental Analytical Chemistry, 59*, 59-67, 1995.

Short, R.D., and H.S. Munro, Conclusions drawn from a study of cellulose nitration in technical mixed acids by X-ray photoelectron spectroscopy and ^{13}C nuclear magnetic resonance, *Polymer, 34*, 2714-2719, 1993.

Short, R.D., H.S. Munro, R. Matthews, and T. Pritchard, ^{13}C n.m.r. study of cellulose nitrates: a comparison between nitration in nitric acid dichloromethane mixes and technical mixed acids, *Polymer Communications*, 1989.

Talley, L.D., An Okhotsk Sea water anomaly: implications for ventilation in the North Pacific., *Deep Sea Research, 38(1)*, 171-190, 1991.

Tang, K., X. Feng, and G.J. Ettl, The variations in δD of tree rings and the implications for climatic reconstruction, *Geochimica et Cosmochimica Acta, 64*, 1663-1673, 2000.

Taylor, C.B., Tritium in Southern Hemisphere Precipitation 1953-1964, *Tellus, 18*, 105-131, 1966.

Taylor, C.B., Influence of 1968 French thermonuclear tests on tritium fallout in the southern hemisphere, *Earth and Planetary Science Letters, 10*, 196-198, 1971.

Terwilliger, V.J., and M.J. DeNiro, Hydrogen isotope fractionation in wood-producing avocado seedlings: Biological constraints to paleoclimatic interpretations of δD values in tree ring cellulose nitrate, *Geochimica et Cosmochimica Acta, 59*, 5199-5207, 1995.

Thiele, G., and J.L. Sarmiento, Tracer Dating and Ocean Ventilation, *Journal of Geophysical Research, 95*, 9377-9391, 1990.

Thiemens, M.H., and S.K. Bhattacharya, New quantum chemical isotope effects: Applications to the pre-solar nebula, planetary atmospheres and interstellar space, in *From Mantle to Meteorites: A Garland of Perspectives. Festschrift for Devendra Lal*, edited by K. Gopalan, V.K. Gaur, B.L.K. Somayajula, and J.D. Macdougall, pp. 35-59, Indian Academy of Sciences, 1990.

Van Scoy, K.A., R.A. Fine, and H.G. Östlund, Two decades of mixing tritium into the North Pacific Ocean, *Deep Sea Research, 38* (Suppl. 1), S191-S219, 1991.

Warner, M.J., J.L. Bullister, D.P. Wisegarver, R.H. Gammon, and R.F. Weiss, Basin-wide distributions of chlorofluorocarbons CFC-11 and CFC-12 in the North Pacific:1985-1989, *Journal of Geophysical Research, 101*, 20,525-20,542, 1996.

Warner, M.J., and G.I. Roden, Chlorofluorocarbon evidence for recent ventilation of the deep Bering Sea, *Nature, 373*, 409-412, 1995.

Weiss, W., and W. Roether, Der Tritiumabfluss des Rheins 1961-1973, *Deutsche Gewässerkundliche Mitteilungen, 19*, 1-5, 1975.

Weiss, W., and W. Roether, The rates of tritium input to the world oceans, *Earth and Planetary Science Letters, 49*, 435-446, 1980.

Weiss, W., W. Roether, and E. Dreisigacker, Tritium in the North Atlantic: inventory, input and transfer into the deep water, in *The Behaviour of Tritium in the Environment*, pp. 315-336, International Atomic Energy Agency, Vienna, 1979.

Whistler, R.L., and C.L. Smart, *Polysaccharide Chemistry*, 493 pp., Academic Press inc. New York, 1953.

White, J.W.C., The Climatic Significance of D/H Ratios in White Pine in the Northeastern United States, PhD Thesis, Columbia University, 1983.

White, J.W.C., E.R. Cook, J.R. Lawrence, and W.S. Broecker, The D/H ratios of sap in trees: Implications for water sources and tree ring D/H ratios, *Geochimica et Cosmochimica Acta, 49*, 237-246, 1985.

White, J.W.C., J.R. Lawrence, and W.S. Broecker, Modelling and interpreting D/H ratios in tree rings: A test case of white pine in the northeastern United States, *Geochimica et Cosmochimica Acta, 58*, 851-862, 1994.

Wong, C.S., R.J. Matear, H.J. Freeland, F.A. Whitney, and A.S. Bychkov, WOCE line P1W in the Sea of Okhotsk 2. CFCs and the formation rate of intermediate water, *Journal of Geophysical Research, 103*, 15,625-15,642, 1998.

Woods, F.W., and D. O'Neal, Tritiated Water as a Tool for Ecological Field Studies, *Science, 147*, 148-149, 1965.

Yakir, D., Variations in the natural abundance of oxygen-18 and deuterium in plant carbohydrates, *Plant, Cell and Environment, 15*, 1005-1020, 1992.

Yapp, C.J., and S. Epstein, A reexamination of cellulose carbon-bound hydrogen δD measurments and some factors affecting plant-water D/H relationships, *Geochimica et Cosmochimica Acta*, *46*, 955-965, 1982a.

Yapp, C.J., and S. Epstein, Climatic significance of the hydrogen isotope ratios in tree cellulose, *Nature*, *297*, 636-639, 1982b.

Yapp, C.J., and S. Epstein, Seasonal Contributions to the Climatic Variations Recorded in Tree Ring Deuterium/Hydrogen Data, *Journal of Geophysical Research*, *90*, 3747-3752, 1985.

Yasuda, I., K. Okuda, and Y. Shimizu, Distribution and Modification of North Pacific Intermediate Water in the Kuroshio-Oyashio Interfrontal Zone, *Journal of Physical Oceanography*, *26*, 448-465, 1996.

Zahn, A., V. Barth, K. Pfeilsticker, and U. Platt, Deuterium, oxygen-18 and tritium as tracers for water vapour transport in the lower stratosphere and tropopause region, *Journal of Atmospheric Chemistry.*, *30*, 25-47, 1998.